

**Biochemical and structural characterization
of spliceosomes purified at defined stages of
assembly from the yeast *S. cerevisiae***

Dissertation

zur Erlangung des mathematisch-naturwissenschaftlichen Doktorgrades

“Doctor rerum naturalium”

der Georg-August-Universität zu Göttingen

im Promotionsprogramm Biologie

der Georg-August-University School of Science (GAUSS)

vorgelegt von

Julia Dannenberg

aus Braunschweig

Göttingen, 2013

Betreuungsausschuss

Prof. R. Lührmann, Abteilung für Zelluläre Biochemie/MPI-bpc Göttingen

Prof. R. Ficner, Abteilung für Molekulare Strukturbioogie, GZMB Göttingen

Mitglieder der Prüfungskommission

Referent: Prof. R. Lührmann, Abteilung für Zelluläre Biochemie/MPI-bpc Göttingen

Korreferent: Prof. R. Ficner, Abteilung für Molekulare Strukturbioogie, GZMB
Göttingen

Weitere Mitglieder der Prüfungskommission:

Prof. J. Enderlein, Abteilung für Biophysik, III. Physikalisches Institut der Universität
Göttingen

Prof. H. Stark, Abteilung für Elektronenmikroskopie, MPI-bpc Göttingen

Prof. J. Wienands, Abteilung für Zelluläre und Molekulare Immunologie, Universität
Göttingen

Prof. H. Krebber, Abteilung für Molekulare Genetik, Institut für Mikrobiologie und
Genetik

Tag der mündlichen Prüfung: 8. April 2013

Table of content

1. Introduction.....	8
1.1 From Genes to Proteins	8
1.2 Conserved sequences and pre-mRNA splicing.....	8
1.3 The chemistry of the splicing mechanism	10
1.4 SnRNPs – the building blocks of the spliceosome	11
1.5 Assembly of the spliceosome	15
1.6 DExD/H box proteins as the driving force for spliceosome remodeling	17
1.7 Spliceosome associated non-snRNP factors – proteins of the NTC	19
1.8 Structural rearrangements of the Spliceosomal RNA-RNA network	19
1.9 Approaches for the isolation of native spliceosomal complexes	21
1.10 Yeast as a model organism.....	24
1.11 Investigation and characterization of yeast spliceosomal complexes via mass spectrometry and electron microscopy	24
1.11.1 Mass spectrometry.....	25
1.11.2 Electron microscopy	25
1.12 Dual Color Fluorescence Cross-Correlation Spectroscopy – an excellent technique to study protein dynamics within the spliceosome	26
1.13 Aim of this study	28
2. Materials and Methods.....	33
2.1 Materials.....	33
2.1.1 Chemicals and media.....	33
2.1.2 Enzymes and enzyme inhibitors	35
2.1.3 Nucleotides.....	35
2.1.4 DNA oligonucleotides and plasmids.....	36
2.1.4.1 DNA oligonucleotides	36
2.1.4.2 Plasmids.....	36
2.1.5 Yeast and bacterial strains.....	37
2.1.5.1 Yeast strains	37
2.1.5.2 Bacterial strains.....	38

2.1.6	Commercial kits	38
2.1.7	Chromatography materials and consumables	38
2.1.8	Common buffers	39
2.1.9	Machines and working equipment	40
2.2	Methods	42
2.2.1	General molecular biology methods	42
2.2.1.1	Concentration determination of nucleic acids	42
2.2.1.2	Purification and manipulation of DNA	42
2.2.1.3	Agarose gel electrophoresis	42
2.2.1.4	Polymerase chain reaction	43
2.2.1.5	Transformation of yeast and E. coli	43
2.2.1.6	Phenol-chloroform-isoamylalcohol (PCI) extraction and ethanol precipitation	44
2.2.1.7	Proteinase K digestion	45
2.2.1.8	In vitro transcription	45
2.2.1.9	Denaturing polyacrylamide gel electrophoresis of RNA (splicing products)	47
2.2.1.10	Silver staining of RNA gels	48
2.2.1.11	Northern blot analysis	48
2.2.2	Protein-biochemistry standard methods	49
2.2.2.1	Concentration determination of proteins	49
2.2.2.2	Ethanol precipitation of proteins for Mass Spectrometric analysis	49
2.2.2.3	Denaturing Polyacrylamide Gel Electrophoresis (PAGE)	50
2.2.2.4	Coomassie staining of protein gels	50
2.2.2.5	Silver Staining of Protein Gels	51
2.2.2.6	Western blot analysis	51
2.2.3	Purification of recombinant proteins	52
2.2.3.1	Cloning strategy and overexpression	52
2.2.3.2	Purification of proteins	53
2.2.4	Purification of MS2MBP Protein	54
2.2.5	Cell culture and extract preparation	55
2.2.5.1	Cultivation of bacteria	55
2.2.5.2	Cultivation of yeast cells	55
2.2.5.3	Preparation of yeast whole cell extracts and immunodepletion	56
2.2.6	Special methods	57
2.2.6.1	In vitro splicing reactions	57

2.2.6.2	Purification of spliceosomal complexes.....	58
2.2.6.3	Non-denaturing Complex gels.....	59
2.2.7	Reconstitution of functional spliceosomes for FCCS.....	59
2.2.7.1	Treatment of complexes for RNA PAGE.....	59
2.2.7.2	Reconstitution on Amylose Matrix.....	60
2.2.7.3	In-solution.....	60
2.2.8	Mass spectrometry.....	61
2.2.9	Electron Microscopy.....	61
2.2.10	Labeling Methods.....	62
2.2.10.1	Preparation of yeast strains expressing EGFP-tagged proteins.....	62
2.2.10.2	Pre-mRNA labeling with a fluorescent dye.....	62
2.2.11	Fluorescence Cross Correlation Spectroscopy (FCCS).....	63
2.2.11.1	Setup.....	63
2.2.11.2	Measurement protocol.....	64
3.	Results.....	65
3.1	Pre-mRNA constructs and conditions used for the isolation of yeast spliceosomal complexes.....	65
3.2	Preliminary work for stalling and isolating active spliceosomal complexes from yeast at defined stages.....	66
3.3	Purification of yeast spliceosomes.....	68
3.3.1	Purification of the pre-catalytic B complex.....	69
3.3.2	Affinity-purified complex B is functionally committed for subsequent activation and splicing catalysis.....	71
3.3.3	Purification of the activated B ^{act} complex.....	72
3.3.4	Purification of the first step spliceosome complex C.....	74
3.4	Protein composition of purified yeast spliceosomes.....	77
3.4.1	The proteome of the pre-catalytic B complex.....	78
3.4.2	The proteome of the activated B ^{act} complex.....	79
3.4.3	The proteome of the step1 spliceosome C complex.....	81
3.5	Electron microscopy of Yeast spliceosomes.....	85
3.5.1	Electron microscopy of yeast spliceosomal complexes Complex B, B ^{act} and C.....	86

3.6	Isolation and characterization of early spliceosomal complexes isolated from the Yeast <i>S. cerevisiae</i>	88
3.6.1	Inactivation or removal of Prp5 stalls the spliceosome assembly at the stage of the CC complex.....	89
3.7	Investigation of the protein rearrangements at the catalytic core of the spliceosome as revealed by dual color FCCS.....	92
3.8	Generation of doubly labeled spliceosomes for dcFCCS measurements	94
3.8.1	Stability of the binding of EGFP fusion proteins to the B ^{actΔPrp2} complex under dcFCCS conditions.....	96
3.8.2	Cwc24 and Cwc27 leave the spliceosome during Prp2-mediated catalytic activation under near-physiological conditions.....	98
3.8.3	Cwc24 is essential for the first step of splicing in vitro but it is not required for catalysis of the splicing reaction per se	101
3.8.4	The U2-associated SF3a and SF3b proteins Prp11 and Cus1 remain bound to the B* complex under physiological conditions, but their affinity is weakened at high salt	102
3.8.5	The binding of the RES complex protein Bud13 is weakened during catalytic activation	103
3.8.6	Binding of Yju2 to the spliceosome is strengthened upon catalytic activation.....	105
3.8.7	Prp2-mediated catalytic activation of the spliceosome creates also a high affinity binding site for Cwc25 in the spliceosome	106
4.	Discussion	110
4.1	The structural dynamics of the spliceosome are modulated by multiple DExD/H-box RNA helicases, the driving forces of the spliceosome.....	110
4.2	The protein composition of yeast spliceosomes is less complex than that of metazoan spliceosomes	111
4.3	Isolation and characterization of early spliceosomal complexes from yeast	112
4.4	Evolutionary conservation of yeast spliceosomes	114
4.5	Spliceosomal dynamics during catalytic activation	117
4.6	Compositional dynamics correlate with structural changes	122
4.7	Suitability of dual color Fluorescence Cross Correlation Spectroscopy (dcFCCS) for investigating spliceosomal protein dynamics	123

4.8	Prp2-mediated transformation of the B ^{act} into the B* complex substantially alters the binding affinity of several proteins at the catalytic core of the spliceosome ...	124
4.9	Cwc24 functions in the generation of an active spliceosome but is not required for splicing catalysis per se.....	125
4.10	Sf3a/b proteins remain bound to the B* spliceosome under near-physiological conditions, but their binding is reduced at high salt.....	126
4.11	Prp2 action creates high-affinity binding sites for the step 1 factors Yju2 and Cwc25 in the catalytically activated spliceosome	127
4.12	Substantial Prp2-mediated remodeling during catalytic activation of the spliceosome	128
5.	Future perspectives	131
6.	References.....	133
7.	Appendix.....	141
7.1	List of abbreviations	141
7.1	Curriculum vitae	144
7.2	List of publications	145
7.3	Conferences	145
7.4	Acknowledgment	146
7.5	Erklärung.....	149

Abstract

Splicing of pre-messenger RNA (pre-mRNA) is catalyzed by the spliceosome, a multimegadalton ribonucleoprotein (RNP) comprising several small nuclear (sn) RNPs and numerous proteins. The spliceosome assembles on its pre-mRNA substrate in an ordered process that begins with recognition of the 5' end of the intron (5' splice site, 5'SS) by the U1 snRNP. Thereafter the U2 snRNP binds to the pre-mRNA's branch point sequence (BPS), forming complex A. Complex A then binds the pre-formed U4/U6·U5 tri-snRNP to form complex B, which contains a full set of snRNAs in a pre-catalytic state. Complex B is then activated for catalysis by a major rearrangement of its RNA network and its overall structure; this remodeling includes dissociation of the U1 and U4 snRNAs and the formation of the activated spliceosome B^{act}. In the catalytically activated complex (termed B*) step 1 catalysis takes place: the adenosine at the BPS attacks the 5'SS, generating a cleaved 5' exon and intron-3' exon intermediate. The resulting complex C then catalyzes step 2 catalysis, in which the intron is cleaved at the 3' splice site (3'SS) with concomitant ligation of the 5' and 3' exons to form mature mRNA. Thus, the spliceosome is a particularly dynamic RNP machine that undergoes many changes in composition and conformation. The structural dynamics of the spliceosome are facilitated by the action of multiple DExD/H-box RNA helicases. Among these are Prp5 and Prp2, which are essential ATPases required prior to the first step of pre-mRNA splicing. Prp5 enables stable U2 snRNP association with the branch site and Prp2 promotes a structural rearrangement that transforms the B^{act} into the catalytically activated B* complex.

The pathway of spliceosome assembly and the main features of its catalytic chemistry appear to be conserved between metazoans and yeast. Thus, I set out to study isolated spliceosomal complexes from the lower eukaryote *Saccharomyces cerevisiae* as it was already known to possess a basic (constitutive) spliceosomal machinery similar to that of primates. Each new round of splicing generates a catalytic centre *de novo* during the transitions from complex B to B^{act} to B* and to the product of step 1 of splicing, complex C. Here, I focused on the isolation and characterization of complex B, the activated complex B^{act} and complex C. Each complex was stalled via truncation or modification of the actin pre-mRNA used during the splicing reaction or adjustment of the ATP concentration in the splicing reaction. Each complex was then

isolated by centrifugation and affinity-selection, their proteomes determined by mass spectrometry (in collaboration with Prof. Henning Urlaub) and their structures examined by electron microscopy (in collaboration with Dr. Berthold Kastner and Prof. Holger Stark), for the first time. The analysis of the three stalled yeast spliceosomal “snapshots” isolated here has made it possible to pinpoint the window of function for important spliceosomal proteins. For instance, the number, characteristics and time of recruitment of evolutionarily conserved proteins involved in the formation and stabilization of the U2/U6/pre-mRNA network of the catalytic center in complex B^{act} remained so far elusive. The data revealed several evolutionarily conserved proteins recruited at the time of pre-catalytic activation (i.e. Cwc2, Cwc24, Yju2, Prp2 and Spp2) and also provided important hints for those proteins involved in promoting step 1 catalysis and the formation of complex C (i.e. Cwc25). Compared to metazoan spliceosomes the number of proteins associated with purified yeast spliceosomes at any stage is less than a half, yet more than 85% of these have evolutionarily conserved counterpart in humans. The less complex protein composition of yeast spliceosomes offers also a significant advantage for three-dimensional (3D) structure analyses. The EM analyses show for the first time images of *S. cerevisiae* spliceosomal complexes at well defined stages of function. These are at an unprecedented quality level, and they are well suited for 3D structure investigations, based on criteria such as their structural integrity and homogeneity.

In this work I have also applied dual-color fluorescence cross-correlation spectroscopy (dcFCCS, in collaboration with Prof. Jörg Enderlein, III. Institute of Physics, University of Göttingen), to measure the binding affinity of splicing factors – which were detected in the first part of this work – to the yeast spliceosome and to follow their binding dynamics during the catalytic activation of the spliceosome promoted by the RNA helicase/ATPase Prp2 and its co-activator Spp2. dcFCCS is a sensitive and versatile optical technique that allows the direct analysis of the dynamic association and dissociation events among proteins and/or RNAs in complex systems in solution at low nanomolar concentrations and in equilibrium, without requiring biochemical or physical perturbation of the sample. For this purpose I have employed a recently described purified splicing system developed in our laboratory which recapitulate catalytic activation and step 1 of splicing *in vitro* and consists of B^{act}

complexes assembled in extracts where Prp2 is thermo sensitive and can be heat-inactivated. These B^{act} complexes lacking Prp2 are then purified to near homogeneity and complemented with recombinantly expressed Prp2 and Spp2 splicing factors. To perform dcFCCS, the B^{act} complexes were assembled on pre-mRNA labeled with a red fluorescent dye. In addition, spliceosomal proteins of interest were labeled *in vivo* by fusing them with the green fluorescent protein EGFP, by genetic modification in yeast. The purified doubly-labelled spliceosomes were then analyzed before and after catalytic activation by Prp2 and the weakening or strengthening of the binding of the EGFP-labeled protein to the spliceosome was analyzed by measuring the cross-correlation between the green label and the red fluorescent dye. The analysis and evaluation of the dcFCCS data in this work was done in collaboration with Prof. Jörg Enderlein and Mira Prior (III. Institute of Physics, University of Göttingen).

The data revealed that the binding affinity of quite a number of proteins is significantly changed during the Prp2-mediated catalytic activation of the spliceosome. Specifically, the essential zinc finger protein Cwc24, was quantitatively displaced from the B* complex. Consistent with this, we show that Cwc24 is required for step 1 but not for catalysis *per se*. Interestingly, the U2-associated SF3a and SF3b proteins Prp11 and Cus1 were destabilized during catalytic activation. Indeed, they remained bound to the B* spliceosome under near-physiological conditions (i.e. 75 mM), but their binding was reduced at higher salt. As the U2 SF3a/b proteins bind near the branch point sequence, this indicated that the branch site must be remodeled in complex B* as a prerequisite for step 1 catalysis. On the other hand, high affinity binding sites were created for the step 1 factors Yju2 and Cwc25 during catalytic activation, consistent with their requirement for step 1 catalysis. In conclusion, These results shed light on the nature of the structural remodeling mediated by Prp2 in the spliceosome and suggest that during catalytic activation the spliceosome undergoes significant rearrangements.

1. Introduction

1.1 From genes to proteins

The blueprint of cells is encoded in their DNA. The flow of information from genes to proteins requires two main steps, termed transcription and translation. Transcription is a DNA-controlled process where DNA is “transcribed” into RNA; translation is the RNA-controlled synthesis of proteins. In eukaryotic cells, genes are expressed as *precursor messenger RNAs (pre-mRNAs)* due to the fact that in higher eukaryotes the coding sequences of genes, the exons are interrupted by non-coding sequences, the introns. These *mosaic structure* or *split genes*, is only found in eukaryotes. First, the precursor is synthesized/transcribed by the polymerase II. After transcription and before the transport out of the nucleus into the cytoplasm, the precursor RNA has to undergo a maturation process or so-called RNA processing step. Due to the split gene character, the non-coding sequences have to be removed from the precursor messenger RNA by a mechanism called splicing. During this process, introns are removed from the precursor and the flanking sequences, the exons, are joined to build the functional mature RNA. RNA processing includes in addition to splicing, the modification of both ends of the pre-mRNA: capping of the 5' end and polyadenylation of the 3' end. Both modifications play an important role in mRNA export, stability and translation and occur co-transcriptionally. After RNA processing the mature RNA can be transported from the nucleus to the cytoplasm, where it is used by ribosomes as a template for the synthesis of the amino-acid sequence, leading to the formation of a protein.

1.2 Conserved sequences and pre-mRNA splicing

Splicing itself is catalyzed by a macromolecular machinery, the spliceosome and requires a set of specific sequences contained within the intron. The boundaries of exons and introns must be precisely identified by the spliceosome, because an error of only one nucleotide would result in a shift of the gene's reading frame and would lead to the translation of a non-functional protein.

The process of pre-mRNA splicing is highly conserved from yeast to humans; however the degree to which it occurs is clearly different (Ast, 2004). Whereas nearly all human genes contain introns, the yeast *Saccharomyces (S.) cerevisiae* has introns in only ~3-4% of its genes (Lopez and Seraphin 1999). Interestingly, about 70% of genes encoding for ribosomal proteins contains an intron. Introns vary in their length and sequences and exon-intron boundaries are only defined by very short sequence stretches, which makes the process of splicing challenging, but both organisms, humans and yeast are suitable models for *in vitro* studies and for understanding the highly conserved splicing process. In pre-mRNA transcripts three conserved sequences are found which are recognized by different factors during the splicing process. The sequences are the 5' splice site (5'SS), the branch point sequence (BPS) and the 3' splice site (3'SS).

In the yeast (*S. cerevisiae*) these elements are highly conserved (Fig. 1.1).

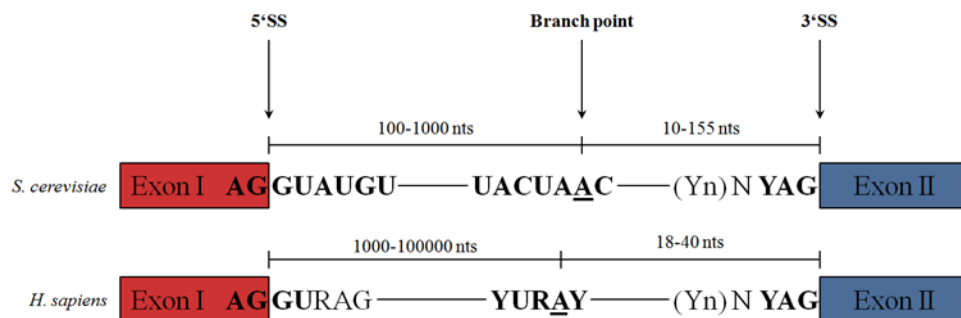


Figure 1.1: Conserved sequences in intron of *S.cerevisiae* and *Homo sapiens*

(kindly provided by Dr. Nicolas Rasche)

The (5'SS) sequence defines the boundary between an exon and a downstream intron and is composed of R/GUAUGU ('R' is a purine, '/' indicates the exon/intron boundary)(Lopez and Seraphin 1999). While in *S. cerevisiae* the 5'SS is 90% conserved, the human consensus sequence AG/GUAGU is rather degenerated.

The (3'SS) sequence defines the boundary between an intron and a downstream exon and is composed of YAG/ ('Y' is a pyrimidine, '/' indicates the exon/intron boundary) in *S. cerevisiae* as well as in *H. sapiens*. In many introns the 3'SS is preceded by a stretch of 8-12 pyrimidines called the polypyrimidine tract, which

usually ends one nucleotide upstream of the 3'SS. The polypyrimidine tract seems to be more important for splicing of human than for splicing of yeast introns.

Another conserved sequence element surrounds the adenosine (branch adenosine, branch point, BP), - which forms a branched intermediate in the course of the first step of splicing. This sequence is therefore called branch point sequence (BPS). The consensus sequence is composed of UACUAAC and in yeast it is usually located 10-60 nucleotides upstream of the 3'SS (Spingola, Grate et al. 1999).

1.3 The chemistry of the splicing mechanism

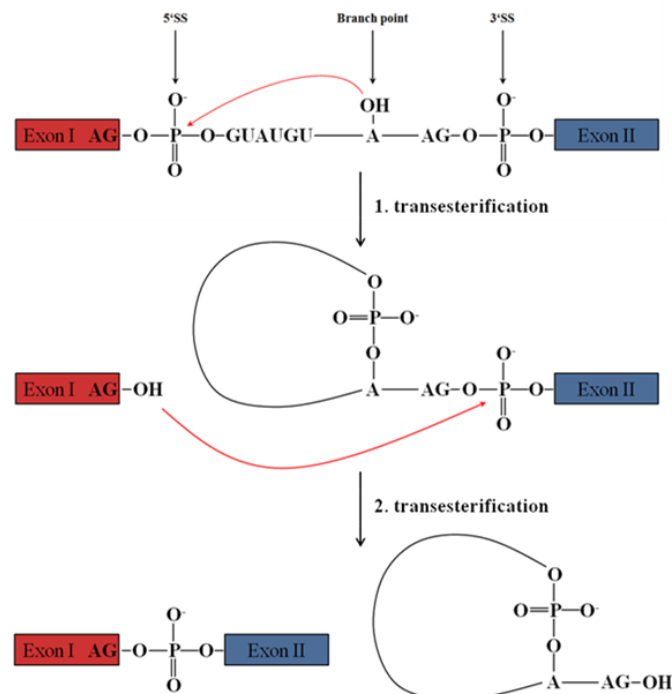


Figure 1.2: The chemistry of the pre-mRNA splicing reactions (Figure was kindly provided by Dr. Nicolas Rasche) Pre-mRNA splicing is carried out via a two transesterification step mechanism. Step 1 results in formation of a free 5' exon and a lariat-3' exon (lariat intermediate). Step 2 produces the ligated exons and an intron lariat structure. Nucleophilic attack by the reactive groups is shown as dashed lines in red.

The process of pre-mRNA splicing consists of a two steps mechanism involving two consecutive transesterification reactions (Moore, Query et al. 1993; Moore and Sharp 1993) . In the first step, the 2'-hydroxyl group (OH) of the conserved branch point adenosine as a nucleophile attacks the phosphate at the 5'SS (5'exon/intron junction) resulting in a free 5' exon which contains a 3' terminal OH group and a branched lariat intermediate which contains an unusual 2'-5' phosphodiester bond at the branchpoint adenosine (Fig. 1.2). In the second step, the 3' OH of the 5' exon attacks the phosphate at the intron/3' exon boundary (3'SS) followed by the ligation of the 5' and 3' exons and the release of the intron lariat. Subsequently, the mRNA is transported to the cytoplasm, whereas the intron lariat is degraded (Nilsen 1998); (Will and Luhrmann 2011). The splicing process is dependent on ATP.

1.4 SnRNPs – the building blocks of the spliceosome

The snRNPs are the main building blocks of the spliceosome. Each of these consists of a snRNA molecule (or two in the case of U4/U6), seven Sm proteins (B/B', D3, D2, D1, E, F, and G) that are shared by all of the spliceosomal snRNPs and several other, particle specific proteins (Brow 2002); (Will and Luhrmann 2011); (Wahl, Will et al. (2009); (Valadkhan and Jaladat (2011)). More than 50 proteins are associated with the snRNPs and more than 100 non-snRNP proteins are in the spliceosome as revealed by mass spectrometry studies (Wahl, Will et al. 2009). In total five spliceosomal snRNAs are found in the yeast *S.cerevisiae* termed U1, U2, U4, U5 and U6. U5 exist in two isoforms: U5 long and U5 short, which originate from the same precursor transcript, but are differently cleaved at the 3'-stem loop by RNaseIII (Chanfreau, Elela et al. (1997).

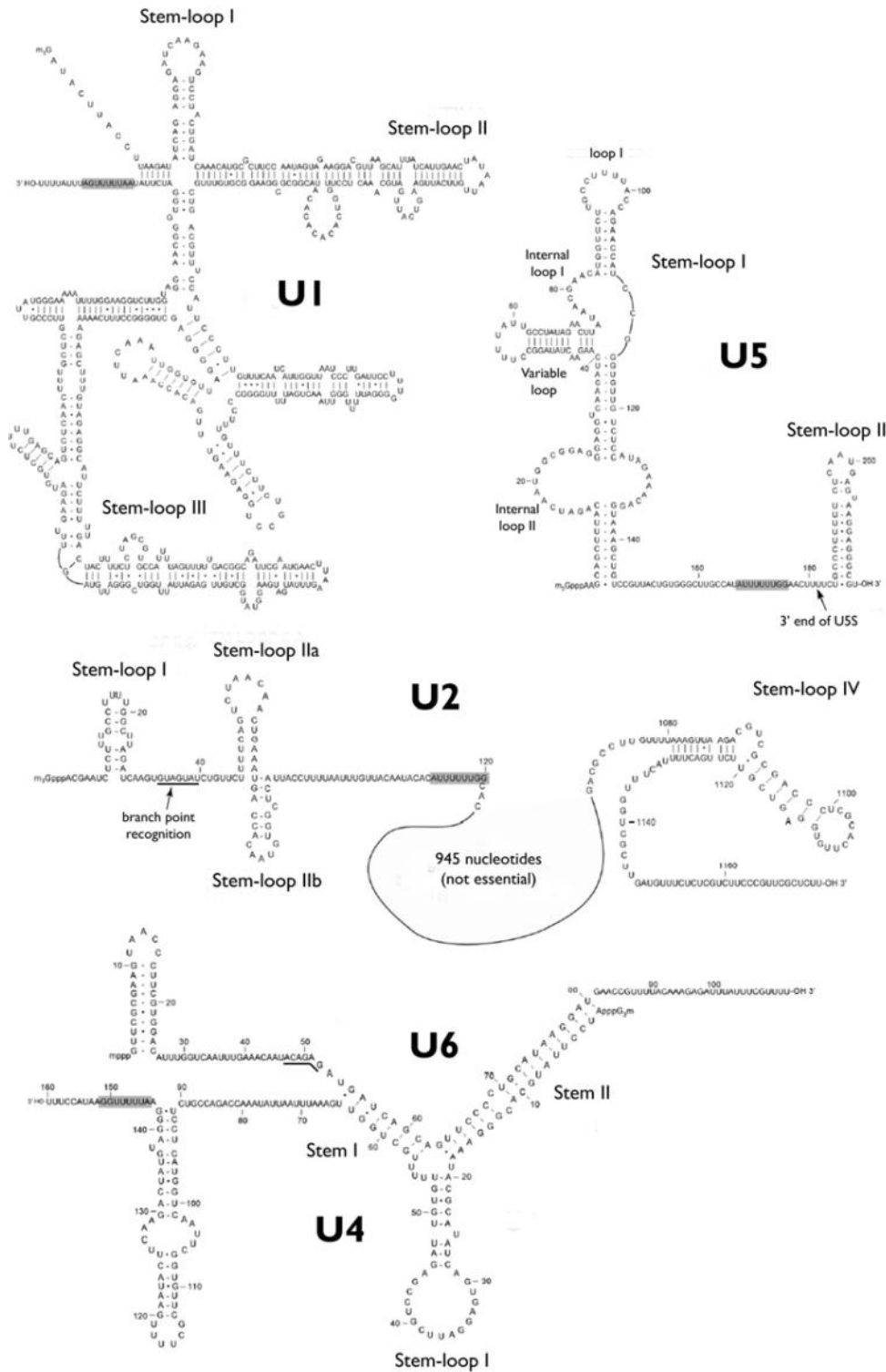


Figure 1.3: Secondary structures for the yeast U snRNAs

Schematic representation of proposed secondary structures of yeast snRNAs. The Sm binding site is indicated with a grey shadow. The conserved ACAGAGA box motif in U6 snRNA is underlined (adapted from Kretzner, Krol et al. (1990)(U1); (Shuster and Guthrie 1988)(U2); Frank, Roiha et al. (1994); (Will and Lührmann 2006)(U5); (Brow and Guthrie 1988)(U6, U4/U6)).

The U snRNAs, except U6, are transcribed by the RNA polymerase II as snRNA precursors that acquire an m⁷G cap. U6 snRNA is transcribed by the polymerase III and bears a γ -monomethyl phosphate cap at its 5'-end (Singh and Reddy 1989). These pre-U snRNAs are subsequently exported to the cytoplasm where the snRNP assembly occurs (Kiss and Jady 2004);(Will and Lührmann 2001). In the cytoplasm, the seven Sm proteins bind to the Sm RNA site, a uridine rich consensus sequence, found in each of the snRNAs, except U6, and form a doughnut-shaped structure around the Sm binding site. In contrast, U6 bears a so-called Sm-like binding site (Lsm) at its 3' end, which also shows a high uridine content. To the Lsm site of U6, seven proteins, Lsm 2-8, are recruited during U6 snRNP biogenesis. These proteins are homologous to the Sm proteins. This binding process of Sm proteins with the snRNAs is an important step for later hypermethylation of the cap structure. In yeast this hypermethylation is catalyzed by a RNA-methyltransferase termed Tsg1, which is recruited by binding at the Sm site (Mouaikeel, Verheggen et al. 2002). After assembly in the cytoplasm, the particle is transported back to the nucleus for assembly of the spliceosome.

As already mentioned above and illustrated in Fig. 1.4, each yeast U snRNP contains, beside the described seven Sm (Lsm) proteins, its particle-specific set of proteins. Both, common and particle specific proteins are evolutionarily conserved between organisms, outlining the importance of the protein composition for the mechanism of pre-mRNA splicing. If one compares for example the yeast U1 snRNP with the human U1 snRNP, one recognizes immediately that the yeast particle is more complex than the human one. While the human U1 snRNP is only composed of the Sm proteins and three snRNP specific proteins, U1A, 70K and U1C, the yeast U1 snRNP has ten specific proteins (Gottschalk, Tang et al. (1998); (Neubauer, Gottschalk et al. 1997). Three of these proteins are homologues of the human U1 proteins. Mud1 is the homologue of the human U1A protein, Snp1p of the human 70K and Yhc1 of the human U1C protein. The function of the specific U1 proteins is to stabilize the binding of U1 snRNA to the 5'SS (Gottschalk, Tang et al. 1998); (Rosbash and Séraphin 1991). The U2 snRNP in yeast consists of twelve snRNP specific proteins; eleven of which are homologues to the human U2 snRNP proteins. The U2 associated proteins are Lea1 (homologue of U2A'), Msl1 (homologue of U2B''), as well as the factors of the SF3a and SF3b complex: Prp9, Prp11 and Prp21

(homologues of the human proteins of the SF3a complex: SF3a120, SF3a66, SF3a60), Cus1, Hsh49, Hsh155, Rse1 Rds3 and YSF3 (homologues of the human SF3b proteins) (Brow 2002); (Casparly and Séraphin 1998); (Wang and Rymond 2003). The snRNAs of the U4/U6 di-snRNP are base-paired with each other and in addition to the Sm and Lsm proteins, have five particle specific proteins, Snu13 (homologue of 15.5K), Prp3 (homologue of 90K), Prp4 (homologue of 60K), Prp31 (homologue of 61K) and Prp6 (homologue of 102K). In the human system, 102K/yeast Prp6 is associated with the U5 snRNA (Abovich, Legrain et al. 1990). The U5 particle contains six particle-specific proteins, Prp8 (homologue of 220K), Brr2 (homologue of 200K), Snu114 (homologue of 116K), Prp28 (homologue of 100K), Snu40 (has no homologue in human) and Dib1 (Stevens, Barta et al. 2001). Most of the yeast U5 proteins have highly conserved human homologues (Bach, Winkelmann et al. 1989; Bach and Lührmann 1991). The U5 specific protein Snu114 shows similarity to GTPases (Fabrizio, Lagerbauer et al. 1997), while Brr2 and Prp28 belongs to the family of the DExD/H-box proteins and are important driving forces during the splicing cycle (see chapter 1.6). The pre-assembled U4/U6.U5 tri-snRNP has, beside the particle specific proteins of U4, U5 and U6 also factors which only associates with the tri-snRNP, Snu66, Prp38, Snu23 and Spp381 (Gottschalk, Neubauer et al. 1999; Stevens, Barta et al. 2001).

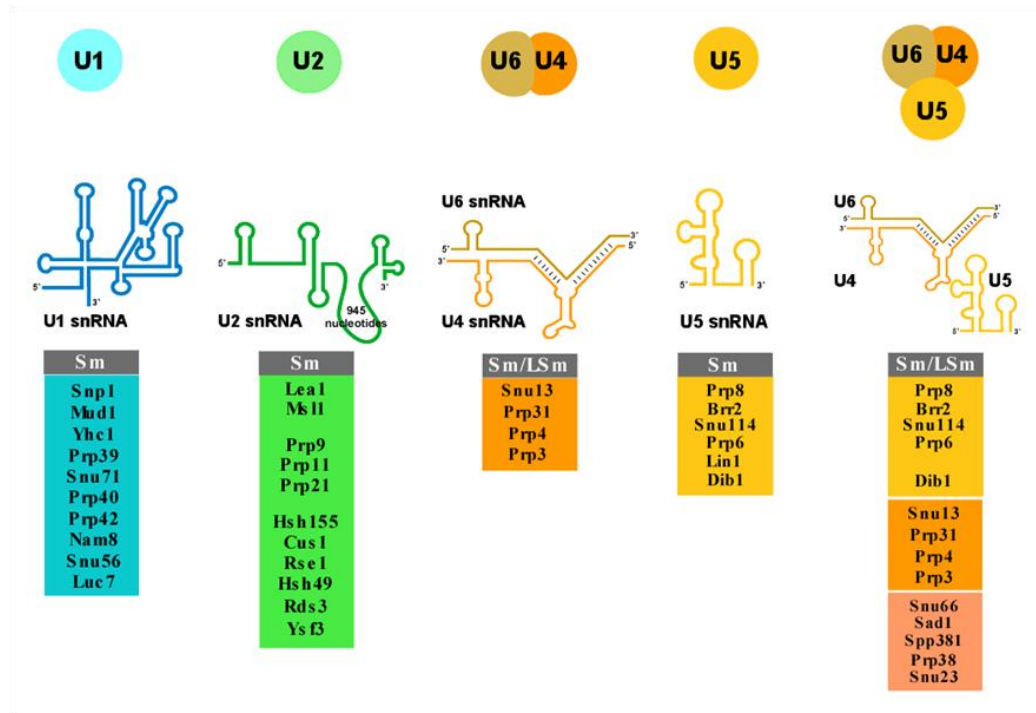


Figure 1.4: Composition of the yeast U snRNPs. Each U snRNP consists of a RNA molecule and the common Sm- or Sm-like proteins (Lsm) and several particle specific proteins. The common Sm proteins are grey boxed, the particle specific proteins are in the same color as the U snRNA of the particle which is shown above (scheme was kindly provided by Dr. Patrizia Fabrizio).

1.5 Assembly of the spliceosome

The assembly of the spliceosome in the course of the pre-mRNA splicing process occurs in a stepwise manner. The spliceosome is a highly dynamic protein-rich molecular machinery and is composed of the previously described five snRNPs. *In vitro* studies in humans and yeast showed that the spliceosome consists of several different complexes which are formed stepwise one after another termed as E, A, B, B^{act}, C complex and postspliceosome (in this work yeast complexes are named after human spliceosomes). The assembly starts with the recognition of the 5'SS by U1 snRNP (see Figure 1.3) and the ATP-independent binding of U1 snRNA to the 5'SS in the early phase of spliceosome assembly leading to the early E complex (yeast Commitment complex; CC). After formation of the early complex, the BPS is recognized by the U2 snRNP, forming the spliceosomal A complex or pre-spliceosome in an ATP dependent manner (Das, Zhou et al. 2000).

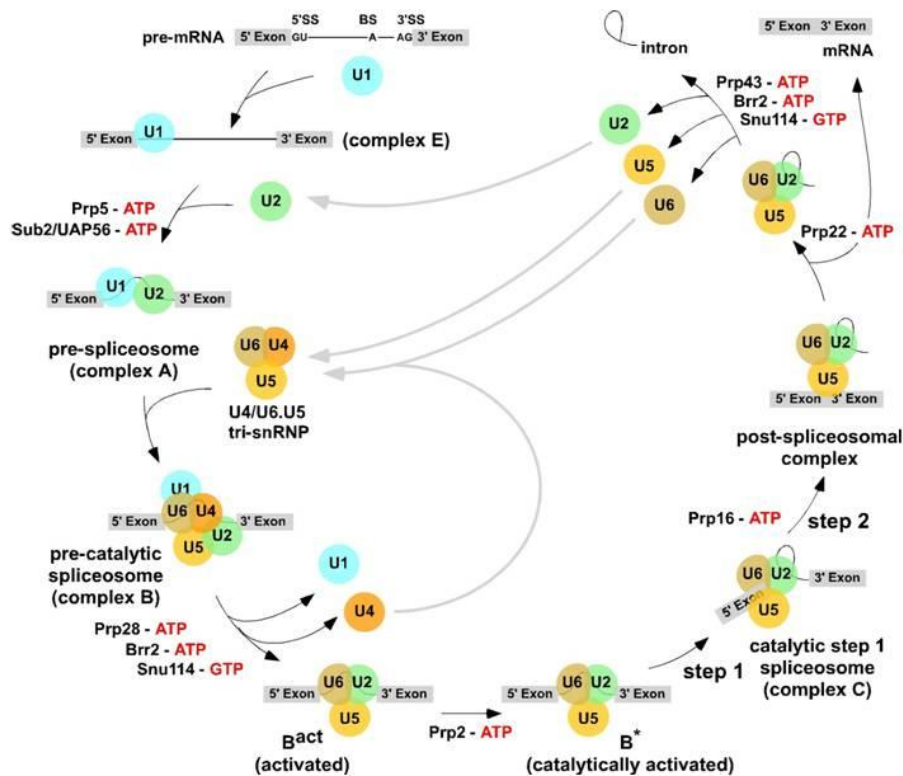


Figure 1.5: The assembly cycle of the spliceosome. The stepwise assembly of the spliceosome is initiated by the binding of U1 to the 5'SS in an ATP-independent manner, forming the early spliceosome or commitment complex. This early step is followed by the stable interaction of the U2 snRNP with the branch site generating the A-complex. After recruitment of the pre-formed tri-snRNP U4/U6.U5 to the A-complex, complex B is formed. The U1 and U4 snRNPs are released from the spliceosome and dramatic rearrangements of the RNA network lead to the activated B^{act} complex. After catalytic activation, step 1 occurs, forming the C complex. After step 2, the spliceosome disassembles and the mature RNA is released (Figure was kindly provided by Dr. Patrizia Fabrizio)

In this step the conserved sequence of U2 snRNA $G\psi\text{AGUA}$ (ψ is pseudouridine) allows the branch point adenosine to bulge out of the helix, which is essential for the first step of splicing (Query, Moore et al. 1994). The pre-catalytic spliceosomal B-complex is formed upon recruitment of the pre-assembled tri-snRNP U4/U6.U5 to the spliceosomal A-complex. Even if the spliceosome contains now a full set of U snRNPs, it is still catalytically inactive. For the activation of the spliceosome a major rearrangement of the RNA network is required, including the release of the U1 snRNP and the U4 snRNP from the spliceosome. This step leads to the formation of

the activated B complex, termed B^{act} . At this stage, U1 is replaced by U6 at the 5'SS and U6 snRNA contacts also the U2 snRNA forming the catalytic centre, which is not catalytically active yet. The B^{act} complex is then catalytically activated to generate the B^* complex, which catalyzes the first step of splicing and thus generates the spliceosomal C complex. Prior to catalysis of the second step of splicing, the network undergoes another rearrangement (Konarska, Vilardeell et al. 2006). In the second step, the lariat-3'exon intermediate is cleaved at the 3'SS and the 5'- and 3'-exon are ligated. The mature RNA is released from the spliceosome and the spliceosome dissociates, the intron is degraded and the U snRNPs are recycled for another round of splicing.

1.6 DExD/H box proteins as the driving force for spliceosome remodeling

The dynamic interactions of the RNA network during spliceosome assembly described above require driving forces at distinct stages. Therefore, members of the protein family of DExD/H-box RNA dependent ATPases play an important role in the splicing mechanism. This group of enzymes plays a major role at the stage of disrupting RNA-RNA, RNA-protein and protein-protein interactions during rearrangement (Wahl, Will et al. 2009); (Staley and Guthrie 1998); (Valadkhan and Jaladat 2011), 2010); (Cordin, Hahn et al. 2012). At least eight of these proteins are conserved between human and yeast and function at various steps during the spliceosomal cycle (see table 1.1)

DExD/H-box ATPase	Human homologue	Stage in splicing cycle
Sub2	UAP56	Pre-spliceosome
Prp5	hPrp5	Pre-spliceosome
Prp28	U5-100 kD	Early activation
Brr2	U5-200 kD	Early activation
Prp2	hPrp2	Late step-1 activation
Prp16	hPrp16	Step-2 activation
Prp22	hPrp22	mRNA release
Prp43	hPrp43	Disassembly

Tabelle 1.1: Comparison of yeast and human ATPases and their involvement in the splicing cycle. The function of each ATPase is described in the main text below (scheme was adapted from Brow, 2002)

At the early stage of spliceosome assembly, both helicases Sub2 and Prp5 promote the displacement of the spliceosomal factor SF1/BBP from the branchpoint region in an ATP-dependent manner to prepare the binding of U2 snRNA to the branchpoint (Kosowski, Keys et al. 2009); (Valadkhan and Jaladat 2011) 2010; (Wahl, Will et al. 2009). Prp5 is thought to play also a role in the remodeling of the U2 snRNA that is required for stable binding of U2 snRNP to the pre-mRNA branch site (Abu Dayyeh, Quan et al. 2002); (Staley and Guthrie 1998); (Wiest, O'Day et al. 1996); (Xu and Query 2007). The early binding of the U1 snRNA with the 5'SS has to be disrupted to free this position for binding of U6 snRNA with the 5'SS. This step is promoted by the protein Prp28 which is involved in the release of U1. Simultaneously, the U4/U6 snRNA duplex has to be unwound to release U4 from the spliceosome and to ensure the proper base-pairing of U6 snRNA with U2 snRNA. Responsible for this step is the helicase Brr2. Since Brr2 remains bound to the spliceosome during assembly, and seems to be required at a later step in the splicing cycle, has to be controlled very strictly (Small, Leggett et al. 2006). One of the major actors during catalysis is the helicase Prp2 and its co-activator Spp2. Prp2 acts immediately before the first step of splicing. ATP hydrolysis by Prp2 is the main driving force for catalytic activation of the spliceosome (transition from B^{act} complex to B* complex), because its action leads to dramatic changes in the spliceosomal network (Kim and Lin 1996); (Fabrizio, Dannenberg et al. 2009); (Warkocki, Odenwalder et al. 2009) (Ohrt, Prior et al. 2012). It is interesting to note that the action of Prp2 leads to the destabilization of the U2

proteins (SF3a and SF3b proteins), most probably in order to expose the branch point for catalysis (Lardelli, Thompson et al.); (Warkocki, Odenwalder et al. 2009). At the stage of the C complex, another helicase, Prp16 is needed. After the action of Prp16, the C complex catalyses the second step of splicing. The DExD/H-box helicase Prp22 acts subsequent to exon ligation and promotes the release of the mature mRNA from the spliceosome (Company, Arenas et al. 1991); (Schwer and Gross 1998). Finally, the spliceosome disassembles, the intron-lariat complex has to be degraded and the splicing components have to be recycled for another round of splicing. This process is triggered by the helicase Prp43 (Arenas and Abelson 1997). Hereby, the splicing factor Ntr2 is needed to recruit Prp43 to the spliceosome and Ntr1 is needed to activate the helicase activity of Prp43 (Tsai, Fu et al. 2005; Tsai, Tseng et al. 2007); (Boon, Auchynnikava et al. 2006); (Tanaka, Aronova et al. 2007); (Valadkhan and Jaladat 2011).

1.7 Spliceosome associated non-snRNP factors – proteins of the NTC

In the work of Tarn et al. in 1993, *in vitro* studies in yeast revealed the existence of a pre-assembled complex associated with the Prp19 protein, the NTC (nineteen complex). It was postulated that the NTC most likely plays a major role during the transition from the pre-catalytic B complex to the activated B^{act} complex (Tarn, Lee et al. 1993). It was also shown that the NTC enters the spliceosome subsequently after the dissociation of U1 and U4 and stabilizes the U5 and the U6 interaction with pre-mRNA. The yeast NTC consists of eight proteins, Prp19, Ntc20, Ntc25, Isy1, Syf1, Syf2, Clf1 and Cef1. In human there are also eight proteins within the NTC which is named Prp19/CDC5 complex, among others the protein CDC25 which is the human orthologue to yeast Cef1 is found. The Prp19/CDC25 complex plays also an important role in human spliceosomes (Makarova, Makarov et al. 2004).

1.8 Structural rearrangements of the Spliceosomal RNA-RNA network

During the assembly of the spliceosome major rearrangements have to occur. The catalytical activation is hallmarked by a dramatic rearrangement at the RNA-RNA

and the RNA-protein interactions (Staley and Guthrie 1998); (Brow 2002); (Wahl, Will et al. 2009); see Fig. 1.6).

At the early steps of spliceosome assembly, U1 snRNA contacts the 5'SS and base-pairs with its complement sequence in the pre-mRNA in an ATP-independent manner. In the next step, the U2 snRNA base-pairs with the BPS in an ATP-dependent manner to form the spliceosomal A complex. At the stage of the pre-catalytic B complex the pre-formed U4/U6.U5 tri-snRNP is recruited to the spliceosome. At this point the spliceosome consists of a full set of snRNPs but it is still in its pre-catalytic form, as long as the catalytically important regions of the U6 snRNA are still base-paired with the U4 snRNA. During activation, base-pairing between U4/U6 snRNA is disrupted and the U1 snRNP is replaced at the 5'SS by the U6 snRNP. U6 snRNA binds with its conserved ACAGAGA-box motif at the 5'SS of the pre-mRNA. This step is important to determine the 5'SS and to initiate the first step of catalysis (Fabrizio and Abelson 1990); (Lesser and Guthrie 1993). During this step, the U1 and U4 snRNPs are released from the spliceosome. U6 snRNA base-pairs with U2 snRNA in form of short helices (U6/U2 helices Ia, Ib and II). Another important role of U6 snRNA is the capacity to bind metal ions during catalysis by forming an intramolecular stem loops (U6-ISL) (Yean, Wuenschell et al. 2000); (Sontheimer 2001). After the recruitment of the tri-snRNP, U5 snRNA binds with its loop I to nucleotides of the exon upstream of the 5'SS. After the first step of splicing, U5 snRNA contacts also nucleotides of the exon downstream of the 3'SS. This mechanism is thought to juxtapose both exons of the pre-mRNA for the catalysis of the second step of the splicing reaction (Newman 1997).

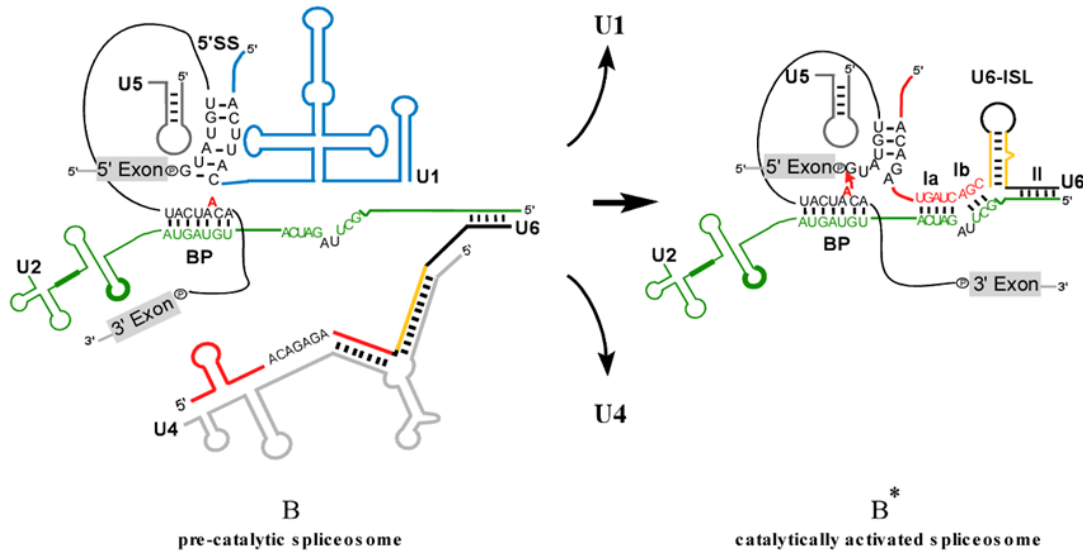


Figure 1.6: Structural dynamics during catalytic activation. On the left hand site the pre-catalytic form of the spliceosome, the pre-catalytic B complex is shown. After dramatic rearrangements of the RNA-RNA network and the subsequent release of the U1 and the U4 snRNPs, the catalytically activated spliceosome, the B* complex is generated. Both exons are grey-boxed, the different snRNAs are shown in different colors. The branch point adenosine is highlighted in red (kindly provided by Dr. Patrizia Fabrizio)

1.9 Approaches for the isolation of native spliceosomal complexes

As mentioned above, spliceosomes are very dynamic molecular machines, thus, during their formation/catalytic activity, they go through many intermediate assembly/functional stages (i.e., E, A, B, B^{act}, B* and C complex) (Fig.1.5).

Two general methods have been employed to isolate native spliceosomal complexes. The first is to target a protein component of the spliceosome. To isolate a specific spliceosomal complex, ideally such a component should transiently interact with the spliceosome at a specific stage of its assembly/function. Anti-peptide antibodies raised against such a protein would allow immunoprecipitation and subsequent peptide-induced elution of only those spliceosomal complexes that contain the targeted protein. Using anti-peptide antibodies directed against spliceosomal proteins that are transiently, but stably associated with the spliceosome, activated spliceosomes from HeLa nuclear

extract have been previously isolated (Makarov, Makarova et al. 2002), as well as spliceosomal complex B lacking the U1 snRNP (Makarova, Makarov et al. 2002).

A second approach for the isolation of spliceosomal complexes is targeting the pre-mRNA by adding an aptamer sequence to its 5' or 3' end (e.g. the hairpin structures bound by tobramycin or the MS2 protein). Either prior to or after allowing spliceosomal complexes to form under splicing conditions in HeLa nuclear extract or in yeast *S. cerevisiae* whole cell extract (this work), the aptamer is bound by its ligand (e.g. tobramycin or MS2 protein fused to the maltose binding protein), which binds or is covalently attached to a solid support. After washing, complexes can then be eluted under native conditions by the addition of an excess of the aptamer or ligand. This approach has been successfully used to isolate a mixture of spliceosomal complexes (Zhou, Licklider et al. 2002), as well as spliceosomes at a more defined stage of assembly and function such as the A, B, B^{act}, B* or C complexes from human, *Drosophila* and yeast cells (this work, Fig. 1.7) under mild, physiological conditions (Jurica, Licklider et al. 2002); (Hartmuth, Urlaub et al. 2002); (Deckert, Hartmuth et al. 2006); (Bessonov, Anokhina et al. 2008); (Behzadnia, Golas et al. 2007); (Herold, Will et al. 2009); (Warkocki, Odenwalder et al. 2009), (Bessonov, Anokhina et al. 2010). A general problem of *in vitro* splicing is that spliceosome assembly is not synchronized; at a given incubation time point a heterogeneous population of spliceosomal complexes are assembled on the pre-mRNA. Thus, if a specific spliceosomal complex is to be isolated, additional measures must be undertaken to isolate a more homogeneous population. One approach is to stall spliceosome assembly at a given point. For example, an accumulation of human spliceosomal complex C can be achieved by removing the 3' splice site and the 3' exon of the pre-mRNA (Bessonov, Anokhina et al. 2008). Affinity-purified C complexes formed on such a pre-mRNA substrate can even be chased through the catalytic steps of splicing and catalyze exon ligation in the absence of added factors. This provides a means to verify the functional integrity of the purified complexes (Bessonov, Anokhina et al. 2008).

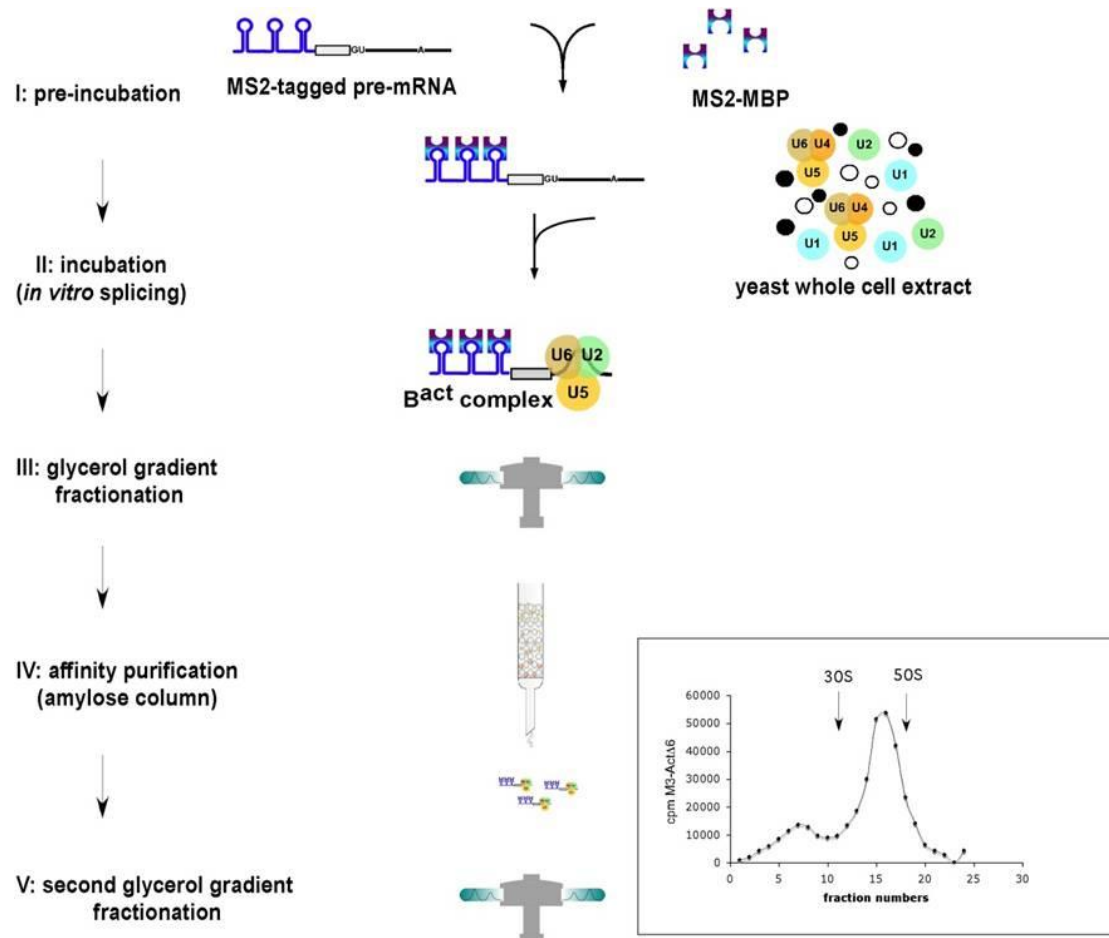


Figure 1.7: Schematic of the purification protocol for the isolation of yeast spliceosomes. Purification of the B^{act} spliceosome is depicted. *In vitro* splicing is carried out using yeast whole cell extract. The reactions are first separated via glycerol gradient centrifugation and subsequently purified on an amylose matrix. A second glycerol gradient centrifugation is carried out if very high purity is required. (This figure was kindly provided by Dr. Patrizia Fabrizio, department of cellular biochemistry, MPI-BPC).

Alternatively, splicing can be carried out for only very short periods of time, so that predominantly only early spliceosomal complexes such as E, A and B will have time to form (Hartmuth, Urlaub et al. 2002; Deckert, Hartmuth et al. 2006). Especially in yeast there is one distinctive feature, which provides another tool for stalling the spliceosomal assembly cycle at defined stages: the existence of temperature-sensitive strains for various spliceosomal factors, in particular for most of the essential DExD/H-box helicases. For example, it was shown in previous studies that the inactivation of Prp5, an essential DEAD-box helicase, known to function in A

complex formation, leads to the accumulation of the early pre-spliceosomal Commitment complex in yeast (O'Day, Dalbadie-McFarland et al. 1996); (Dalbadie-McFarland and Abelson 1990). To isolate and to purify yeast spliceosomes stalled at the commitment complex (CC) stage prior to the formation of pre-spliceosomal A complex, we used in this work, a temperature-sensitive yeast strain which carries a mutant of Prp5 and thus, can be heat-inactivated to accumulate Commitment complexes for subsequent biochemical and structural investigations.

1.10 Yeast as a model organism

Saccharomyces cerevisiae has been considered a model for molecular biology studies like pre-mRNA splicing. The benefit is the easy handling of this organism. Over the last few decades a set of well-established selection markers and protocols has been established which make genetic manipulation of this organism easy and rapid. Therefore, a number of different strains, recombinant spliceosomal factors or different RNA constructs, especially for studying the mechanism of pre-mRNA splicing, have accumulated. Screenings for synthetic lethality and genetic interactions have greatly widened our understanding of the complex mechanisms involved in pre-mRNA splicing. Moreover, one major aspect is the existence of temperature-sensitive strains for various spliceosomal factors in yeast as described above. This has provided a perfect device to block the spliceosomal cycle at distinct stages in yeast. Using wild-type pre-mRNAs that carry all sequences essential for pre-mRNA splicing, the purification of spliceosomal complexes that are functional intermediates can be performed. This feature and the accumulated knowledge of the last decades allow the stepwise reconstitution of the splicing machinery and its assembly *in vitro* in *S. cerevisiae* and will be described in more details in this work.

1.11 Investigation and characterization of yeast spliceosomal complexes via mass spectrometry and electron microscopy

In former biochemical and genetic studies, numerous proteins were found and characterized as spliceosomal factors, but their exact function is still partially

unknown. To understand better their contribution and function in pre-mRNA splicing several special methods are required to investigate and characterize them.

1.11.1 Mass spectrometry

Mass spectrometry (MS) is one of the major analytical technologies for the identification of unknown protein factors and to determine the proteomic composition of highly complex samples like spliceosomal complexes. Large and complex biomolecules can be analyzed after ionization by either matrix-assisted laser desorption ionization (MALDI MS), electrospray ionization (ESI MS) or tandem MS (LC-MS/MS). The electrospray leads to formation of micrometer-sized droplets that accelerate in electric field with simultaneous evaporation of the solvent, so that only peptide ions enter the mass spectrometer (reviewed by (Fenn, Mann et al. 1989). In the mass spectrometer, the ions are separated according to their mass to charge ratio (m/z) and detected. For sequence information, one of the ions (peptides) is isolated and fragmented, typically by collision-induced dissociation and the fragments are detected. Finally, the set of masses obtained from MS analysis is used to search against a protein database to identify the peptides, and thus the proteins, contained in the sample. On the basis of peptide assignment quality, number of assigned total and unique peptides, and sequence coverage, a protein can be identified as a component of the spliceosome. MS gives fast and authentic identification of protein factors and it is an essential tool for studying protein dynamics (reviewed in (Mann, Hendrickson et al. 2001).

MS analyses of the spliceosomes purified in our laboratory have been performed in collaboration with the MS facility and research group of Prof. Henning Urlaub at the MPI-bpc.

1.11.2 Electron microscopy

To gain insights into the structure and function of highly dynamic and complex structures like the splicing machinery, electron microscopy (EM) is another indispensable tool to obtain insights into the three-dimensional structure of the yeast splicing machinery. In addition, to learn more about the three-dimensional structure of macromolecular complexes in living cells can be considered an approach towards understanding better their function and mechanism. One of the major techniques to study EM structures is the *single-particle-cryo-electron microscopy*, which revealed

promising results for the analysis of multiprotein complexes with a high resolution ($< 10\text{\AA}$) (Golas, Sander et al. 2003). This technique is ideally suited to investigate the structure of spliceosomal complexes in the yeast *S.cerevisiae*. Previous work from our laboratory, Deckert et al. and Bessonov et al. have shown that when single-particle cryo electron microscopy was used, higher order structures at a resolution of 30 - 40 \AA were obtained for the human spliceosomal B Δ U1 and C complexes (Deckert, Hartmuth et al. 2006), (Bessonov, Anokhina et al. 2008).

The structural analysis of spliceosomal complexes isolated from yeast, done in this work, was performed according to the protocol of Kastner et al. with the *Grafix*-method. Therefore, spliceosomal complexes were affinity purified under native conditions according to the protocol described in this work and in Fabrizio et al. and Dannenberg et al., and were then sedimented on a second glycerol gradient containing 0.1 % Gluteraldehyd. Gluteraldehyd is a light chemical cross-linker which fixes the complexes under analysis during gradient centrifugation. The fixation step in this preparation allows longer absorption time of the particle on the grid for later analysis by the electron microscope (Kastner, Fischer et al. 2008) and Methods). For what concerns the 2D EM structure of spliceosomal complexes from the yeast *S.cerevisiae* nothing was known at the start of my work and it is one of the aims of this thesis.

EM analyses of the spliceosomes purified in our laboratory have been performed in collaboration with the EM facility and research group of Prof. Holger Stark at the MPI-bpc.

1.12 Dual Color Fluorescence Cross-Correlation Spectroscopy – an excellent technique to study protein dynamics within the spliceosome

Standard MS methods are only semi-quantative and can only give good indications about the relative abundance of a certain protein associated with various spliceosomal complexes. A feature of the spliceosome, however, is the ordered recruitment and subsequent release of spliceosomal factors. The spliceosome must therefore create binding sites for recruited partners at the correct phase of assembly cycle or existent binding sites are modulated to switch from low affinity to high affinity and vice versa. Therefore the elucidation of recruited partners, the definition of the exact time points

of recruitment/release events and the assignment of dissociation constants for spliceosomal factors at different stages of the spliceosomal cycle is crucial in understanding molecular mechanism of the splicing process in depth.

A method that appears to meet the requirements for obtaining this much-needed information is dual-color fluorescence cross-correlation spectroscopy (dcFCCS). This is a sensitive and versatile optical technique that allows the direct analysis of the dynamics of the association and dissociation events among proteins and/or RNAs in complex systems in solution, at low nanomolar concentrations and in equilibrium without requiring a biochemical/physical perturbation of the sample (see Materials and Methods/Results). In brief, dcFCCS is based on the confocal microscope and requires particles labelled with two spectrally separated colours (e.g. green and red). The fluorescence of the labelled molecules is spectrally separated and detected in two channels. The signals are analysed by computing the auto-correlation of each channel and their cross-correlation. If molecules bearing different labels are not part of the same complex, then they will diffuse independently through the confocal volume. In that case, there will be no cross-correlation between both signals. However, if the molecules are part of the same complex, they will form doubly labeled entities. Co-diffusion of the two labels will generate correlated signals in both detection channels and therefore a cross-correlation. The amplitude of the cross-correlation is proportional to the number of doubly labelled molecules and can therefore be used to monitor binding and release reactions (Fig.1.8) (Ricka and Binkert 1989; Schwille, Meyer-Almes et al. 1997; Földes-Papp 2005; Mütze, Ohrt et al. 2011). For a detailed mathematical description of the auto-correlation function refer to Schwille and Haustein, 2002 and to Sauer, Hofkens and Enderlein, 2011, as this is beyond the scope of this introduction. The computation and evaluation of the dcFCCS data in this work was done in collaboration with Prof. Jörg Enderlein and Mira Prior (III.Institute of Physics, University of Göttingen) (Kettling, Koltermann et al. 1998); (Foldes-Papp and Rigler 2001); (Ohrt, Staroske et al.).

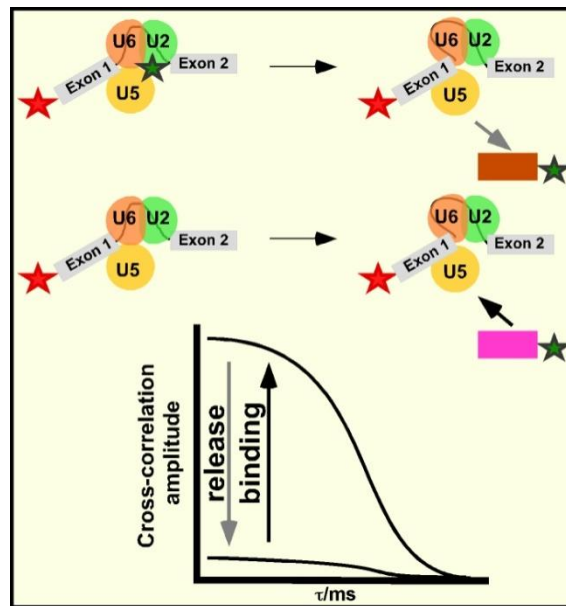


Figure 1.8: The cross-correlation amplitude is proportional to the amount of doubly labeled species

Binding and release of a fluorescently labeled protein (brown or pink rectangles with a “green fluorophor”) to a larger assembly of molecules (i.e.the spliceosome with a “red fluorophor”) are shown schematically. The effects of the two events on the cross- correlation curves are indicated in the middle (adapted from (Ohrt, Prior et al. 2012)).

1.13 Aim of this study

The spliceosome is a protein-rich molecular machine that catalyzes the removal of a pre-mRNA intron. Proteomic studies of purified spliceosomes, assembled *in vitro* at defined stages of function, have primarily been carried out with splicing extracts from human HeLa cells. Human spliceosomes contain more than 50 proteins associated with snRNPs and more than 100 non-snRNP proteins as revealed by mass-spectrometric studies. Such studies showed that the spliceosome's protein complement varies substantially from one stage of the splicing cycle to another (Deckert, Hartmuth et al. 2006; Bessonov, Anokhina et al. 2008). One aim of this work was to expand these studies to the yeast *Saccharomyces cerevisiae*, since there is no alternative splicing in yeast cells and thus regulatory splicing factors such as SR and hnRNP proteins are absent. Nonetheless, the pathway of spliceosome assembly and the main

features of its catalytic chemistry appear to be conserved between metazoans and yeast. The study of the extent of conservation is not only relevant for tracing evolutionary relationships, but it can also lead to conclusions about the mechanisms of conformational changes, such as those resulting in spliceosome activation or catalysis. Therefore, a comprehensive proteomic analysis of the yeast spliceosomes should reveal the minimum set of proteins required for driving the spliceosomal dynamics and for catalyzing the removal of a pre-mRNA intron.

Towards this goal we set up a strategy to purify and isolate spliceosomal complexes from yeast under native conditions for the first time, to learn more about the dynamics of protein recruitment and release during catalytic activation and step 1 of splicing. To isolate biochemically homogenous B, B^{act} and C complexes, we used an actin pre-mRNA and modifications thereof. For MS2 affinity-purification, three MS2 binding sites were fused to the 5' end of the various pre-mRNA constructs. Previous studies showed that truncation/modification of the actin pre-mRNA and adjustment of the ATP concentration in the splicing reaction can lead to stalling of the spliceosomal cycle (Rymond and Rosbash 1985; Cheng 1994). The intron in the actin pre-mRNA contains the yeast consensus branch point (BPS) sequence UACUAAC. The pre-mRNA Act Δ 6 and Act Δ 31 were truncated 6 and 31 bases, respectively, after this sequence, and thus, lack the 3' SS and the 3' exon. These truncated precursors led to stalling at the stage of complex B^{act} and C, respectively, when 2 mM ATP was used. The inclusion of only 0.05 mM ATP in the splicing reaction led to stalling at the stage of complex B. The various spliceosomal complexes were isolated by a three-step purification procedure developed in yeast during my PhD work and involves glycerol gradient centrifugations and affinity-selection of the MS2 tagged spliceosomal complexes with amylose beads. The protein composition of the B, B^{act} and C complexes have been determined by mass spectrometry (MS), and the proteins that dissociate or are recruited during the transition from one complex to the next have been characterized for the first time. MS revealed a dramatic exchange of proteins during spliceosome assembly and activation. Specifically, we learned that in yeast, activation (B to B^{act} transition) is accompanied by the stable recruitment of ~20 proteins, whereas ~35 proteins, including all U1 and U4/U6-associated proteins, are lost. Nine additional proteins are recruited during the transition from the B^{act} to the C

complex. At the same time the DEAH-box helicase Prp2 and its co-activator Spp2, as well as the U2 SF3a and SF3b complexes, are also destabilised. However, it was not yet clear whether the U2 SF3a/SF3b proteins are subsequently lost from the spliceosome.

A fundamental outcome of this work is that it provides an inventory of the evolutionarily conserved splicing factors that are stably associated with three “snapshots” of spliceosome assembly, activation and catalysis and offer insights into the window of function of the proteins exchanged during the transition from one stage to the next. Another important outcome of this work is that it revealed that in yeast and human, the same homologous proteins dissociate and are recruited during the transition from the B to the B^{act}, and from the B^{act} to the C complex, indicating that these compositional changes are an evolutionarily conserved design principle of the spliceosome.

The isolation of intact yeast spliceosomal complexes has already provided an important background not only for further biochemical, biophysical and functional studies (see below), but also for initial structural studies. Because of its dynamic and complex nature, obtaining structural information about the spliceosome represented a major challenge so far. Nevertheless in this work, electron microscopy (EM) of the three isolated “snapshots” of the yeast spliceosome revealed a quite homogenous general morphology of the B, B^{act} and C complexes and also their significant differences in shape and structural details, consistent with their substantial compositional differences. Thus, these studies have paved the way to obtain a topographic map of the spliceosome, and will also provide novel insights into the structural remodeling events occurring during the spliceosome cycle.

Significantly, the moderate number of phylogenetically conserved proteins recruited to the yeast complexes B^{act} and C has made possible targeted investigations of the mechanism of activation and catalysis in a fully-defined biochemical reconstitution system in our laboratory (Warkocki, Odenwalder et al. 2009). In the latter studies was shown that the DEAH-box helicase Prp2 remodels substantially B^{act} into the catalytically activated B* complex prior to the formation of the C complex. During this Prp2-mediated remodeling, the binding of several proteins to the spliceosome is

weakened. Interestingly, these included the proteins of the U2 SF3a/SF3b subunits and further suggested that the ATPase Prp2 may facilitate the spliceosome's catalytic activation by inducing destabilisation of U2 SF3a/SF3b proteins. This rearrangement is important since it is believed to expose the BPS adenosine as a crucial preliminary to step 1. In addition, we observed that there were potentially several other proteins whose binding affinity to the spliceosome might have been changed by Prp2 action as revealed by the comparative MS analyses of purified spliceosomes described above. These included the RES (REtention and Splicing) complex proteins, the NTC-related proteins Cwc24 and Cwc27, and the essential catalytic step 1 factors Yju2 and Cwc25.

Thus, a second aim of this work was to study these events in a quantitative manner, toward this goal we established a dual color Fluorescence Cross Correlation Spectroscopy setup (in collaboration with Dr. Thomas Ohrt, Mira Prior and Prof. Jörg Enderlein). In this work, the technique of dcFCCS was applied for the first time to investigate the compositional dynamics of yeast spliceosomes in more details. Specifically, we have studied the modulation of the binding strength of various proteins to the yeast spliceosome during catalytic activation by Prp2 to finally shed some light on the nature of the release/loss of splicing factors during this crucial remodeling step. For this purpose, spliceosomes were stalled before step 1 by using the temperature-sensitive yeast mutant *prp2-1* and affinity-purified to near homogeneity, yielding a $B^{\text{act}\Delta\text{Prp2}}$ spliceosome. Highly purified $B^{\text{act}\Delta\text{Prp2}}$ can be catalytically activated to form B^* when supplemented with recombinant Prp2 and Spp2 splicing factors (Warkocki, Odenwalder et al. 2009). We have used purified $B^{\text{act}\Delta\text{Prp2}}$ complexes assembled on actin pre-mRNA labeled at its 5' end with the red fluorescent dye Atto647N. We labeled proteins by fusing the protein of interest with a fluorescent protein EGFP (enhanced green fluorescent protein) by genetic modification; the fluorescently labeled protein is uniquely produced in the modified yeast strain and is, therefore, quantitatively and selectively labeled in purified spliceosomes assembled in splicing extracts derived from such strains. The purified doubly-labeled spliceosomes were then analyzed before and after catalytic activation by Prp2 and the weakening or strengthening of the binding of the EGFP-labeled protein to the spliceosome was measured by dcFCCS.

Using dcFCCS we show that the binding affinity of quite a number of proteins is significantly changed during the Prp2-mediated catalytic activation of the spliceosome. Finally, we convincingly demonstrate that the U2 SF3a/SF3b proteins Prp11 and Cus1 remain bound to the B* spliceosome under near-physiological conditions, and that their binding is reduced only when high salt is included. Furthermore, high affinity binding sites are created for Yju2 and Cwc25 during catalytic activation, consistent with their requirement for step 1 catalysis. This work suggests that Prp2-mediated structural remodeling of the spliceosome leads to multiple rearrangements and show that dcFCCS is a powerful tool, ideally suited to investigate quantitatively the compositional dynamics of the spliceosome during its catalytic activation. In addition, this is the first example where purified, catalytically active spliceosomes were investigated directly in solution and in equilibrium. In conclusion, by combining biochemical, biophysical approaches and ultrastructural studies by EM, this work gives new insights and useful information about protein dynamics and structural changes occurring during spliceosome activation and catalysis.

2. Materials and Methods

2.1 Materials

2.1.1 Chemicals and media

2-Mercaptoethanol	Roth, Germany
Acetic acid	Merck, Germany
Acetone	Merck, Germany
Agarose, electrophoresis grade	Invitrogen, Netherlands
Ammoniumperoxodisulfate (APS)	Merck, Germany
Ampicillin	Sigma-Aldrich, Germany
Bacto agar	BD, USA
Bacto yeast extract	BD, USA
Bacto peptone	BD, USA
Bradford-assay solution	Bio-Rad, Germany
Brilliant Blue G-Colloidal concentrate	Sigma-Aldrich, Germany
Bromphenol blue	Merck, Germany
D(+)-glucose monohydrate	Merck, Germany
Dipotassiumhydrogenphosphate	Merck, Germany
DNA-molecular weight marker	Gibco, New Zealand
DTT (Dithiothreitol)	Roth, Germany
EDTA (Disodium salt dihydrate)	Roth, Germany
Formaldehyde	Merck, Germany
Formamide	Merck, Germany

Glycerol	Merck, Germany
Glycoblu	Ambion, USA
HEPES (N-2-Hydroxyethylpiperazin-N-2-ethansulfonic acid)	Calbiochem, USA
Imidazole	Merck, Germany
Lithium acetate	Sigma-Aldrich, Germany
Maltose	Merck, Germany
Methanol	Merck, Germany
Polyethylene glycol (PEG)	Sigma-Aldrich, Germany
Ponceau S	Serva, Germany
Potassium Chloride	Merck, Germany
Potassiumdihydrogenphosphate	Merck, Germany
Pre-stained protein-molecular weight marker	Bio-Rad, Germany
Roti-Phenol-Chloroform-Isoamyl alcohol (PCI)	Roth, Germany
Rotiphorese Gel 30 solution	Roth, Germany
Rotiphorese Gel 40 solution	Roth, Germany
Rotiphorese Gel A and B solution	Roth, Germany
Silver nitrate	Merck, Germany
Sodiumdodecylsulfate (SDS)	Serva, Germany
Sodiumacetate	Merck, Germany
TEMED (N, N, N', N'-Tetramethylethylendiamine)	Sigma-Aldrich, Germany
Tris-(hydroxymethyl)aminomethane (Tris)	Roth, Germany
Triton X-100	Merck, Germany
tRNA <i>E. coli</i>	Boehringer, Germany
Nonidet P-40 (Igepal CA-630)	Sigma-Aldrich, Germany
Urea	Merck, Germany
Xylene cyanol FF	Fluka, Switzerland

2.1.2 Enzymes and enzyme inhibitors

Aprotinin	Serva, Germany
Benzamidine	Serva, Germany
Chymostatin	Serva, Germany
Complete™ protease inhibitor tablets EDTA-free	Roche, Germany
Leupeptin	Serva, Germany
Pepstatin A	Serva, Germany
Phenylmethylsulfonylfluoride (PMSF)	Merck, Germany
Phusion® High-Fidelity DNA Polymerase	New England Biolabs, Germany
Proteinase K	Sigma-Aldrich, Germany
Recombinant RNasin® Ribonuclease Inhibitor	Promega, USA
Restriction Enzymes	New England Biolabs, Germany
RNasin (RNase inhibitor; 40 U/μl)	Promega, USA
RQ DNase I (1 U/μl)	Promega, USA
SP6 RNA polymerase	New England Biolabs, Germany
T7 RNA polymerase	dept. Lührmann
Taq DNA polymerase	Promega, USA

2.1.3 Nucleotides

Nucleoside-5'-triphosphate (ATP, CTP, GTP, UTP 100 mM each):

Pharmacia, Germany

Deoxynucleoside-5'-triphosphate Mix (dATP, dCTP, dGTP, dTTP 10 mM each):

New England Biolabs, Germany

Radionucleotides: [α -³²P]-UTP, [α -³²P]-dATP, [α -³²P]-ATP:

Perkin-Elmer, Germany

2.1.4 DNA oligonucleotides and plasmids

2.1.4.1 DNA oligonucleotides

Name	sequence (5' to 3')	description
Sp6_for	ATTTAGGTGACACTATAG	used for the generation of template DNA for <i>in vitro</i> transcription
Act_rev	GGAATTCCCCTTCATCACCAA	used for the generation of template DNA for <i>in vitro</i> transcription
Act+13+24	GATGGTGCAAGC	used for RNase H directed cleavage of M3Act pre-mRNA during C-complex purification

2.1.4.2 Plasmids

<u>Name</u>	<u>description</u>
pUC18_T7_M3Act_wt	template for <i>in vitro</i> transcription, generated by Dr. Thomas Ohrt
pUC18_T7_M3Act_Δ6	template for <i>in vitro</i> transcription, generated by Dr. Thomas Ohrt
pMal_MS2-MBP	expression of MS2-MBP fusion protein, provided by Robin Reed and Josep Vilardell
pKT209	used for the amplification of the yEGFP cassette by PCR; Euroscarf, Frankfurt am Main

2.1.5 Yeast and bacterial strains

2.1.5.1 Yeast strains

BJ2168	<i>MATa, leu2, trp1, ura3, prb1-1122, pep4-3, prc1-407, gal2</i> This strain carries deletions in protease genes.
<i>prp2-1</i> (3.2 AID)	<i>MATalpha, prp2-1, ade2, his3, lys2-801, ura3</i> kindly provided by R-JLin. This strain carries a G360D mutation in Prp2, rendering it heat labile.
<i>prp5-1</i>	<i>MATa prp5-1, ade2-101, his3-1200 tyr1 ura3-52</i> (single base change in the <i>PRP5</i> gene which lead to the substitution of glycine 293 with aspartate (G293D) in the protein. This substitution is 12 residues upstream of the glycine-lysine-threonine (GKT) triplet in the highly conserved, nucleotide-binding motif 1 within the putative helicase domain)
YTO13	Snu114-yEGFP <i>MATalpha, prp2-1, ade2, his3, lys2-801, ura3; SNU114::yEGFP-CaURA3 C-terminus</i>
YTO15	Cus1-yEGFP <i>MATalpha, prp2-1, ade2, his3, lys2-801, ura3; CUS1::yEGFP-CaURA3 C-terminus</i>
YTO17	Prp11-yEGFP <i>MATalpha, prp2-1, ade2, his3, lys2-801, ura3; PRP11::yEGFP-CaURA3 C-terminus</i>
YTO18	Cwc24-yEGFP <i>MATalpha, prp2-1, ade2, his3, lys2-801, ura3; CWC24::yEGFP-CaURA3 C-terminus</i>
YTO20	Cwc27-yEGFP <i>MATalpha, prp2-1, ade2, his3, lys2-801, ura3; CWC27::yEGFP-CaURA3 C-terminus</i>
YTO21	Yju2-yEGFP <i>MATalpha, prp2-1, ade2, his3, lys2-801, ura3; YJU2::yEGFP-CaURA3 C-terminus</i>

YTO25 **Bud13-yEGFP** *MAT* α , *prp2-1*, *ade2*, *his3*, *lys2-801*, *ura3*;
BUD13::yEGFP-Ca*URA3* C-terminus

2.1.5.2 Bacterial strains

BL21-CodonPlus(DE3)-RIL cells, F- *ompThsdSB* (*rB-* *mB-*) *gal dcm lacY1*,
 pRARE22 (CMR) pAR5615 (APR) Novagen, USA

2.1.6 Commercial kits

ECL western blot detection kit	GE Healthcare, UK
Prime It II random primer labeling kit	Stratagene, USA
Qiagen gel extraction kit	Qiagen, Germany
Qiagen plasmid preparation kit	Qiagen, Germany

2.1.7 Chromatography materials and consumables

Amylose resin	New England Biolabs, Germany
Cassettes for film exposure	Kodak, USA
Concentrator	Millipore, USA
Dialyses membranes MWCO 6000-8000 Da	SpektraPor, USA
Heparin Sepharose TM 6 Fast Flow	GE Healthcare, UK
HisTrap TM FF crude columns	GE Healthcare, UK
IgG Sepharose 6 Fast Flow	GE Healthcare, UK
Nylon membrane Hybond XL	GE Healthcare, UK
Parafilm	Roth, Germany
Poly-Prep columns	Bio-Rad, USA
ProbeQuant TM G-50 micro columns	GE Healthcare, UK
ProbeQuant TM G-25 micro columns	GE Healthcare, UK
Protein A-Sepharose CL 4B	GE Healthcare, UK

Protran Nitrocellulose membrane	Schleicher & Schüll, Germany
Slide-A-Lyzer dialysis units (MWCO 6 kDa)	Pierce, USA
Sterile filters 0.2 µm or 0.45 µm	Sarstedt, Germany
Superdex 75 16/60 column	GE Healthcare, UK
Whatman 3MM Paper	Whatman Paper, UK
X-ray films BioMax MR	Kodak, USA

2.1.8 Common buffers

Media, buffers, and solutions were prepared with deionized water (Millipore) and autoclaved if necessary (121 °C, 20 min, 1 bar). Solutions with heat-labile components were filter sterilized (0.22 µm).

5x DNA loading dye	30% glycerol 5 mM EDTA, pH 8.0 0.25% (w/v) bromophenol blue 0.25% (w/v) xylene cyanol
4x Separating gel buffer	1.5 M Tris 0.4% (w/v) SDS adjust to pH 8.8
4x Stacking gel buffer	0.5 M Tris 0.4% (w/v) SDS adjust pH to 6.8
10x TBE	0.89 M Tris 0.89 M boric acid 25 mM EDTA pH 8.0
Protein loading dye	75 mM Tris-HCl, pH 6.8 1.25 mM EDTA, pH 8.0 20% (v/v) glycerol

	2.5% (w/v) SDS
	0.125% (w/v) bromophenol blue
	50 mM DTT
RNA loading dye	80% formamide
	1 mM EDTA pH 8.0
	0.05% (w/v) bromophenol blue
	0.05% (w/v) xylene cyanol
Slab 4 Buffer	50 mM Tris
	105 mM glycine
	0.1% (w/v) SDS
SDS-PAGE Running buffer	25 mM Tris-HCl, pH 6.8
	192 mM glycine
	1% (w/v) SDS
10x TBS	200 mM Tris
	1.37 M NaCl
	adjust to pH 7.6
Western blotting buffer	1.5 L Slab4 Buffer
	0.6 L methanol
	0.9 L ddH ₂ O

2.1.9 Machines and working equipment

ÄKTA Prime	GE Healthcare, UK
ÄKTA Explorer	GE Healthcare, UK
Autoclaves	H+P Labortechnik, Germany
Biofuge fresco	Kendro, USA
Biofuge pico	Kendro, USA

DNA Thermal Cycler	Hybaid Omni Gene, UK
Gel documentation unit	Bio-Rad, USA
Gelelectrophoresis apparatus	in-house
Geldryer Model 583	Bio-Rad, USA
Gradient Master	BioComp Instruments, Canada
‘head-over-tail’	Rotor Cole-Parmer, USA
Heating blocks	Eppendorf, Germany
Hybridization oven	Hybaid Biometra, UK
Megafuge 1.0R	Kendro, USA
Milli-Q-water supply apparatus	Millipore, USA
Nanodrop	Thermofisher, Germany
pH-Meter	Mettler Toledo, Switzerland
Phosphorimager Typhoon 8600	Amersham Pharmacia, Germany
Power supply EPS 2A 2000	Hoefer Pharmacia Biotech, USA
Power supply EPS 3501/XL	Amersham Pharmacia, Germany
Liquid Scintillation Analyzer Tri-Carb 2100 T	Packard, USA
Sorvall SLC-6000 rotor	Kendro, USA
Sorvall SS-34 Rotor	Kendro, USA
Sorvall TH660 Rotor	Kendro, USA
Sorvall T865 Rotor	Kendro, USA
Sorvall T647.5 Rotor	Kendro, USA
Speed Vac Concentrator 5301	Eppendorf, Germany
Spectrophotometer Ultrospec 3000 pro	Amersham Pharmacia, Germany
Surespin 630 rotor	Thermo Fisher Scientific, USA
Tabletop centrifuges	Heraeus, Germany
Trans-Blot Cell	Bio-Rad, USA
Ultracentrifuge Evolution	Kendro, USA
UV lamps (254 nm)	Bachofer, Reutlingen
Vortex	Janke & Kunkel, Germany
X-ray film developer X-Omat 2000	Kodak, USA
Liquid scintillation analyzer	Packard, USA

2.2 Methods

2.2.1 General molecular biology methods

Unless otherwise stated all described methods for standard molecular biology are essentially performed according to Sambrook et al., 1989. When a commercial reaction set was used, the manufacturer's instructions were followed.

2.2.1.1 Concentration determination of nucleic acids

The concentration determination of RNA or DNA is based on the absorption maximum of the aromatic ring system of nucleic acids at a wavelength of 260 nm. The concentration and purity of nucleic acids was estimated using the empirical standard values shown below. The ratio between OD₂₆₀ and OD₂₈₀ allows to assess contaminations with proteins or phenol.

2.2.1.2 Purification and manipulation of DNA

Plasmid DNA was obtained from *E. coli* cells using QIAGEN Plasmid Purification Kits according to the manufacturer's instructions. QIAGEN plasmid purification protocols are based on a modified alkaline lysis procedure, followed by binding of plasmid DNA to QIAGEN Anion-Exchange Resin under appropriate low-salt and pH conditions. Restriction endonucleases were obtained from New England Biolabs (NEB) and the reactions were performed according to the manufacturer's instructions. Generally 1-10 units of enzyme were used to cut 1 µg of DNA within 1h under the recommended conditions. DNA fragments were analyzed and purified by agarose gel electrophoresis.

2.2.1.3 Agarose gel electrophoresis

DNA-fragments generated by PCR were analyzed by agarose gel electrophoresis. Gels contained 1-2% agarose (w/v) and 0.4 µg/ml ethidiumbromide in 0,5x TBE buffer. DNA samples were supplemented with DNA loading dye and separated

together with a DNA ladder as size marker at 110 Volts (constant voltage), in 0.5x TBE. Nucleic acids were visualized with UV-light at 254 nm.

2.2.1.4 Polymerase chain reaction

The polymerase chain reaction (PCR) was used to amplify DNA fragments either for analytic (e.g. “colony PCR”) or preparative purposes (e.g. transcription templates). A typical reaction mixture contained 0.4 ng/μl of template, 0.2 mM of each dNTP, 0.6 μM of each primer, the appropriate reaction buffer and the enzyme. Different kinds of polymerases (Taq-, Pfu- or Phusion-polymerase) were used depending on the purpose of the application.

A typical setup for a PCR included the following steps:

- | | | | | |
|----|------|--------|----------------------|-------------------------------------|
| 1. | 94°C | 5 min | initial denaturation | |
| 2. | 94°C | 1 min | cycle denaturation | |
| 3. | 52°C | 1 min | primer annealing | |
| 4. | 72°C | 1 min | elongation | steps 2 to 4 were repeated 35 times |
| 5. | 72°C | 10 min | final elongation | |

For purification of DNA fragments for subsequent *in vitro* transcriptions, PCR reactions were purified with the PCR-clean-up Kit provided by Macherey-Nagel. The manufacturer’s instructions were followed and DNA fragments were eluted in TE buffer. 5’- and 3’-DNA fragments for subsequent site-overlap extension PCRs were separated by agarose gel electrophoresis, visualized by ethidiumbromide and UV light. The DNA band was cut out with a razor blade and transferred to a 2 ml-reaction tube. DNA was extracted from the agarose and purified with the PCR-clean-up Kit by Macherey-Nagel according to the manufacturer’s instructions.

2.2.1.5 Transformation of yeast and *E. coli*

For transformations, chemically competent cells of *S.cerevisiae* and *E. coli* were used. 50 ml cultures of *E.coli* were grown to an OD₆₀₀ of 0.3-0.5 and the cell pellet was washed twice with an ice cold solution of 50 mM CaCl₂. After the addition of glycerol to a final concentration of 10% the cells were frozen in liquid nitrogen and

stored at -80°C . For transformation competent cells were mixed with 50 ng plasmid DNA and incubated on ice for 30 min, followed by a heat shock at 42°C for 1 min. Subsequently, the cells were incubated for 1h at 37°C in LB medium before being transferred to Petri dishes containing a selection medium.

50 ml cultures of *S. cerevisiae* were grown to an OD_{600} of 0.6-0.8. The cells were sedimented by brief centrifugation at $2500 \times g$ and washed with buffer containing 10 mM Tris, pH 7.5. Subsequently, the pellet was resuspended in a buffer containing 10 mM Tris, pH 7.5 and 100 mM lithium acetate (LiT-buffer) and incubated shaking slowly at RT for 40 min. After a brief centrifugation the cells were resuspended in 800 μl LiT-buffer and the designated DNA construct (250 ng for plasmids, 40 μg for PCR constructs) was mixed with 100 μl of cell suspension. As a carrier, salmon sperm DNA (1 mg/ml final concentration) was used and a solution of PEG 3350 (0.5 g PEG/ml LiT final concentration) was added. A heat shock(?) treatment was performed for 5 min at 42°C (except ts strains) before the cells were transferred to YPD medium and incubated at 37°C (or 25°C if the strain was temperature sensitive) for 1h. Petri dishes containing a selection medium were used to select for successful transformants. Positive clones were checked for the correct integration of the construct via colony PCR.

2.2.1.6 Phenol-chloroform-isoamylalcohol (PCI) extraction and ethanol precipitation

The PCI extraction is used to separate nucleic acids from proteins. Phenol and chloroform denature proteins and keep them in the organic phase, while nucleic acids stay in the aqueous phase. Samples were thoroughly mixed with an equal volume of PCI (phenol/ chloroform/ isoamylalcohol, pH 7.5-8.0 in the ratio 25:24:1, commercially available from Roth). Phase separation was accelerated by centrifugation at $16000 \times g$ for 5 min. The aqueous phase was transferred into a new tube and nucleic acids were precipitated by adding 3 volumes of absolute ethanol, 0.1 volume of 3M sodium acetate pH 5.3 and, in case of nucleic acid concentrations below 200 ng/ μl , 10 $\mu\text{g}/\text{ml}$ Glycoblue (Ambion) was added as a carrier. Proteins were precipitated from the organic phase by adding 5 volumes of absolute ethanol or acetone. Both, RNA and protein samples were kept at -20°C for at least 30 min. The

precipitates were sedimented by centrifugation at 16000 x g for 20 min. The pellet was washed with 70% ethanol (v/v), subsequently dried and resuspended in the desired solution.

2.2.1.7 Proteinase K digestion

Proteinase K digestion of (reconstitution) reactions were performed to obtain protein-free RNA samples. All proteinase K digestions were done at a final concentration of 0.2 % (w/v) SDS, 10 mM EDTA and 0.3 mg/ml proteinase K. Reactions were mixed thoroughly and incubated for 30 min at 37 °C. Subsequently, reactions were filled up to 200 µl with “stop- splicing” buffer and RNAs were extracted by PCI and precipitated with ethanol.

“stop-splicing” buffer

50 mM NaOAc (pH 5,3)

0,27 mM EDTA

0,1 % (w/v) SDS

2.2.1.8 In vitro transcription

In vitro transcriptions of RNA were carried out using different DNA templates derived from PCR reactions or linearized plasmid DNA (plasmid was restricted with *Acc651* and then purified via PCI and ethanol precipitation). Depending on the type of the promoter of DNA templates, either Sp6 or T7 were used as DNA-dependant RNA polymerases. The synthesis of radioactively labeled pre-mRNA was performed using [α -³²P] UTP in a small reaction whereas the transcription of “cold” pre-mRNA was carried out in a preparative scale. For subsequent labeling of pre-mRNAs with a fluorescent dye, α -GMPS was used in a 10:1 ratio over α -GTP to be used as a starter nucleotide (for details see “pre-mRNA labeling”). The transcription reactions were incubated for 2,5 h at 37 °C or 40 °C (for T7 and Sp6 polymerases, respectively). The reaction mixture was then loaded on a 5 % denaturing polyacrylamide RNA gel containing 8 M urea. In the case of radioactively labeled RNA, the transcript was detected by autoradiography whereas cold transcript was visualized by UV-

shadowing at 312 nm. The RNA bands were cut out from the gel and transferred to a 2ml reaction tube, 1,8 ml of RNA elution buffer was added to the tube and the elution of the pre-mRNA from the gel piece was carried out by shaking at 4°C over night. The next day, the supernatant without gel pieces was transferred to a chromatography column and filtered followed by ethanol precipitation as described above. The resulting pellet was resuspended in ddH₂O and stored at -20 °C. The concentration of the cold RNA was determined as described above. From the radioactively labeled pre-mRNA, 1 μl was counted in a scintillation counter and the specific activity of the transcript was calculated with the formula:

$$RNA (pmol) = \frac{total\ cpm}{2.2 \times 10^6\ cpm} \times \frac{2 + (age\ of\ 32P)}{2 \times SA_{32P} (\mu\frac{Ci}{pmol})} \times \frac{[UTP (\mu M)]}{[32P\ UTP (\mu M)] \times (\#\ of\ Us)}$$

where age of 32P is in weeks; SA 32P = specific activity of 32P, usually 3μCi/pmol;
of Us = number of U residues per transcript.

Radioactively Labeled Transcription

Template	0.1 μg /μl
RNA polymerase buffer (NEB)	1x
rNTPs	A,C+G [0.5 mM]; U [0.1 mM]
RNasin (Promega)	2 U/μl
α - ³² P] UTP (3000 Ci/mmol)	1 μl/4 μl reaction

Unlabeled Transcription

Template	0.05-0.1 μg/μl
Selfmade transcription buffer	1x
rNTPs	2.5 mM each
RNasin (Promega)	2 U/μl
Pyrophosphatase (NEB)	0.02 U/μl
RNA polymerase (Sp6/T7)	2 U/μl

5x selfmade transcription buffer

200 mM	Tris pH 8.0
150 mM	MgCl ₂
10 mM	Spermidine
50 mM	DTT

2.2.1.9 Denaturing polyacrylamide gel electrophoresis of RNA (splicing products)

Denaturing polyacrylamide gel electrophoresis was mainly used to separate RNA species up to 1500 bp in size. The gels contained 8M urea as denaturing agent and were used with acrylamide concentrations between 5% and 10%. The acrylamide polymerization was initiated by adding ammonium persulfate and TEMED. RNA samples were resuspended in RNA loading dye and denatured at 70°C for 3 min prior to gel loading. The electrophoresis was performed in 1x TBE buffer at a constant voltage. To allow a better separation of the splicing products and intermediates, an optimized ratio of acrylamide to bisacrylamide (29:1) was used. RNAs were visualized either by silver staining or autoradiography. In case of preparative separations e.g. electrophoresis of *in vitro* transcriptions, UV highlighting was sufficient to visualize the RNA fragments.

RNA Gel solutions (per 20 ml):

8 M (w/v) Urea

5 % to 10 % acrylamide (either Rotiphorese Gel 40 solution or a 29:1 mixture of Rotiphorese Gel A and B)

2 ml 10 x TBE

100 μ l 10 % (w/v) APS & 10 μ l TEMED

percentage of acrylamide [%]	Xylene Cyanol FF [bases]	Bromophenol blue [bases]
5	130	35
6	106	29
8	76	26
10	55	12
20	28	8

2.2.1.10 Silver staining of RNA gels

Silver staining of RNA gels was essentially performed as described by (Merril, Goldman et al. 1981). First, the gel was fixed in a solution of 40% methanol and 10% acetic acid for at least 30 min or overnight. The gel was then washed twice with a solution of 10% ethanol and 5% acetic acid for 15 min. Afterwards, it was briefly rinsed with ddH₂O and subsequently stained with a solution of 12 mM AgNO₃ for 30 min. The stained gel was briefly rinsed with ddH₂O again and then incubated with the developing solution (0.28 M Na₂CO₃, 0.0185% formaldehyde) until RNA bands became visible. The developing reaction was stopped by the addition of 5% acetic acid.

2.2.1.11 Northern blot analysis

Northern blotting was used to detect specific RNAs, using radioactively labeled DNA probes complementary to the respective RNA.

RNA samples were separated using denaturing polyacrylamide gel electrophoresis (see 2.2.1.9) and subsequently transferred to a nylon membrane via a semidry blotting procedure. The transfer was carried out in 0.5x TBE at 3mA/cm² of gel surface for 2h. After blotting, the RNAs were crosslinked to the membrane via UV irradiation with 1200 µJoule x100. Before adding the probes, the membrane was incubated with pre-hybridization buffer (see Table 2.1) at 42°C for 2h. The pre-hybridization buffer was exchanged with fresh hybridization buffer containing the radioactive probes, and the hybridization was carried out for 24-48h at 42°C.

Pre-/ Hybridization Buffer

25 mM Na₃PO₄ pH 6.5

6 x SSC

5 x Deinhardt's solution

0.5 % (w/v) SDS

50 % (v/v) Deionized formamide

0.1 mg/ml Salmon sperm DNA (5 min denat.)

20 x SSC

300 mM Na-Citrate

3 M NaCl

100 x Deinhardt's solution

2 % (w/v) Polyvinylpyrrolodase

2 % (w/v) BSA

2 % (w/v) Ficoll 400

Wash Buffer 1

2 x SSC

0.5 % (w/v) SDS

Wash Buffer 2

2 x SSC

0.1 % (w/v) SDS

Table 2.1: Solutions for Northern blotting

After hybridization, the membrane was washed twice at RT for 5 min with wash buffer 1 and twice with wash buffer 2. A third wash step with wash buffer 2 was performed for 30 min at 50°C. The radioactive probes were visualized via autoradiography.

The radioactive probes were generated using the Prime It II random primer labeling kit according to the manufacturer's instructions.

2.2.2 Protein-biochemistry standard methods**2.2.2.1 Concentration determination of proteins**

To determine the concentration of proteins mainly the Bradford protein assay was used. This method involves the binding of Coomassie Brilliant Blue G-250 dye to proteins (Valadkhan and Jaladat 2010). The dye exists in three forms: cationic (red), neutral (green), and anionic (blue). Under acidic conditions, the dye is predominantly in the cationic form with an absorption maximum at 470 nm. When the dye binds to protein, it is converted to the blue form and the absorption maximum shifts to 595 nm. Using a protein standard, it is possible to determine the concentration of a protein solution. During this work the Bradford protein assay kit from Biorad was used, according to the manufacturer's instructions.

2.2.2.2 Ethanol precipitation of proteins for Mass Spectrometric analysis

For mass spectrometry analyses of proteins associated with spliceosomal complexes, the peak fractions of the respective second glycerol gradient were combined in low-protein binding 1.5 ml reaction tubes (Eppendorf). 350 µl of combined fractions (in case it was more, dried down to ~300µl) were supplemented with 40 µg glycoblu, 35

μl of 3 M NaOAc (pH 5.2) and 1100 μl of ethanol. After thorough mixing the solution was stored at least over night at $-20\text{ }^{\circ}\text{C}$ and then centrifuged for 30 min at 13.000 rpm and 4°C in a table top centrifuge. Subsequently, the pellet was washed with 70 % ethanol, dried in a vacuum dryer and resuspended in 1x SDS PAGE loading buffer from invitrogen.

2.2.2.3 Denaturing Polyacrylamide Gel Electrophoresis (PAGE)

To analyze proteins via denaturing PAGE either pre-casted NuPAGE® Bis-Tris gels (4-12%) or self-casted polyacrylamide gels which were use for mass spec only were prepared according to the procedure established by Laemmli (1970). Commercial gels were used according to the manufacturer's instructions. For self-casted gels typical gel compositions are listed below:

<u>stacking gel</u>		<u>8% separating gel</u>	
4x stacking gel buffer	375.0 μl	4x separating gel buffer	1250.0 μl
Rotiphorese Gel 30	250.5 μl	Rotiphorese Gel 30	1332.5 μl
H ₂ O	874.5 μl	H ₂ O	2417.5 μl
APS	10.0 μl	APS	16.75 μl
TEMED	1.0 μl	TEMED	16.75 μl

Protein samples were dissolved in protein loading dye and heated up to 95°C for 5 min prior to loading. Electrophoresis was typically performed at 150-200V for 45 min using Biorad mini gel systems. The gels were stained either with Coomassie Brilliant Blue or with silver.

2.2.2.4 Coomassie staining of protein gels

Coomassie Brilliant Blue G-250 is a triphenylmethane dye forming strong non covalent complexes with proteins. Coomassie staining of protein gels was essentially performed as described in (Sambrook, Russell et al. 1989). For preparing a staining solution, 80 mg Coomassie Brilliant Blue G-250 were dissolved in 11 ddH₂O and stirred for at least 2 h. Subsequently, 3.5 ml of 37.5 % HCl was added to the solution and the solution was stored in an amber glass bottle at room temperature. For

Coomassie staining of proteins, gels were first fixed for 30 min with 40% methanol/10% acetic acid at room temperature on a shaker. After rehydration of the gel in ddH₂O pre-heated, staining solution was added to the gel. After incubation for at least 1 h at room temperature under gentle shaking the gel was destained over night with water. Finally, the gel was scanned and lanes were cut into 23 slices and analyzed by mass spectrometry in Prof. Urlaub's department.

Coomassie staining solution:

50% (v/v) Methanol

10% (v/v) Acetic acid

0.25% (w/v) Coomassie Brilliant Blue G-250

Destaining solution:

50% (v/v) Methanol

10% (v/v) Acetic acid

2.2.2.5 Silver Staining of Protein Gels

Silver staining of protein gels was performed according to Blum (1987). First, the gel was fixed in a solution of 50% (v/v) Methanol/ 12% (v/v) acetic acid for at least 30 min or overnight. Subsequently, the gel was washed twice with 50% (v/v) ethanol and once with 30% (v/v) ethanol for 20 min each. The gel was then treated with a solution of 0.8 mM Na₂S₂O₃ for 60 s and briefly rinsed with water. Afterwards, the gel was stained with a solution of 12 mM AgNO₃/ 0.026 % formaldehyde for 20 min. The staining solution was removed and the gel was rinsed with water, before adding the developing solution (56 mM Na₂CO₃, 0.0185% formaldehyde, 16 μM Na₂S₂O₃). To stop developing, the gel was transferred in a solution of 50% (v/v) Methanol/ 12% (v/v) acetic acid.

2.2.2.6 Western blot analysis

For western blot analysis, proteins were transferred to a nitrocellulose membrane (Protan BA83 nitrocellulose, 0.2 μm by Schleicher & Schuell) by a wet blot procedure. A Biorad Mini Trans-Blot cell was used according to the manufacturer's instructions. The transfer usually was performed at 250 mA for 2h and a Slab4, methanol, H₂O mixture (in a ratio of 5:2:3) was used as transfer buffer. After the blot, the membrane was stained with Ponceau S to check for a proper transfer. The stain

was removed by washing with a TBS-Tween solution (1x TBS, 0.1% Tween) 2-3 times for 5 min each. Next, the membrane was incubated for 1h at RT in a TBS-Tween solution containing 5% fat free milk powder, to block unspecific interactions between the antibody and the membrane. The antibody was then added to the blocking solution in the designated dilution and incubated at RT for 1h. Afterwards, the membrane was briefly rinsed with TBS-Tween twice, and then 2 times with TBS-Tween for 20 min each. If a second antibody was needed, it was added after this step and the previous steps were repeated.

2.2.3 Purification of recombinant proteins

Cloning of the genes and purification of the recombinant proteins described in this work was performed by Dr. Jana Schmitzová, Group of Dr. Pena, MPI-BPC Göttingen.

2.2.3.1 Cloning strategy and overexpression

Genes, coding for the proteins used in this study, were cloned as described in Warkocki et al., 2009: full length *PRP5*, *PRP2* and *CWC25* genes (genes are always in italics) and the N-terminally truncated form of *SPP2* (aa 36-185) were amplified by standard PCR and ligated into the following vectors: *PRP2*, *SPP2* into *pET21a* (Novagen). This resulted in fusion proteins with a C-terminal hexahistidine tag. *CWC2* was ligated into *pETM11*, resulting in N-terminal hexahistidine tagged fusion proteins. Here the tag was cleavable with a tobacco etch virus (TEV) protease. For subsequent labeling of Cwc25, an N-terminal or C-terminal Cysteine tag was introduced by standard PCR and the resulting DNA was cloned as done for the wildtype *CWC25*. After verification of the constructs by sequencing, the plasmids were transformed into the *E.coli* strain Rosetta II (Novagen) and cultures were grown in 2xYT medium or in autoinducing medium containing antibiotics for selection of the plasmids (Studier, 2005). In the case of 2xYT medium, cultures were induced by adding 0.6 mM IPTG for His-tagged proteins and by 0.1 mM IPTG for GST-tagged

proteins. After 20 h (or 48 h in the case of auto-inducing medium) at 17°C, the cells were harvested, the pellets were washed and stored at -80°C.

2.2.3.2 Purification of proteins

All purification steps were performed at 4°C. First, the cell pellets were resuspended in 5 ml lysis buffer per 1g of cells and lysed with a microfluidiser at 80 psi for six times (Microfluidics). After pelleting insoluble material by centrifugation for 40 min at 10,000 rpm in a Sorval SS34 rotor, the supernatant was applied to HisTrap HP FF crude or GSTrap HP columns (GE Healthcare) which were equilibrated with the respective lysis buffer using the Äkta Prime system (GE Healthcare). For His-tagged proteins the column was first washed with 10 column volumes (CV) of Hislysis buffer, then with 2 CV of washing buffer, again with 2 CV of lysis buffer and finally with 3 CV of 5% elution buffer in lysis buffer. After additional washing with 2 CV each of 10, 15 and 20 % elution buffer, proteins were eluted in a 20 CV gradient of 20-100 % elutionbuffer. For GST-tagged proteins the columns were washed with 10 CV of GST-lysis buffer, then with 2 CV of washing buffer followed by 2 CV of GST-lysis buffer. The proteins were eluted with 2 CV of 30 mM reduced glutathione containing lysis buffer. Eluted proteins were dialyzed against His-lysis buffer containing 20 mM imidazol for Histagged proteins and against GST-lysis buffer for GST-tagged protein versions. The tags were cleaved by the addition of TEV (Cwc25) proteases. The proteases were removed by affinity chromatography, retaining the proteases on the matrix, while purified proteins were eluted in the flow-through. Proteins were finally concentrated using Centricon concentrators (Millipore) and underwent further purification by gel filtration chromatography in buffers containing 20 mM HEPES-NaOH pH7.5, with salt concentrations between 100 and 300 mM NaCl (depending on the protein), 2 mM DTT and 5 % glycerol. Fractions of the gel filtration step were analyzed by SDS-PAGE and Coomassie staining. Fractions with 97 % or higher purity were aliquoted, deep-frozen in liquid nitrogen and stored at -80°C. Concentration was determined as described above using BCA protein assay standard kit.

His-tag Lysis buffer

50 mM HEPES pH 7.5
600 mM NaCl

His-tag Elution buffer

50 mM HEPES pH 7.5
600 mM NaCl

2 mM β -Mercaptoethanol
 10 % glycerol
 20 mM Imidazole

2 mM β -Mercaptoethanol
 10 % glycerol
 250 mM Imidazole

His-tag Wash buffer

20 mM HEPES-NaOH pH 7.5
 2M LiCl
 5% glycerol

Buffer for gelfiltration of His-tagged proteins

20 mM HEPES pH 7.5
 200 mM NaCl
 2 mM DTT
 5% glycerol

2.2.4 Purification of MS2MBP Protein

The MS2-MBP fusion protein used for the purification of spliceosomal complexes was expressed and subsequently purified from electrocompetent BL21 DE pLysS cells. Cells containing the plasmid encoding the MS2-MBP protein were grown to an $OD_{600} = 0.3-0.6$ at 37°C in LB medium supplemented with the respective antibiotics. To induce the expression, IPTG was added to a final concentration of 0.1 mM and the cells were incubated further until they reached an $OD_{600} = 2-2.5$. The cultures were harvested by centrifugation and the cell pellets were subsequently washed with ddH₂O. For cell lysis, the pellet was resuspended in 5 ml lysis buffer (20 mM Tris-HCl, pH 7.6, 200 mM NaCl, complete EDTA-free protease inhibitors from Roche according to the manufactures instructions) per gram of cells and processed with a microfluidiser (Microfluidics) at 80 psi for 2-3 times. The lysate was separated from cell debris by centrifugation (12000 x g, 4°C , 40 min) and incubated head-over-tail with 500 μl of amylose resin per 10 ml of lysate for 2h. Afterwards, the suspension was transferred into a Bio-Spin chromatography column (Biorad) and the resin was washed with 10 column volumes (CV) of wash buffer (20 mM HEPES, pH 7.9, 150 mM NaCl, 0.05% NP-40). To decrease the salt concentration in view of the next

purification step the amylose resin was washed with 5 CV of 5 mM Na₂HPO₄, pH7.0 before the protein was eluted with 5 mM Na₂HPO₄ containing 20 mM maltose. The eluate was loaded onto a heparin agarose column equilibrated with 5 mM Na₂HPO₄, pH7.0. After washing with 10 CV of 5 mM Na₂HPO₄, pH7.0, the MS2-MBP protein was eluted using a higher salt concentration within the elution buffer (20 mM HEPES/KOH, pH 7.9, 100 mM KCl, 15% Glycerol, 0.5 mM DTT). The protein was shock frozen in liquid nitrogen and stored at -80°C.

2.2.5 Cell culture and extract preparation

2.2.5.1 Cultivation of bacteria

E. coli cells were grown in lysogeny broth (LB) medium (Sambrook, Russell et al. 1989), 2xYT medium or in autoinducing medium (Studier 2005). The medium was autoclaved for 15 min at 121°C. For the selection of antibiotic resistances the medium contained Ampicillin (100 µg/ml), Chloramphenicol (30 µg/ml) or Kanamycin (30 µg/ml). Cells were stored for long term at -80°C by adding 15% glycerol as a cryopreservative.

2.2.5.2 Cultivation of yeast cells

S. cerevisiae yeast cells were cultivated according to standard methods in YPD medium or on YPD-plates. To prepare YPD plates, first YP-medium including agar was autoclaved for 15 min at 121°C and cooled down to 60 °C. Subsequently, 40 ml of sterile 50 % glucose was added per liter of YP medium (final concentration of 2 %). Subsequently, about 20-25 ml of this medium was poured into Petri dishes. Plates were cooled down for ca. 1 h at roomtemperature and kept at room temperature for long-term storage. To start cultivation of a yeast strain, yeast cells were picked from a glycerol stock and streaked on a YPD-plate. The plate was then incubated for 2-3 days at 25°C or 30°C depending on the phenotype of the cells (BJ2168 at 30°C, *prp2-1* and *prp5-1* at 25°C). In the case of a replica-assay (named also frog-assay), a serial dilution of the yeast strain of interest was spotted on four different YPD-plates which

were then incubated at 16°C, 25°C, 30°C and 37°C. Cell growth was checked after 1-3 days and documented. For a long-term storage of the cells, the plates were sealed with parafilm and kept at 4°C up to 2 months. For subsequent extract preparation, a single colony of yeast cells from the YPD-plate was transferred to 50 ml YPD-medium in a 250 ml Erlenmeyer flask and incubated under shaking at the optimal temperature (25°C -30 °C) depending on the yeast strain. OD₆₀₀ of the cells in the pre-culture was determined and usually 20 OD of cells was inoculated into 2 liters of YPD medium in a 5 L Erlenmeyer flask. Alternatively, 100 L of YPD medium in a fermenter were inoculated with 1000 - 2500 OD₆₀₀ of yeast cells (depending on the strain) and supplemented with 4 L 50% glucose and tetracycline and ampicillin (10 µg/ml final concentration each) and incubated at the optimal temperature. Usually after 18-22 hours, cells reached an OD₆₀₀ of 3-5 / ml and were harvested. For a longer storage in YPD medium, 800 µl of yeast cells were mixed with 400 µl of sterile 50% glycerol and kept at -80°C.

YPD-medium

2 % (w/v) Bacto pepton

1 % (w/v) Yeast extract 2 % (w/v) Glucose (sterile filtered)

1 % (w/v) Bacto agar in the case of YPD-plates

2.2.5.3 Preparation of yeast whole cell extracts and immunodepletion

The preparation of yeast whole cell extracts for subsequent use during *in vitro* splicing reactions was performed essentially as described by Gottschalk, Neubauer et al. (1999). Yeast cells from the strains BJ2168, *prp5-1* or *prp2-1* (and its tagged derivatives), were grown overnight at 30°C (or 25°C for temperature sensitive strains) up to an OD₆₀₀ of 3.5-4.5/ml in 5 L flasks or 10 L up to 100 L fermenter. Cells were pelleted for 10 min at 5000 rpm in an SLC-6000 rotor. The pellet was washed twice with cold H₂O and subsequently resuspended in cold AGK buffer (20 mM HEPES/KOH pH 7.9, 200 mM KCl, 1.5 mM MgCl₂, 8% (v/v) glycerol) supplemented with 0.5 mM DTT, 0.5 mM PMSF, 2 mM benzamidine, 1 µM leupeptin, 2 µM pepstatin A, 4 µM chymostatin, and 2.6 µM aprotinin. Alternatively, AGK buffer was supplemented with 0.5 mM DTT, 0.5 mM PMSF, 2 mM benzamidine and one EDTA-free complete protease inhibitor tablet from Roche per 50 ml of AGK buffer. The

volume of the suspension was measured and the concentration of KCL was adjusted to 200 mM again. To obtain yeast beads 2-5 mm in diameter, the cell suspension was dripped into liquid nitrogen, using a separating funnel. For cell lysis, these beads were ground in liquid nitrogen at 18000 rpm using a centrifugal mill (Retsch). The powder formed during the grinding process was slowly thawed at RT, and the cell debris were separated from the extract by centrifugation (25000 x g, 4°C, 30 min). A second centrifugation step at high speed was used in order to clarify the extract (100000 x g, 4°C, 1h). During the centrifugation the extract was separated into three phases. The upper phase contained lipids and liposomes, the middle phase was clear and the pellet contained ribosomes, DNA and fine cell debris. The middle phase was recovered and dialyzed twice against 50-100 volumes of buffer D (20 mM HEPES/KOH pH 7.9, 50 mM KCl, 0.2 mM EDTA, 0.4 mM MgCl₂, 20% (v/v) glycerol, 0.5 mM DTT, 0.5 mM PMSF, 2 mM benzamidine) for 1.5h each. After dialysis, the extract was centrifuged at 17000 x g for 5 min and subsequently frozen in liquid nitrogen. The extract was stored for long term at -80°C.

2.2.6 Special methods

2.2.6.1 In vitro splicing reactions

In vitro splicing reactions were performed essentially as described by Fabrizio, McPheeters et al. (1989). A splicing reaction usually contained 40% total yeast extract, 1x splice cocktail (see below) and 40.000 cpm (0.4 nM) of radioactively labeled Actin WT pre-mRNA. The reactions were incubated at 23°C for 0-60 min and aliquots were taken at several time points. The reactions were stopped by storing them on ice. Afterwards, Proteinase K digestion was used to strip off completely the proteins of the RNA. A typical Proteinase K reaction included the sample to be digested, 0.2% SDS (w/v), 10 mM EDTA and 0.3mg/ml proteinase K. The reactions were incubated at 37°C for 30 min. Subsequently, 200 µl of “Stop-splicing” buffer were added, PCI extraction was performed followed by ethanol precipitation (2.2.1.6). The RNAs were separated by denaturing PAGE and the gels were analyzed by autoradiography.

5x splicing cocktail:

„stop splicing“ buffer

50 mM NaOAc (pH 5.3)

0.27 mM EDTA

0.1 % (w/v) SDS

300 mM phosphate buffer, pH 7.3*
15 % (w/v) PEG 8000
10 mM ATP
12.5 mM MgCl₂
10 mM spermidine

*phosphate buffer at pH 7.3 was prepared by mixing solutions of K₂HPO₄ and KH₂PO₄ according to Sambrook, Russell et al. (1989).

2.2.6.2 Purification of spliceosomal complexes

To isolate spliceosomal complexes under native conditions according to the protocol of Fabrizio, Dannenberg et al. (2009); (Dannenberg, Fabrizio et al. 2012) the M3-Act pre-mRNA wild type or truncated substrate was bound to the MS2-MBP fusion protein by incubating a 30-35 times molar excess of MS2-MBP with the designated pre-mRNA and 20 mM HEPES-KOH, pH 7.9 on ice for 30 min.

Depending on the required amount of spliceosomal complexes, a 6–72 ml splicing reaction containing 1.8 – 2.5 nM of ³²P-labeled M3-Act pre-mRNA (specific activity 20–300 cpm/fmol) was performed in 60 mM K-PO₄ (pH 7.4), 3% PEG 8000, 2.5 mM MgCl₂, 2.0 mM ATP, 2.0 mM spermidine, and 40% yeast extract in buffer D (20 mM HEPES-KOH, pH 7.9, 50 mM KCl, 0.2 mM EDTA pH 8.0, 20% (v/v) glycerol, 0.5 mM DTT, and 0.5 mM PMSF). The complexes were assembled by incubating at 23°C for 50 min. Complex C was treated additionally with a 125-fold molar excess of a DNA oligonucleotide complementary to nt +13 to +24 of the actin intron and the reaction was incubated for 10 min at 30 °C to allow cleavage by RNaseH present in the extract (Fabrizio, Dannenberg et al. 2009); (Bessonov, Anokhina et al. 2008) During this procedure, the endogenous RNase H present in the extract digests the RNA intron of early spliceosomal complexes whose presence would complicate the purification.

After this procedure, six ml aliquots of the splicing reaction were loaded onto 36-ml linear 10-30% (w/w) glycerol gradients containing GK150 buffer (20 mM HEPES-KOH pH 7.9, 1.5 mM MgCl₂, 150 mM KCl). Gradients were centrifuged for 14 h at 23.000 rpm in a SureSpin 630 rotor (Thermo Scientific) and harvested manually in 1500-µl fractions from the top. Fractions were analyzed by Cherenkov counting in a

scintillation counter and peak fractions containing complexes were pooled and loaded onto columns containing 250–300 μl of amylose matrix equilibrated with GK150 buffer. The matrix was washed two times with 10 ml GK150 buffer and two times with GK75 buffer supplemented with 5% glycerol and 0.01% NP40, and spliceosomal complexes were eluted dropwise with 750 μl elution buffer (GK75 buffer containing 12 mM maltose, 5% glycerol and 0.01% NP40). The elution fractions were either used directly for reconstitution assays or for FCCS.

2.2.6.3 Non-denaturing Complex gels

First, a standard splicing assay is performed. After the incubation time of the splicing reaction (10 μl sample volume) 2 μl Stop Heparin Mix* has to be added to each sample. Keep on ice, treat the sample gently. Do NOT vortex. Then, 3.0 μl of each sample has to be loaded on a complex gel* 4% (80:1). The gel should be poured one day before and wrapped with foil. Keep at 4°C. Run the gel at 300V for 30 min and then at 230V for 5 h at 4°C. Change the T.E. running buffer every hour. For analysis of the splicing intermediates on denaturing PAGE, PK-digestion has to be performed. Therefore, 40 μl of PK-mix has to be added to the rest of each sample (see PK-digestion of proteins)

“Stop Heparin” Mix:

Complex gel solution 4 %/(80:1; Acrylamide/Bis-Acrylamide):

In T.E 1x (20 mM Tris-HCl, pH 8.0, 1 mM EDTA, pH 8.0)

2.2.7 Reconstitution of functional spliceosomes for FCCS

2.2.7.1 Treatment of complexes for RNA PAGE

10 fmol of $B^{\text{act}}_{\Delta\text{Prp2}}$ complexes from the elution of the amylose matrix were supplemented with 100 fmol (10x molar excess) of recombinant proteins in a 40 μl reaction. After incubating the reconstitution reaction for 10 min on ice, a 10x “rescue” solution was added to the reaction. After thorough mixing the reactions were incubated at 23 °C for 40 to 50 min. After Proteinase K digestion the RNAs were

extracted by PCI and ethanol precipitation and analyzed by an 8% denaturing PAGE followed by autoradiography.

2.2.7.2 Reconstitution on Amylose Matrix

For reconstitution assays on the amylose matrix, complexes were kept on the matrix and transferred to a 1.5 ml reaction tube. Complex concentration was determined by Cherenkov counting and recombinant proteins were added in 10x molar excess. A typical reconstitution reaction was performed with 250 μ l-300 μ l amylose beads in a final volume of 600 μ l (in GK 75 buffer) containing 60 μ l “rescue” solution. Reactions were incubated at 23°C for 45 min and transferred back to a plastic column (one per each reaction). If ATP had to be depleted, the reaction was supplemented with 2 mM glucose and 2 Units recombinant hexokinase and incubated for 10 min at 23 °C before the matrix was transferred back to the column. The reaction was then washed thoroughly with 10 ml of GK75 buffer and the complexes were eluted with 20 mM maltose as described above. If several reactions were to be reconstituted on the amylose matrix, the peak of the SureSpin gradient was divided equally to the appropriate number of chromatography columns containing 250 μ l amylose beads. Reactions were then carried out like described above, but in a final volume of 500 μ l.

2.2.7.3 In-solution

For real-time FCCS measurements, i.e. from reactions carried out in solution, reactions were carried out in a final volume of 60 μ l with a final complex concentration of 0.8 nM-1.1 nM. Recombinant proteins were added in 10 fold excess. Instead of the 10x rescue mix, however, the reaction conditions were only adjusted to final concentrations of 2.5 mM MgCl₂ and 2 mM ATP (or other analogues), as PEG8000 increased the background of the FCCS measurements.

10x “rescue” solution

200 mM phosphate buffer, pH 7.3

10 mM MgCl₂

20 mM ATP

14 % PEG 8000

2.2.8 Mass spectrometry

For Mass spectrometry, proteins recovered from purified spliceosomal complexes (usually between 100-400 fmol), were separated by SDS-PAGE using a 4-12% Bis-Tris-HCL (pH 7.0) NUPAGE polyacrylamide gel (Invitrogen) and stained with Coomassie. Entire lanes were cut into 23 slices and proteins were digested in-gel with trypsin and extracted as described by described Shevchenko, Wilm et al. (1996). Resulting peptides were analyzed in an LC-coupled ESI Q-ToF (QToF Ultima, Waters) and/or OrbitrapXL (ThermoFisher Scientific) mass spectrometer under standard conditions. Proteins were identified by searching fragment spectra against the NCBI nonredundant (nr) database using Mascot as search engine.

2.2.9 Electron Microscopy

Eluted complexes were fixed by loading onto a 3.8 ml linear 10%–30% glycerol gradient containing 0.1% glutaraldehyde in the 30% gradient solution and centrifuged for 107 min at 490,000 g (Kastner, Fischer et al. 2008). Gradients were fractionated from the bottom using a fraction collector. Particles were negatively stained by the double-carbon film method (Golas, Sander et al. 2003). Images were taken at 160 kV and a magnification of 88,000 or 115,000 in eucentric height at a defocus of 1.5 mm in a CM200FEG microscope (FEI, Eindhoven, The Netherlands) at RT on a 4 k 3 4 k CCD camera (TVIPS GmbH, Gauting, Germany) using 2-fold pixel binning. About 10,000 particle images were collected for each data set and were subjected to single-particle image processing at the level of 2D projection images using the IMAGIC-V software package (Image Science GmbH, Berlin, Germany). Good-quality class averages were obtained after several iterations of alignment, multivariate statistical analysis (MSA), and classification.

2.2.10 Labeling Methods

2.2.10.1 Preparation of yeast strains expressing EGFP-tagged proteins

To construct yeast strains with the yEGFP tag at the C terminus of selected proteins, the yEGFP cassette was amplified by PCR from the plasmid pKT209 (purchased from Euroscarf, Frankfurt am Main). We used this PCR product to transform haploid yeast cells from strain 3.2.AID/CRL2101 (Yean and Lin 1991), and transformants were selected on synthetic dextrose dropout medium lacking uracil. The correct integration of the tag in the genome was confirmed by PCR, and on the protein level by western blotting. The resulting strains carry a single chromosomal copy of the gene of interest, containing the yEGFP tag, the *Candida albicans* URA3 marker at their C terminus and in addition a temperature-sensitive Prp2 ATPase (*prp2-1*).

2.2.10.2 Pre-mRNA labeling with a fluorescent dye

Guanosine-5'-O-monophosphorothioate (59-GMPS) can be incorporated as the first nucleotide by T7 or Sp6 RNA polymerase (dependent of the used promoter) *in vitro*. 5'-GMPS-containing mature actin pre-mRNA was prepared by *in vitro* transcription of Acc65I digested pUC18-Actin-wt plasmid DNA with T7(Sp6) RNA polymerase (40 mM Tris-HCl, pH 8.0, 30 mM MgCl₂, 10 mM DTT, 2 mM spermidine, 0.1 U yeast inorganic pyrophosphatase (NEB), 0.5 U RNasin (Promega), 4 mM ATP, 4 mM CTP, 4 mM UTP, 1 mM GTP, 10 mM 5'-GMPS (Biolog); 37°C, 3 h). Transcripts were purified by electrophoresis through 5% polyacrylamide, 8 M urea gels and passively eluted into 0.5 M NaOAc, pH 5.3, 1 mM EDTA, pH 8.0, 2.5% phenol-chloroform-isoamyl alcohol. To link the 5'-GMPS-modified pre-mRNA covalently to the fluorescent dye Atto647N, Atto647N-maleimide was incubated with the pre-mRNA in the presence of 100 mM NaPO₄ (pH 7.2) at RT for 4 h. The Atto647N-labeled pre-mRNA was prepurified by 4x ethanol precipitation and several washing steps to remove unreacted dye, resulting in nearly 100% labeled pre-mRNA. The dye:RNA stoichiometry was calculated according to the manufacturer's protocol (Molecular Probes).

The thiol group of the pre-mRNA and the maleimide group of the dye form a thioether linkage and are therefore covalently attached to each other. The labelling

efficiency was determined by measuring the absorption of the RNA molecules at 260 nm and the absorption of the attached dye at 647 nm. Efficiency in % is then calculated with the formula:

$$\text{labeling efficiency \%} = \frac{A(\text{dye})}{A(\text{RNA})} \times \frac{\varepsilon(\text{RNA})}{\varepsilon(\text{dye})} \times \# \text{ of nt}$$

where ε is the molar extinction coefficient, # is the number of nucleotides of the respective pre-mRNA and A is the absorption. Usually a labeling efficiency of more than 98 % was obtained.

2.2.11 Fluorescence Cross Correlation Spectroscopy (FCCS)

2.2.11.1 Setup

The two-color-dual-focus setup is based on an inverse epi-fluorescence microscope (MicroTime 200, PicoQuant GmbH, Berlin, Germany). The system is equipped with two identical pulsed 470 nm diode lasers (LDH-P-C-470 B, PicoQuant GmbH, Berlin, Germany) and two identical pulsed 635 nm diode lasers (LDH-P-635, PicoQuant GmbH, Berlin, Germany) with linear polarization and a pulse duration of 50 ps (FWHM). The lasers are pulsed alternately with an overall repetition rate of 10 MHz (PIE mode) corresponding to a delay between pulses of 25 ns (PDL 828 “Sepia II”, PicoQuant GmbH, Berlin, Germany). The light of each of the two pairs of identical wavelength lasers is combined by two polarizing beam splitters (Ealing Catalogue, St. Asaph, UK) into single beams. These beams are combined by a dichroic mirror (490 dcxr, Chroma Technology, Rockingham, VT, USA) resulting in a single beam containing both wavelengths. The beam is coupled into a polarization-preserving single mode fiber. At the fiber output, the light is collimated and reflected up by a dichroic mirror (Q660LP, Chroma Technology, Rockingham, VT, USA). Before entering the objective, the light is passed through a Nomarski prism (U-DICTHC,

Olympus Europa, Hamburg, Germany) which splits the beam deflects into two slightly different directions depending on their polarization. Then the light is focused into the microscope's objective (UPLAPO 60x W, 1.2 N.A., Olympus Europa, Hamburg, Germany) and one thus obtains two overlapping foci with a fixed lateral distance determined by the properties of the Nomarski prism. Fluorescence is collected by the same objective (epi-fluorescence setup), passed through the Nomarski prism and the dichroic mirror, and focused by a tube lens through a single circular aperture (diameter 150 mm). After the pinhole, the light is re-collimated, split by a polarizing beam splitter cube and a dichroic mirror (640 dcmr, Chroma Technology, Rockingham, VT, USA), and focused onto two single photon avalanche diodes (SPAD, AQR13, Perkin Elmer, Wellesley, MA, USA), respectively for the red and the blue excitation. Emission bandpass filters HC692/40 and HC520/35 (Semrock, USA) for red and blue excitation, respectively, positioned directly in front of each detector, discriminate fluorescence against scattered light. A single-photon counting electronics (HydraHarp 400, PicoQuant GmbH, Berlin, Germany) independently records the detected photons of all detectors with an absolute temporal resolution of 4 ps on a common time frame.

2.2.11.2 Measurement protocol

Spliceosomal complexes were assembled on fluorescently labeled pre-mRNAs (bearing Atto647 as a fluorescent label at the 5'-end) and purified as described above. On the amylose matrix complexes were supplemented with recombinant proteins as described. Complexes were kept on ice until measured by FCCS. Complexes were measured in a volume of 25 μ l at a concentration of 1.1 nM in a reaction chamber consisting of two glass slides connected through a 1 mm spacer. Measurement was then performed for 10 min at room temperature.

3. Results

Spliceosome dynamics comprise a complex, but regulated interplay of several snRNPs and factors that interact sequentially with the pre-mRNA. The purification of spliceosomal complexes at distinct stages is very helpful to learn more about the composition, structure and function of the yeast spliceosome. In the last years, a number of purification strategies have been employed to purify human spliceosomes at different time points *in vitro*. To isolate and characterize biochemically homogeneous B, B^{act} and C complexes from the yeast *S. cerevisiae*, we first had to establish a system which is suitable for stalling the spliceosome assembly at distinct stages of the splicing cycle and allows purifying these complexes under native conditions. To purify the stalled complexes, we made use of an affinity selection method by using pre-mRNAs, modified at their 3' or 5' end, which were fused to three MS2-binding sites (M3) to their 5' end. Each stalled complex was isolated by a three step affinity selection method including centrifugation and affinity-selection (Deckert, Hartmuth et al. 2006); (Jurica and Moore 2002). Their proteomes were determined by mass spectrometry (MS), and their structures were examined by electron microscopy (EM).

3.1 Pre-mRNA constructs and conditions used for the isolation of yeast spliceosomal complexes

To isolate biochemically homogeneous B, B^{act} and C complexes actin pre-mRNA and its modifications were employed. For the later affinity purification, three MS2 binding sites were fused to the 5' end of the various pre-mRNA constructs; the resulting constructs were termed "M3-Act". Previous studies have shown that truncation/modification or mutation of the actin pre-mRNA and adjustment of the ATP concentration in the splicing reaction lead to stalling of the spliceosomal cycle (Cheng 1994); (Vijayraghavan, Parker et al. 1986); (Rymond and Rosbash 1985). The intron in the actin pre-mRNA contains the yeast consensus branch point sequence (BPS) UACUAAC. M3-Act Δ 6 and M3-Act Δ 31 were truncated 6 and 31 bases after

this sequence. Both of these, thus, lacked the 3'SS and the 3' exon. The variant M3-ActACAC contained a mutation in the introns' 3'SS (AGAG to ACAC), which was followed by an unmutated but shortened 3' exon. The inclusion of only 0.05 mM ATP in the splicing reaction led to stalling of the spliceosomal cycle at the stage of the pre-catalytic B complex for the wild-type and for the M3-Act Δ 6 construct, as already observed in previous studies (Tarn, Lee et al. 1993).



Figure 3.1: Pre-mRNA constructs used for the purification of spliceosomes

(adapted from (Fabrizio, Dannenberg et al. 2009))

M3-Act wt is used to assemble either complex B under low ATP concentrations while M3-Act Δ 6 is used to stall B^{act} complexes. M3-Act Δ 6 is truncated six nucleotides downstream of the BPS, M3-Act Δ 31 is truncated 31 nucleotides after the BPS and stalls spliceosome assembly at the stage of complex C. M3-Act ACAC has a mutation in its 3'SS (AGAG to ACAC) and stalls the cycle prior to the second step.

3.2 Preliminary work for stalling and isolating active spliceosomal complexes from yeast at defined stages

Our first goal was to test if our “set up” worked for the isolation of spliceosomal complexes from the yeast *S.cerevisiae* thus, we verified that the presence of the three MS2 hairpins did not interfere with the splicing cycle and that the constructs were able to undergo spliceosome assembly.

For the *in vitro* assembly of yeast spliceosomal complexes we made use of whole cell extract made from the *S.cerevisiae* strain BJ-2168 (a protease deficient strain) and the various M3-Act pre-mRNA constructs mentioned above. The extracts were made according to the protocol (see methods; (Fabrizio, Dannenberg et al. 2009); (Dannenberg, Fabrizio et al. (2012)). A prerequisite for this was to *in vitro* transcribe the pre-mRNA constructs via SP6 or T7 polymerase. For detection of the RNA by autoradiography, the pre-mRNA was radioactively labeled with [³²P] -UTP during transcription. The inclusion of only 0.05 mM ATP in the splicing reaction led to stalling of the splicing cycle at the stage of complex B, both for M3-Act and M3-Act Δ 6 (Fig. 3.2 A lanes 6-8, 14-16). Raising the ATP concentration to 2.0 mM ATP led the splicing reaction to proceed to completion for the M3-act wt construct while the pre-catalytic B complex was converted into the activated B^{act} complex, showing neither splicing intermediates nor mature RNA, which identifies these complexes as pre-catalytic splicing intermediates (Figs. 3.2 A and B lanes 2-4, 10-12). When we applied the same conditions to the M3-Act Δ 31 construct, we observed a different behavior compared to the M3-Act Δ 6 version of pre-mRNA truncation. In this case, the spliceosome assembly could proceed up to the stage of the C complex (Fig. 3.2 A lanes 18-20). The presence of the cleaved 5' exon and intron-3'SS intermediates without products formation (i.e. mRNA and intron-lariat), identified this complex as a C complex which performed the first but not the second step of splicing (Fig. 3.2 B lanes 18-20). The characteristics of splicing using the M3-ActACAC construct was similar to the M3-Act Δ 31 construct, but if one compares the intensities of the band signals on the gels, the yield of C complex was higher (Fig. 3.2 C lanes 2-4).

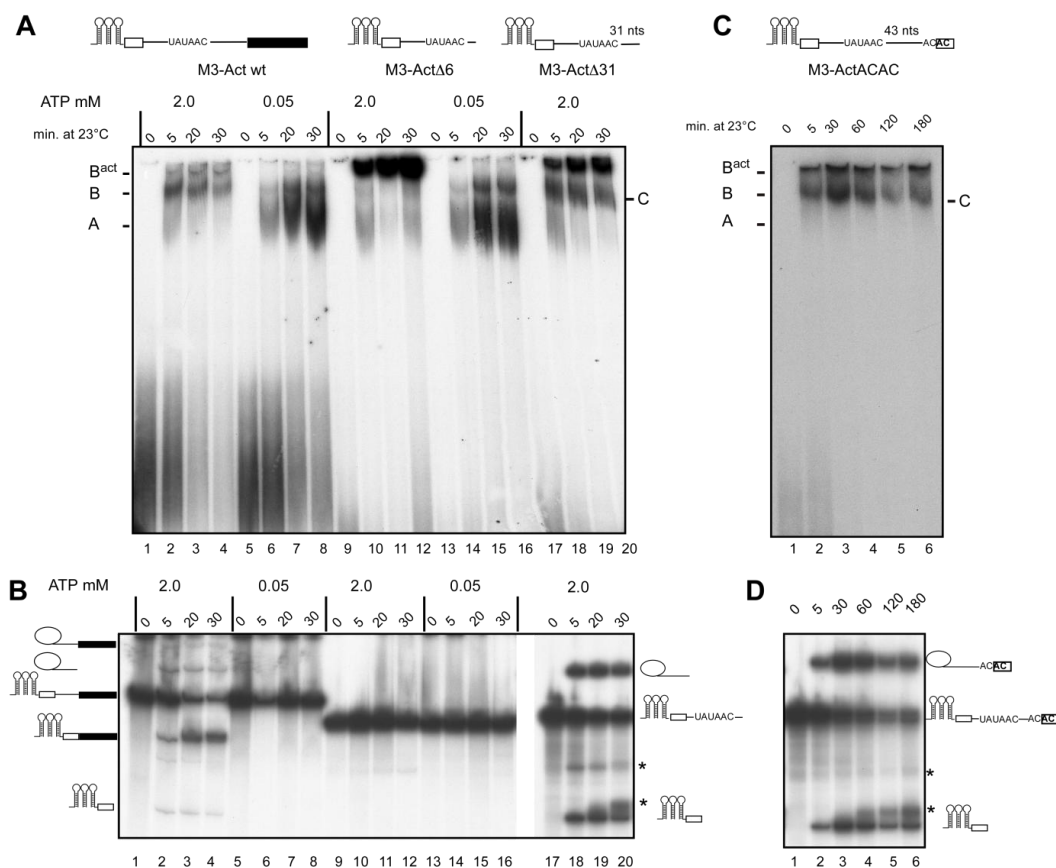


Figure 3.2: Kinetics of splicing and splicing complex formation. Panel A shows the kinetics of *in vitro* splicing complex formation and in panel B splicing is depicted. In lanes 1-8 of both panels M3-Act wt was used; in lanes 9-16, M3-ActΔ6 and in lanes 17-20, M3-ActΔ31 was used. The constructs are shown as a scheme above panel A. The panels C and D show the kinetics of spliceosomal complex formation using the 3' splice site (3'SS) mutant construct M3-ActACAC. Splicing was performed under the same conditions using 2.0 mM ATP in yeast whole-cell extract for 0-180 min. In the panels A and C the splicing complexes were analyzed on non-denaturing RNA-PAGE. In the panels B and D, the RNA substrates were analyzed by denaturing RNA-PAGE. The position of the complexes, the pre-mRNA and the splicing intermediates are indicated as a scheme on the left and right. The asterisks indicate unknown RNA derivatives.

3.3 Purification of yeast spliceosomes

To obtain preparative amounts for the isolation of spliceosomal complexes and for later analysis by mass spectrometry and electron microscopy we performed upscale experiments. Therefore we incubated first each of the different [³²P]-labeled M3-Act substrates with the MS2-MBP fusion protein to allow the binding of the MS2-MBP to the three MS2 hairpins at the 5' end of the pre-mRNA for later affinity-purification on

amylose beads. Yeast whole-cell extracts prepared from the protease-deficient strain BJ2168 were used in these experiments and the reactions were incubated at 23°C for 50-60 min to allow formation of spliceosomal complexes. Mainly, the time point of 50 min was chosen, since after 50 min of incubation, the majority of spliceosomal complexes have formed. In case of low ATP, only pre-catalytic B complexes could be formed, with high ATP but with the M3-Act Δ 6 substrate, spliceosomal assembly stopped at the stage of the activated B^{act} complex. After incubation under splicing conditions, the reaction was placed on ice and subsequently loaded on six linear 10%-30% glycerol gradients in the presence of 150 mM KCl and was centrifuged in a Sorvall SureSpin rotor 630 at 22.100 rpm for 18 h at 4 °C. This step serves as a first isolation step to enrich the B, B^{act} or C complexes and separate them from the majority of other spliceosomal complexes and also to remove unbound MS2-MBP fusion protein. After centrifugation, 23 fractions of 1.5 ml were collected by hand from the top of the gradient and the peak fractions were determined by Cherenkov-counting of all fractions. The peak fractions were located in the 40S-45S region of the gradient, containing the major amount of complex B, B^{act}, or C. These fractions were pooled and bound on an amylose column, pre-equilibrated with wash buffer G-150 (containing 150 mM KCl) at 4°C. The complexes were bound to the matrix by gravity flow and afterward washed two times with ~ 10 ml of G-150 buffer, two times with ~ 10 ml of buffer G-75 (containing 75 mM KCl) and then eluted with a buffer containing 12 mM Maltose, 0.01 % NP40 and 5% glycerol in G-75. The purification was carried out under stringent conditions so that only stably bound proteins would be present. For mass spectrometry or electron microscopy, the eluted complexes underwent a second centrifugation step, this time on a 10%-30% glycerol gradient containing 75 mM KCl for 1h and 47 min at 60,000 rpm in a Sorvall TH660 rotor at 4°C (see methods). Their distribution in the gradient was determined again by Cherenkov-counting and their RNA and protein content were analyzed by denaturing PAGE.

3.3.1 Purification of the pre-catalytic B complex

Spliceosomal B complexes were assembled on M3-Act Δ 6 pre-mRNA substrate under splicing conditions with only 0.05 mM ATP in the reaction. The purification was

carried as described above. The verified sedimentation coefficient known as Svedberg constant (S) is $\sim 40S$ for the B complex.

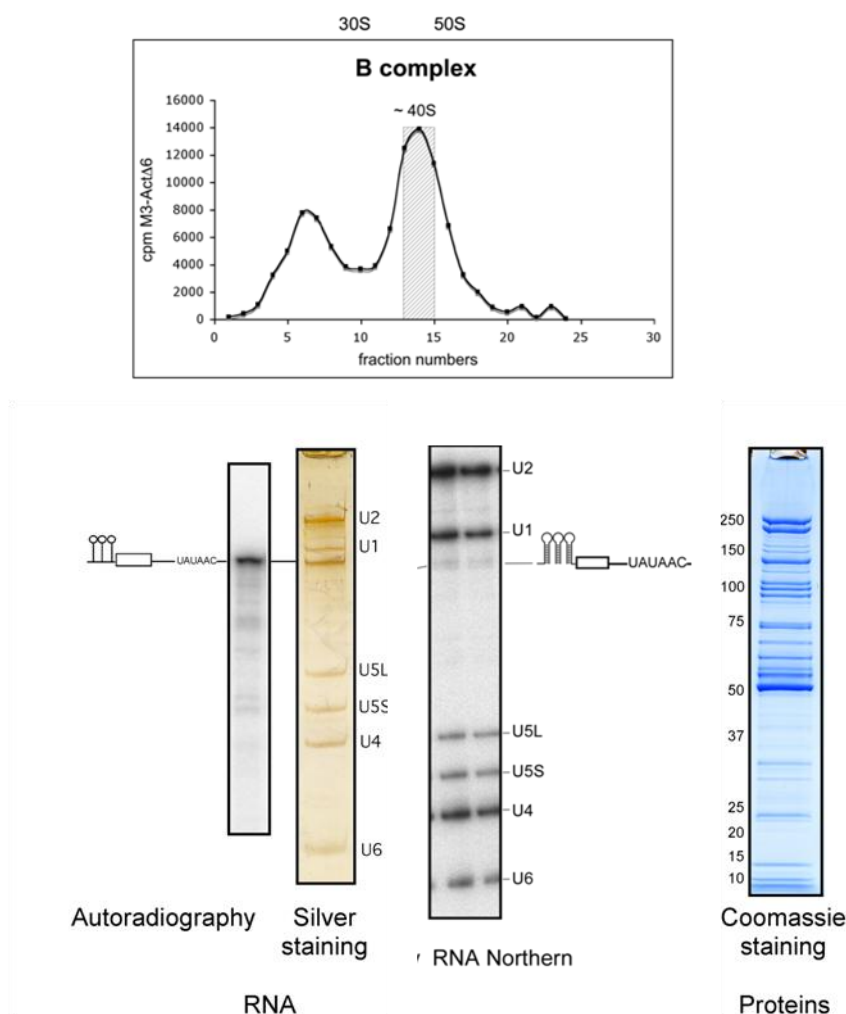


Figure 3.3: Characterization of the pre-catalytic B complex. Upper panel: Profile of purified B complex (specific activity of 100 cpm/fmol) separated on a glycerol gradient. The radioactivity contained in each gradient fraction was determined by Cherenkov counting. Sedimentation was determined by analyzing the UV absorbance of a reference gradient containing prokaryotic ribosomal subunits. Lower panel: RNA from gradient fractions (# 13–14) was recovered, analyzed by denaturing PAGE, and visualized by silver staining, autoradiography, and Northern analysis. RNA identities are indicated on the right. Proteins were separated by SDS-PAGE and Coomassie stained.

The distribution of the main population of the spliceosomal B complexes is shown schematically in Fig. 3.3 A as a graph which corresponds to the gradient profile. After pooling the fractions of the main peak of the gradient, they were analyzed by RNA PAGE and Northern Blot. The autoradiography of the RNA PAGE revealed the pre-mRNA. Silverstaining of the RNA gels afterwards revealed a full set of snRNPs, U2, U4, U5 and U6, in equimolar amounts, whereas U1 was slightly underrepresented. The snRNAs were additionally analyzed by Northern Blot (Fig. 3.3 B). No splicing intermediates were detected by denaturing PAGE, but only unspliced pre-mRNA.

3.3.2 Affinity-purified complex B is functionally committed for subsequent activation and splicing catalysis

To examine whether the affinity-purified B complexes stalled by using 0.05 mM ATP are functionally committed to splicing, we performed “chasing experiments”. Therefore, we assembled them on M3-Act wt pre-mRNA but with 0.05 mM ATP. The complexes isolated as described above were then incubated with a mixture of 2.0 mM ATP and MN-digested extract, where all endogenous snRNAs have been digested by treating with micrococcal nuclease (MN).

In the presence of 2.0 mM ATP and MN-digested extract, the purified B complexes were able to catalyze both steps of splicing (Fig. 3.4, lanes 1 and 2), whereas no splicing was observed when an equimolar amount of only naked [32P]-labeled M3-Actin pre-mRNA was used under the same conditions (Fig. 3.4, lanes 9 and 10). As expected, neither affinity purified B complex nor the naked M3-Actin pre-mRNA underwent splicing in the MN-treated extract when treated with only 0.05 mM ATP (Fig. 3.4, lanes 5-6 and 11-12). Taken together, these experiments demonstrate that our isolated B complexes do not require complementation with any of the spliceosomal U snRNAs for their activity. Thus, we could demonstrate that the B complexes, isolated from the yeast *S.cerevisiae*, were no “dead-end” complexes and were able to perform the subsequent steps of splicing, on the other hand, the incubation of purified B complexes under splicing conditions, but in the absence of MN-extract, did not result in splicing (Fig. 3.4, lanes 3-4 and 7-8). This suggested that likely, these purified complexes lacked one or more factors required for subsequent spliceosome activation and/or catalysis.

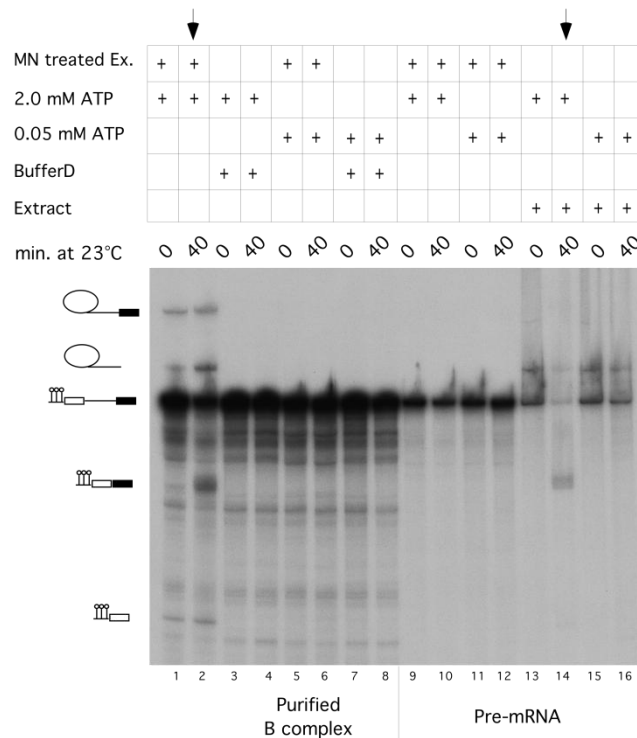


Figure 3.4: Affinity-purified complex B is functionally committed for subsequent activation and splicing catalysis. Affinity-purified B complexes were incubated (0 and 40 minutes) with 2.0 mM ATP and micrococcal nuclease (MN) digested extract under splicing conditions (lanes 1-2), 2.0 mM ATP and Buffers D (lanes 2-3), (MN) digested extract and 0.05 mM ATP (lanes 5-6) and 0.05 mM ATP and Buffer D. An equimolar amount of naked, [32P]-labeled wt M3-Actin pre-mRNA was analyzed under the same conditions (lanes 9-12), or with whole cell extract and 2.0 mM or 0.05 mM ATP (lanes 13-16).

3.3.3 Purification of the activated B^{act} complex

For the activated, but not catalytically active spliceosomal complex B^{act} the purification procedure was the same except the concentration of ATP during the splicing reaction. Complex B^{act} was prepared by using M3-Act Δ 6 as splicing substrate and 2.0 mM ATP. The B^{act} complex has a slightly higher S value than the B complex. The S value changes from 40S to 45S due to the activation of the spliceosome which is accompanied by conformational changes of the RNA network (Fig. 3.5 A).

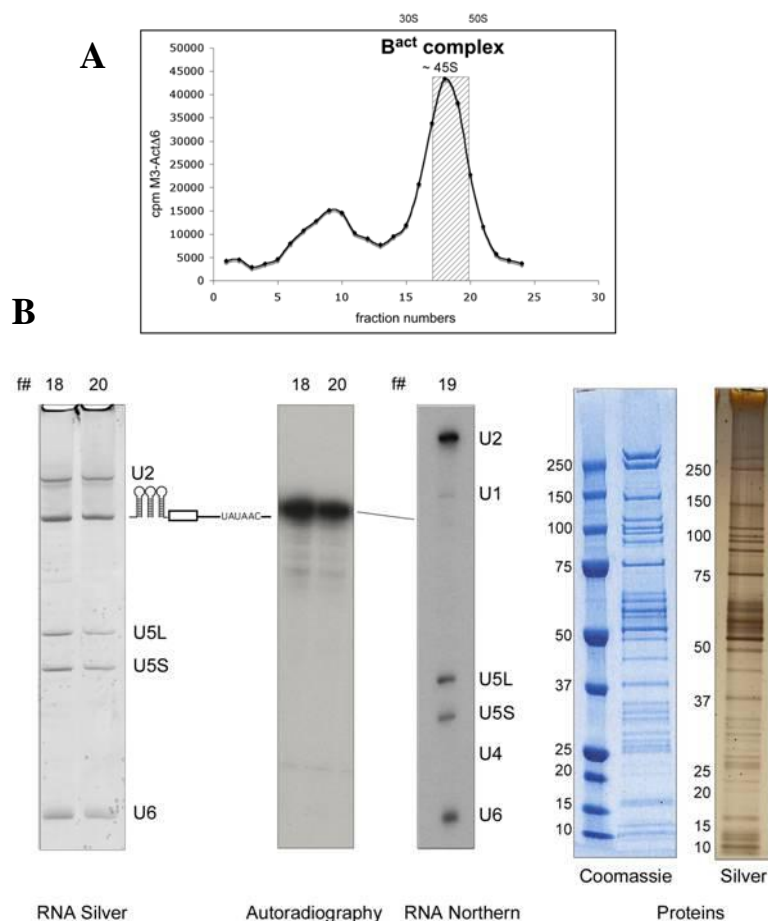


Figure 3.5: Characterization of the purified B^{act} complex. Upper (A): Profile of affinity-purified complex B^{act} (specific activity of 185 cpm/fmole) separated on a glycerol gradient centrifuged for 15 hours at 20.700 r.p.m. (58,257 g) in a Sorvall TH660 rotor. The radioactivity contained in each gradient fraction was determined by Cherenkov counting. Sedimentation coefficients were determined by analyzing the UV absorbance of fractions of a reference gradient containing prokaryotic ribosomal subunits. Lower (B): RNA from gradient fractions (#18-20), were separated by denaturing PAGE and visualized by silver staining, autoradiography and Northern analysis (fraction # 19). RNA identities are indicated on the right. Protein composition of purified complex B^{act}. Proteins were separated by SDS-PAGE and visualized by staining with Coomassie or with Silver, depending on the preparation.

Nearly stoichiometric quantity of unspliced pre-mRNA and U2, U5 and U6 snRNAs were detected by silverstaining, whereas U1 and U4 snRNAs were absent from this complex which is an indication that the isolated complex was the activated B^{act} complex and not the pre-catalytic B complex (Fig. 3.5 B).

3.3.4 Purification of the first step spliceosome complex C

Complex C was assembled on either M3-Act Δ 31 or M3-ActACAC pre-mRNA. The use of the two different constructs was done to determine whether additional factors were recruited to M3-ActACAC as compared to the shorter M3-Act Δ 31 pre-mRNA. To remove earlier pre-catalytic spliceosomal complexes like A, B and B^{act} complexes, we performed oligo-directed RNaseH cleavage immediately after the splicing reaction. RNaseH was not added since the yeast whole cell extract already contains this enzyme. The cleaving procedure was proofed in preliminary experiments with numerous oligos which covered the whole length of our actin pre-mRNA construct to optimize the cleavage; simultaneously, we obtained additional information about the accessibility of the pre-mRNA at the stage of the first step spliceosome (Fig.3.6 A). To control that our pre-catalytic complexes underwent digestion of their pre-mRNAs, we treated also our B and B^{act} complexes with the oligo for RNase H cleavage that we used for our C complex. We demonstrated by non-denaturing PAGE that the C complex was not affected by RNase H cleavage and that only the free pre-mRNA or pre-catalytic complexes were cleaved (Fig.3.7).

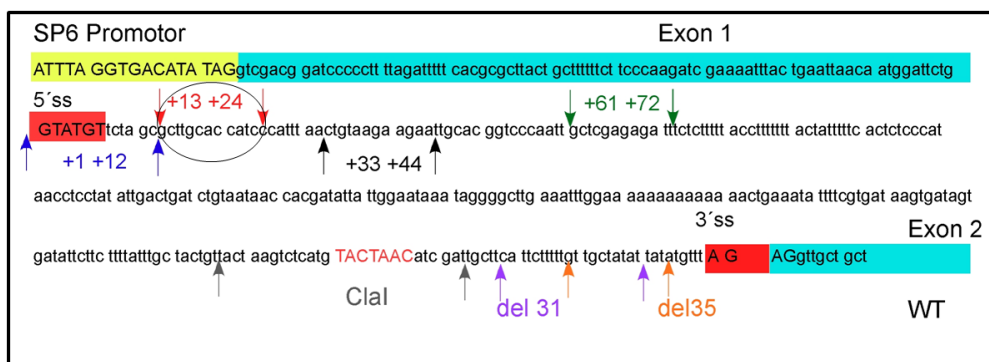


Fig. 3.6 A: Sequence of the actin wt pre-mRNA. The promoter sequence is indicated as a yellow box; both exons are shown in turquoise and the 5' and 3' SS are indicated as red boxes. The numbers stand for the region on the pre-mRNA complementary to the individual oligo. The black circle indicates the oligo used for the oligo-directed RNaseH digestion of actin wt pre-mRNA.

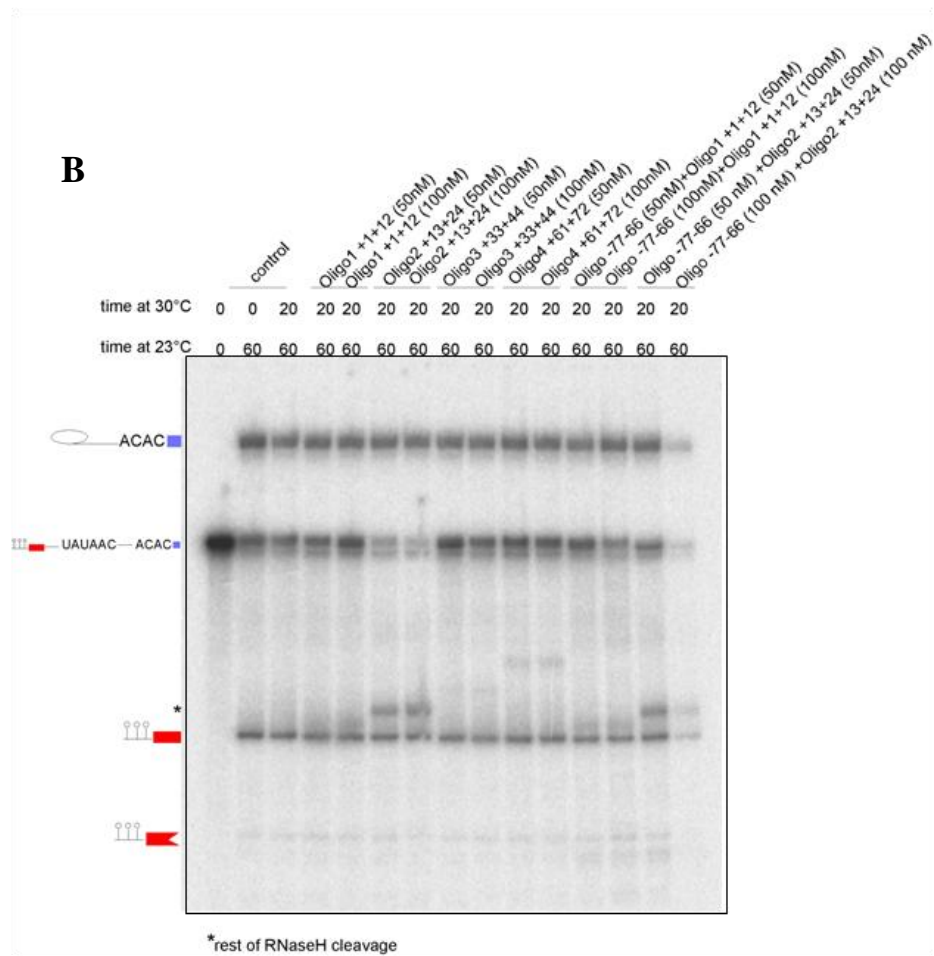


Figure 3.6 B: Test of various oligos for the oligo-directed RNaseH digestion of Actin wt pre-mRNA. RNA-PAGE of actin pre-mRNA after treatment with different oligos for directed RNase H cleavage. Sequence of the individual oligo is indicated above each lane, splicing intermediates are indicated schematically on the left. For details see text.

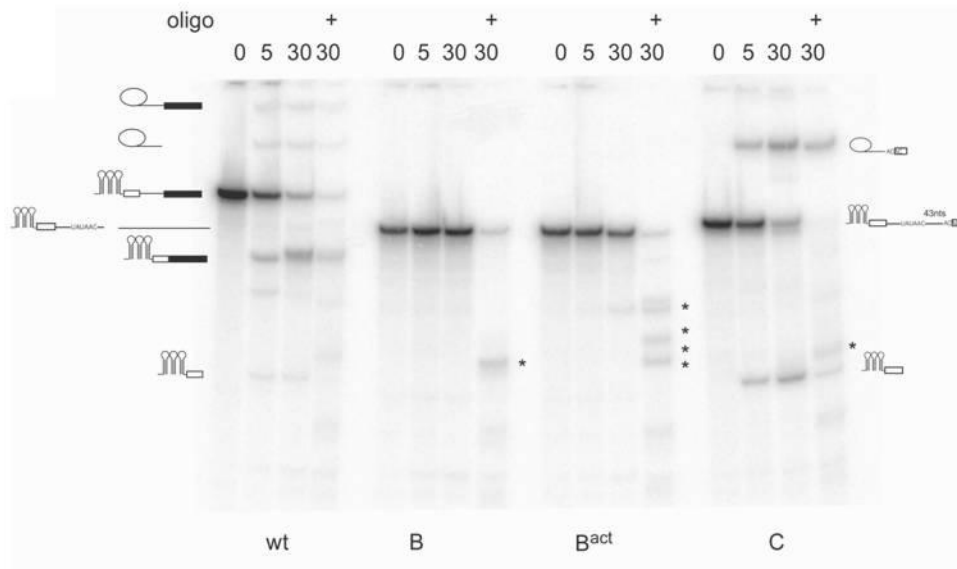


Figure 3.7: Oligo-directed RNaseH digestion of yeast B, B^{act} and C complexes.

Kinetics of *in vitro* splicing with M3-Actin wt, M3-Act Δ 6 and mutated at the 3'ss (see text for details). Splicing was performed at 2.0 or 0.05 mM ATP, in yeast whole cell extract for 0-30 min followed by oligo-directed RNaseH digestion for an additional 20 min at 30 C° (+oligo). RNA was analyzed by denaturing PAGE. Asterisks: RNaseH digestion products.

The cleaving procedure was carried out for 20 min at 30 °C with an oligo complementary to the downstream region of the 5'ss +13+24 (Fig.3.6; Methods).

The purification strategy for complex C was as described for the other complexes. Irrespective of which pre-mRNA was used (M3-Act Δ 31 or M3-ActACAC), complex C exhibited an S value of ~ 40 S and contained similar amounts of U2, U5 and U6 snRNA (see Fig.3.8). Denaturing PAGE revealed an excised 5' exon and intron-3'exon, which confirmed the isolation of the step 1 spliceosome. Quantitative analysis of the radioactive bands as revealed by RNA PAGE, silver staining and Northern blotting showed that only 5%-10% of unspliced pre-mRNA remained in the purified C complex after oligo-directed RNase H cleavage (Fig.3.8).

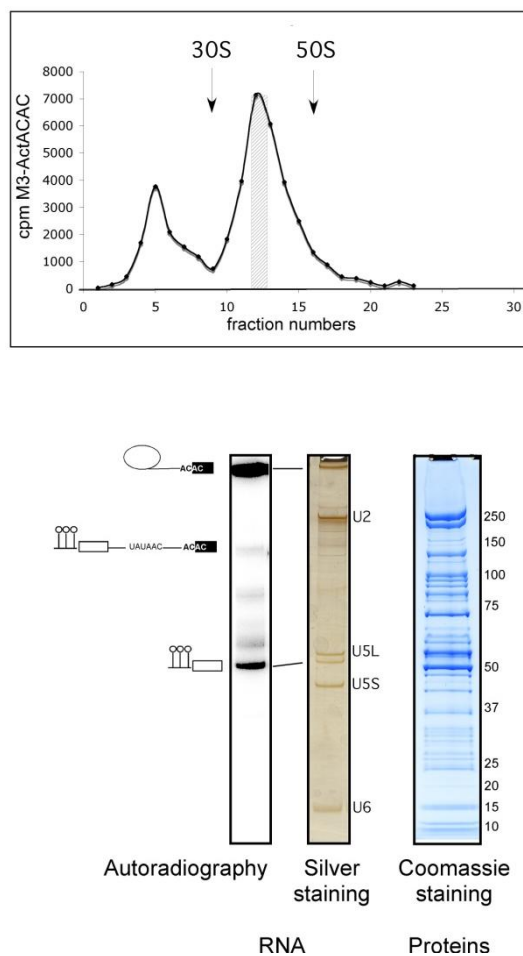


Figure 3.8: Characterization of affinity-purified C complex. Profiles of affinity-purified complex C (specific activity 200, 160 and 180 cpm/fmole, respectively) assembled on M3-Actin pre-mRNAs mutated at the 3' SS, respectively and separated on glycerol gradients. The radioactivity contained in each gradient fraction was determined by Cherenkov counting. Sedimentation coefficients were determined by analyzing the UV absorbance of fractions of a reference gradient containing prokaryotic ribosomal subunits. Splicing was performed in yeast whole cell extract for 60 min at 23 C°, followed by oligo-directed RNaseH digestion for an additional 20 min at 30 C° to allow RNaseH digestion of early spliceosomal complexes. RNA from gradient fractions 12-15 was separated by denaturing PAGE and visualised by silver staining and autoradiography. Splicing substrates intermediates and products as well as snRNAs identity are indicated on the right and left.

3.4 Protein composition of purified yeast spliceosomes

To determine the protein composition of the complexes isolated from the yeast *S.cerevisiae* via the three steps method described above, the peak fractions of the glycerol gradients of each complex derived from the TH660 centrifugation step were

prepared for denaturing SDS-PAGE and the proteins were visualized by Coomassie or silver staining. The Coomassie stained protein gels were subsequently identified by liquid chromatography-coupled tandem mass spectrometry (LC-MS/MS) and scored by the absolute number of peptides found in each preparation. MS analyses were repeated several times, with a minimum of two times for each complex. Proteins which we found only in one out of two or more preparations were considered as contaminants, while the majority of the proteins found in our preparations were reproducibly detected.

3.4.1 The proteome of the pre-catalytic B complex

The pre-catalytic B complex was isolated as described above. After the second centrifugation step in a Sorvall TH660 rotor, the peak fractions of the gradient were pooled and the sample volume was concentrated down to a volume of 500 μ l-350 μ l by drying under vacuum. Samples were precipitated with 2–4 volumes of ethanol 100%, washed with ethanol 70% and the pellet was resuspended in MS sample buffer. The protein sample was separated in 4–12% Bis-Tris-HCl (pH 7.0) NuPage polyacrylamide gels (Invitrogen) and stained with G-colloidal Coomassie Brilliant Blue. An entire lane of the Coomassie-stained gel was cut into 23 slices and proteins were digested in-gel with trypsin and extracted according to (Shevchenko, Wilm et al. 1996). The peptides extracted from the samples were analyzed in an LC-coupled ESI Q-ToF (Q-ToF Ultima, Waters) mass spectrometer under standard conditions. Proteins were identified by searching fragment spectra of sequenced peptides against the NCBI non-redundant database by using the search engine Mascot.

The proteins we found associated with the yeast pre-catalytic B complex revealed a set of ~ 60 proteins and is shown in Table 1. This set was comprised of all known U1- and U2 snRNP specific proteins (U1 snRNP: Prp39, Snu71, Prp40, Prp42, Nam8, Snu56, Snp1/U1-70k, Mud1/U1-A, Luc7/Luc7B1 and Yhc/U1-C; U2 snRNP: Rse1/SF3b130, Hsh155/SF3b155, Prp9/SF3a60, Cus1/SF3b145, Prp21/SF3a120, Prp11/SF3a66, Lea1/U2-A', Hsh49/SF3b49, Msl1/U2-B'', Rds3/SF3b14b and Ysf3/SF3b10). For the U5 snRNP we could detect the U5 specific proteins Prp8, Brr2, Snu114, Prp6 and Dib1. Lin 1 was not detected, because Lin1 is thought to associate only with free U5 snRNP and not together with the tri-snRNP that is

integrated into the B complex. Also all U4/U6 particle specific proteins were found in the B complex as well as the tri-snRNP specific proteins Snu66, Spp381 and Snu23. The RNA helicase Prp28 which is known to displace the U1 snRNA from the 5'SS to allow the formation of a duplex between the 5'SS and U6 snRNA was found in any of our preparations. By RNA-PAGE and Northern blotting we could also observe a slightly underrepresentation of the U1 snRNA (see Fig. 3.3 above). These observations led to the assumption that we isolated a B complex at the stage shortly after Prp28 has acted and from which U1 snRNA is already destabilized from the 5'SS.

In all of our B complex preparations we detected each of the three candidates of the *retention and splicing* complex (RES complex): Bud13, Pml1 and Ist/Snu17 which is consistent with previous studies showing that these proteins associate with the yeast spliceosome before the first step. Another group consisting of eight proteins already known to contribute to splicing is the NTC (Nineteen-complex, proteins associated with Prp19). All eight proteins were found in our purified B complexes. Former experiments indicated that the NTC is required for the catalytic activation of the spliceosome and is recruited after U4 release. Our data show that the NTC is already bound to the spliceosome at the stage of the pre-catalytic B complex, but is underrepresented compared to our Bact and C complexes (see below). Most of the NTC proteins found in yeast have human counterparts, which were also found associated with the human B complex (Deckert et al., 2006). The full set of the 60 proteins together with all the miscellaneous proteins found in the yeast B complex was already described in my Diploma thesis and will not be one of the main focuses of this work. The description of the yeast B complex should only give a brief insight into spliceosome assembly to understand better the transition from the pre-catalytic spliceosome to the activated B^{act} complex and the first step spliceosome, the C complex.

3.4.2 The proteome of the activated B^{act} complex

The method for analyzing the protein content of the purified yeast B^{act} complex was the same as for the B complex and the first step spliceosome. In comparison to the B complex, the proteome of the activated B^{act} complex shows dramatic differences in its

composition (Table 1). The changes in the organization of the proteome included mainly the loss of all U1- and U4/U6 snRNP specific proteins and also the U6 associated Lsm2-8 proteins. This observation is consistent with the published data which showed the destabilization of the Lsm2-8 proteins during activation of the spliceosome (Chan, Kao et al. 2003). The U5 proteins Prp6 and Dib1, all proteins specific for the tri-snRNP, plus Prp5 and Urm1 are slightly underrepresented but likewise present in B complex but not in B^{act}. In conclusion, ~ 35 proteins, more than half of the ~ 60 proteins found in complex B, are released or destabilized and then lost during purification. Proteins recruited to B^{act} which were not present in B complex included ~12 proteins, several of which are well-established splicing factors or were previously detected in the endogenous Cef1-associated complex (Ohi and Gould 2002). Among these are the NTC-related proteins, which are homologous to human proteins that either physically interact with Prp19 or CDCL5 in humans or are present in the human 35 S U5 snRNP. Two of these proteins are also part of the human Prp19/CDCL5 complex – Cwc15/AD002 and Prp46/PRL1 – and are already integrated into human B complex (Deckert, Hartmuth et al. 2006). Two additional proteins of the NTC, termed Bud31 and Ecm2, are homologous to the human Prp19-related proteins G10 and RBM22 (Makarova, Makarov et al. 2004). Another important result of the MS analysis of the protein content of the activated B^{act} complex was the remarkable number of peptides which was sequenced for the RNA helicase Prp2 and its binding partner Spp2. It is already known that both proteins are required prior to step 1. Both of them are recruited during B^{act} formation and their quantity is consistent with B^{act} being pre-catalytic. Indeed, Prp2 action is needed for catalytic activation of the spliceosome, which leads to its release. Other studies showed that another protein factor found in complex B^{act}, Yju2, is also needed for step 1 and is known to promote step 1 after Prp2 function (Liu, Chen et al. 2007). All of the step 2 factors were absent in complex B^{act}, except Prp17, a step 2 factor known to play an important role in step 1 of the splicing reaction (Sapra, Khandelia et al. 2008). In contrast, several well-established spliceosomal proteins known to act during step 2 of splicing were not found in B^{act}, as for example Prp22, Prp16, Slu7 and Prp18, suggesting that B^{act} is very pure. Indeed, this group of proteins is recruited at a later stage. In summary, the transition from the pre-catalytic B to the activated B^{act} complex involves a dramatic change in composition, in which more than 30 proteins

dissociate from the spliceosome, 12 new ones associate and eight, the NTC-complex, are stably bound. Thus, B^{act} is composed of ~ 40 proteins.

3.4.3 The proteome of the step1 spliceosome C complex

For the assembly of complex C, we used the M3-Act Δ 31 or the M3-ActACAC substrate. Both complexes have exactly the same protein composition (compare Table 1) and for both complexes we applied the three steps affinity-purification method. The evaluation of complex B^{act} and C reveals nearly the same protein content, only the number of peptides changes if one compares individual proteins. One prominent example is the RNA helicase Prp2 and its counterpart Spp2. Both show reproducibly a reduced number of peptides in complex C as compared to B^{act}. This observation is consistent with the findings of previous studies, Prp2 binds at the stage of the B^{act} complex and dissociates from the spliceosome concomitant with the first step of splicing (Kim and Lin 1996). Surprisingly, this dissociation was also observed for some of the members of the U2-associated, heteromeric SF3a complex and also for parts of the SF3b, like for example Rse1, Hsh155, Prp11 or Cus1, for which the peptide number decreased more than half. In comparison to Prp2 and the U2 associated proteins, the proteins of the U5 snRNP are present in equal amounts in B^{act} and in C complexes. The proteins associated with Prp19 exhibit a higher number of peptides in complex C which indicates a more stable integration in the spliceosome.

Proteins which are really characteristic for C complex and never found in complex B^{act} or B, are a set of nine proteins, Slu7, Prp18, Prp22, Prp16, Cwc23 and Cwc25, Ntr1 and Ntr2 and Prp43. The most prominent factors are the step 2 factors Prp22, Slu7 and Prp18. Prp17 was already mentioned to be present in the B^{act} complex, while Prp16 could only be detected by one peptide but only in complex C. For Prp16 we have hypothesized that it is only transiently associated with the spliceosome, so it might be that we stalled complex C after Prp16 action. Another possibility is that we purified an intermediate spliceosome stalled after step 1 and before step 2. We found two additional proteins in our C complex preparation, Cwc23 and Cwc25. At least Cwc25 is known to be essential for growth, but the precise function of both proteins was still unknown when I started my PhD work (Ohi and Gould 2002). The helicase Prp43 together with Spp382/Ntr1 and Ntr2 are also recruited at the stage of complex

C (Table 1). This is consistent with earlier observations that Spp382 and Ntr2 associate with Prp43 (forming the NTR complex) and thereby modulate its helicase activity (Tsai, Tseng et al. 2007). The NTR complex is associated with the spliceosome before step 2, but it acts later during the disassembly of the post-spliceosomal complex (Tanaka, Aronova et al. 2007). In summary, the biochemical composition of the spliceosome changes not only during early assembly steps, but also during the transition from B^{act} to C; although this compositional change is not as dramatic as that during the transition from B to B^{act}.

Yeast Protein name	Systematic Gene name	MW (kD)	Number of peptides sequenced in B, B ^{act} and C complex preparations						Penta-snRNP	Cef1 TAP	Human Protein name
			M3-Actin Δ6		M3-Actin Δ6		M3 Actin Δ31	M3 Actin ACAC			
			B #1	B #2	B ^{act} #1	B ^{act} #2	C #1	C #2			
Sm proteins											
B	YER029C	22.4	31	3	49	8	9	33	14	5	<u>B</u>
D1	YGR074W	16.3	22	4	3	5	5	10	8	1	<u>D1</u>
D2	YLR275W	12.8	26	9	27	7	10	6	5	3	<u>D2</u>
D3	YLR147C	11.2	14	4	3	10	6	8	5	2	<u>D3</u>
E	YOR159C	10.4	2	1	6	5	7	1	1		<u>E</u>
F	YPR182W	9.6	20	2	9	4	4	1	2	2	<u>F</u>
G	YFL017W-A	8.5	3	2	4	1	1	1	2	2	G
U1 snRNP proteins											
Prp39	YML046W	74.7	27	8		1			3		
Snu71	YGR013W	71.4	26	8	1	1			3		S164
<u>Prp40</u>	YKL012W	69.0	19	12	1	4			7		FBP11
Prp42	YDR235W	65.0	17	7					2		
Nam8	YHR086W	56.9	5	3	1	3			2		TIA1/TIAR
Snu56	YDR240C	56.5	6	2					4		
Snp1	YIL061C	34.4	18	1					5		<u>U1-70K</u>
Mud1	YBR119W	34.4	14	5	1			1	3		<u>U1-A</u>
Luc7	YDL087C	30.0	1		2				2		LUC7B1
Yhc1	YLR298C	27.0	5						2		<u>U1-C</u>
U2 snRNP proteins											
Rse1	YML049C	153.8	91	63	111	61	32	52	6	1	<u>SF3b130</u>
Hsh155	YMR288W	110.0	93	24	83	23	22	16	9	1	<u>SF3b155</u>
Prp9	YDL030W	63.0	70	25	66	45	14	12	7	2	<u>SF3a60</u>
Cus1	YMR240C	50.2	42	10	71	17	4	8	3		<u>SF3b145</u>

Prp21	YJL203W	33.0	50	4	35	16	5	14	13	2	<u>SF3a120</u>		
Prp11	YDL043C	29.9	30	5	25	22	2	9	11	1	<u>SF3a66</u>		
Lea1	YPL213W	27.2	28	3	47	11	22	17	10	6	<u>U2-A'</u>		
Hsh49	YOR319W	24.5	4	2	41	2	6	2	9		<u>SF3b49</u>		
Msl1	YIR009W	12.8	8		10	4	2	7	7	2	<u>U2-B''</u>		
Rds3	YPR094W	12.3	3		4	1					<u>SF3b14b</u>		
Ysf3	YNL138W-A	10.0	3	1	9	2	1	1			SF3b10		
U5 snRNP proteins													
Prp8	YHR165C	279.5	233	81	166	125	176	306	22	38	<u>220K</u>		
Brr2	YER172C	246.2	197	90	237	197	110	126	30	17	<u>200K</u>		
Snu114	YKL173W	114.0	66	54	159	51	113	130	18	24	<u>116K</u>		
Prp6	YBR055C	104.2	73	37		1	4	11	29		<u>102K</u>		
Prp28	YDR243C	66.6									<u>100K</u>		
Lin1	YHR156C	40.4									52K		
Dib1	YPR082C	16.7	10	1					5		<u>15K</u>		
U4/U6 snRNP proteins													
Prp31	YGR091W	56.3	27	11					12		<u>61K</u>		
Prp3	YDR473C	56.0	27	11					29		<u>90K</u>		
Prp4	YPR178W	52.4	27	14		1		2	12		<u>60K</u>		
Snu13	YEL026W	13.6	2						3		15.5K		
U4/U6.U5 snRNP proteins													
Snu66	YOR308C	66.4	39	14					15		<u>110K</u>		
Sad1	YFR005C	52.2							5		65K		
Spp381	YBR152W	34.0	26	6					3				
Prp38	YGR075C	28.0	21	8	1	1	2	3	7		<u>hPRP38</u>		
Snu23	YDL098C	23.0	33	8					13		<u>hSNU23/ZMAT</u> 2		
Lsm proteins													
<u>L</u> Sm4	YER112W	21.3	16	3		1			5		<u>L</u> Sm4		
LSm7	YNL147W	13.0	3	1					2		LSm7		
LSm8	YJR022W	12.4	3	1					4		LSm8		
<u>L</u> Sm2	YBL026W	11.2	8	4			2		2		<u>L</u> Sm2		
<u>L</u> Sm5	YER146W	10.4	2	1							LSm5		
<u>L</u> Sm3	YLR438C	10.0	1						2		<u>L</u> Sm3		
LSm6	YDR378C	9.4	5	1	1				2		LSm6		
Yeast Protein name	Systematic Gene name	MW (kD)	Number of peptides sequenced in B, B^{act} and C complex preparations								Penta-snRNP	Cef1 TAP	Human Protein name
			M3-Actin Δ6		M3-Actin Δ6		M3 Actin Δ31	M3 Actin ACAC	C				
			B #1	B #2	B^{act}	B^{act}	C						

					#1	#2	#1	#2			
RES complex											
Bud13	YGL174W	30.5	23	4	81	26	11	30		1	MGC13125
Pml1	YLR016C	23.6	6		14	5	1	3	5		<u>SNIP1</u> ? ^a
Ist3/Snu1 7	YIR005W	17.0	3		12	2	3	1	7	1	CGI-79 ? ^a
NTC/Prp19 complex											
Syf1	YDR416W	100.0	28	19	124	67	52	69	8	18	<u>hSYF1/XAB2</u>
Clf1	YLR117C	82.4	16	6	40	18	44	33	12	16	<u>CRNKL1</u>
Cef1	YMR213W	68.0	21	18	87	24	72	69	7	11	<u>CDC5L</u>
Prp19	YLL036C	56.6	49	31	235	50	195	150	13	17	<u>hPRP19</u>
Isy1	YJR050W	28.0	8	1	37	11	14	17	8	2	<u>KIAA1160</u>
Syf2	YGR129W	25.0	11	2	43	16	14	37	2	2	GCIP p29
Snt309	YPR101W	21.0	2	1	21	11	17	10	6	9	<u>SPF27</u>
Ntc20	YBR188C	16.0	11	2	8	1	2	11	3	4	
NTC related proteins											
Prp46	YPL151C	51.0	20	9	97	35	20	28	7	20	<u>PRL1</u>
Prp45	YAL032C	42.5	19	5	70	15	13	37	18	16	<u>SKIP1</u>
Ecm2	YBR065C	41.0			35	5	26	32	1	8	RBM22 ?
Cwc2	YDL209C	38.4			43	19	9	45	11	5	RBM22 ?
Cwc15	YDR163W	20.0			38	10	16	22		3	<u>AD-002/HSPC148</u>
Bud31	YCR063W	18.4			12	1	4	11	10	2	G10
Early splicing factors											
Prp5 ^b	YBR237W	96.4	10	5							hPRP5
Urn1 ^b	YPR152C	54.0	8	5							TCERG1 ^d
Known splicing factors											
<u>Prp2</u>	YNR011C	100.0			116	64	24	19			DDX16
Spp2	YOR148C	20.6			15	6	1	1		5 *	GPKOW/T54
Yju2	YKL095W	32.0			27	8	10	16		5	CCDC130
<u>Cwc21</u>	YDR482C	15.7			14	8	5	6		2	Srm300
Cwc22	YGR278W	67.3			48	17	33	67		2	KIAA1604
Cwc24	YLR323C	28.0			40	20	2	9		4 *	RNF113A
Cwc27	YPL064C	35.0			29	11	2	6		1	NY-CO-10
Cwc23	YGL128C	33.2					2	3		2	DNAJ A1 ? ^c
Cwc25	YNL245C	20.4					2	3		1	CCDC49
Step 2 proteins											
Prp17	YDR364C	52.0			24	10	14	36		5	hPRP17
Prp22	YER013W	130.0					24	68		2	<u>hPRP22</u>
Prp16	YKR086W	121.6						1			hPRP16
Slu7	YDR088C	44.6					2	17		1	<u>hSLU7</u>
Prp18	YGR006W	28.4					7	12			hPRP18

Disassembly proteins ^b										
Prp43	YGL120C	87.6					9	2		hPRP43
Spp382	YLR424W	83.0					2	4		TFIP11
Ntr2	YKR022C	36.6					2			
CBP proteins										
Sto1	YMR125W	100.0	7							<u>CBP80</u> ^d
Cbc2	YPL178W	24.0	1				1			CBP20 ^d

Table 3.1: The table shows the protein content of spliceosomal complexes isolated from the yeast *S.cerevisiae*. Proteins were identified by LC-MS/MS after three steps purification and separation by PAGE. Proteins identified in two out of two preparations are shown. Numbers represent the absolute number of peptides sequenced for a protein found in a particular preparation (i.e., #1 or #2). The table contains information about the *S.cerevisiae* protein, the systematic gene name, the calculated molecular weight in kDa, and the concentration in pmols of each complex are also included (Ohi and Gould 2002);(Stevens, Ryan et al. 2002). The last column contains the name of the human protein to aid comparison with previous studies of human spliceosomal complexes. Proteins are grouped in organizational and/or functional subgroups. Prp28, Lin1 and Sad1 were not detected by MS and are included for completeness.

^aHomologs could not be assigned unambiguously on the basis of BLAST data.

^bNever detected in yeast spliceosomal complexes.

^cExtensiv homology between protein family members prevents assignement of *S.cerevisiae* homologs on the basis of BLAST data.

^dHuman homolog previously detected in one or more human spliceosomal complex.

(Table adapted from Molecular cell Paper,(Fabrizio, Dannenberg et al. 2009)

3.5 Electron microscopy of Yeast spliceosomes

To obtain the insights into the structure and the rearrangements of yeast spliceosomes during the transition from B to B^{act} to C complexes, we purified complexes as described above. After two steps purification we loaded the isolated complexes onto a second glycerol gradient containing glutaraldehyde to fix the particles (Kastner, Fischer et al. 2008). The gradient was collected from the bottom with a gradient collector (see Methods). Particles from the peak fractions were then negatively stained and analyzed by EM. To obtain a better resolution, the single-particle images were classified, and members of each class were averaged. Results are summarized in Figure 3.9, which shows for each particle a typical EM field (left), a gallery of class

averages (middle) and interpretative sketches (right). All three complexes showed monodisperse distributions with a particle size of approximately 40 nm.

3.5.1 Electron microscopy of yeast spliceosomal complexes **Complex B**, **B^{act}** and **C**

The **B complex** shows in most projection classes a triangular or rhombic shape (uppermost block). The most noticeable structural feature of the predominant classes (Fig. 3.9, columns 1 and 2) is an almost straight element, ~30 Å long and 7–10 Å wide; in the orientation shown, this element runs from the bottom of the image (foot) to the upper left (stump). Classes looking approximately like mirror images of the main form are also found but rarely (Fig. 3.9, column 3). Other more frequently seen forms include those shown in columns 4–6. These forms could be attributed to side-on views of complex B.

Complex B^{act}. The images analyzed from the B^{act} complex were very different from those of B. Most classes show a protruding domain resembling that of the foot of complex B (shown pointing downwards in the representations of B^{act}) (Figure 3.9). However, the main body appears more compact. The most frequent images of B^{act} (Fig. 3.9, middle block, columns 1 and 2) display a slightly asymmetrical main body with outlines running left and right at different angles, such that the left appears steeper than the right. A more elongated accumulation of stain is found parallel to the left flank, while on the right there is a point-like accumulation of stain. B^{act} also shows relatively frequent symmetric (Fig. 3.9 column 3) and asymmetric (Fig. 3.9, column 4) variants of the main form. Further typical images of B^{act} are shown in columns 5 and 6 (Fig. 3.9). On the left-hand side, these show a pronounced axis while the right-hand side appears as a wing (Fig. 3.9, column 6).

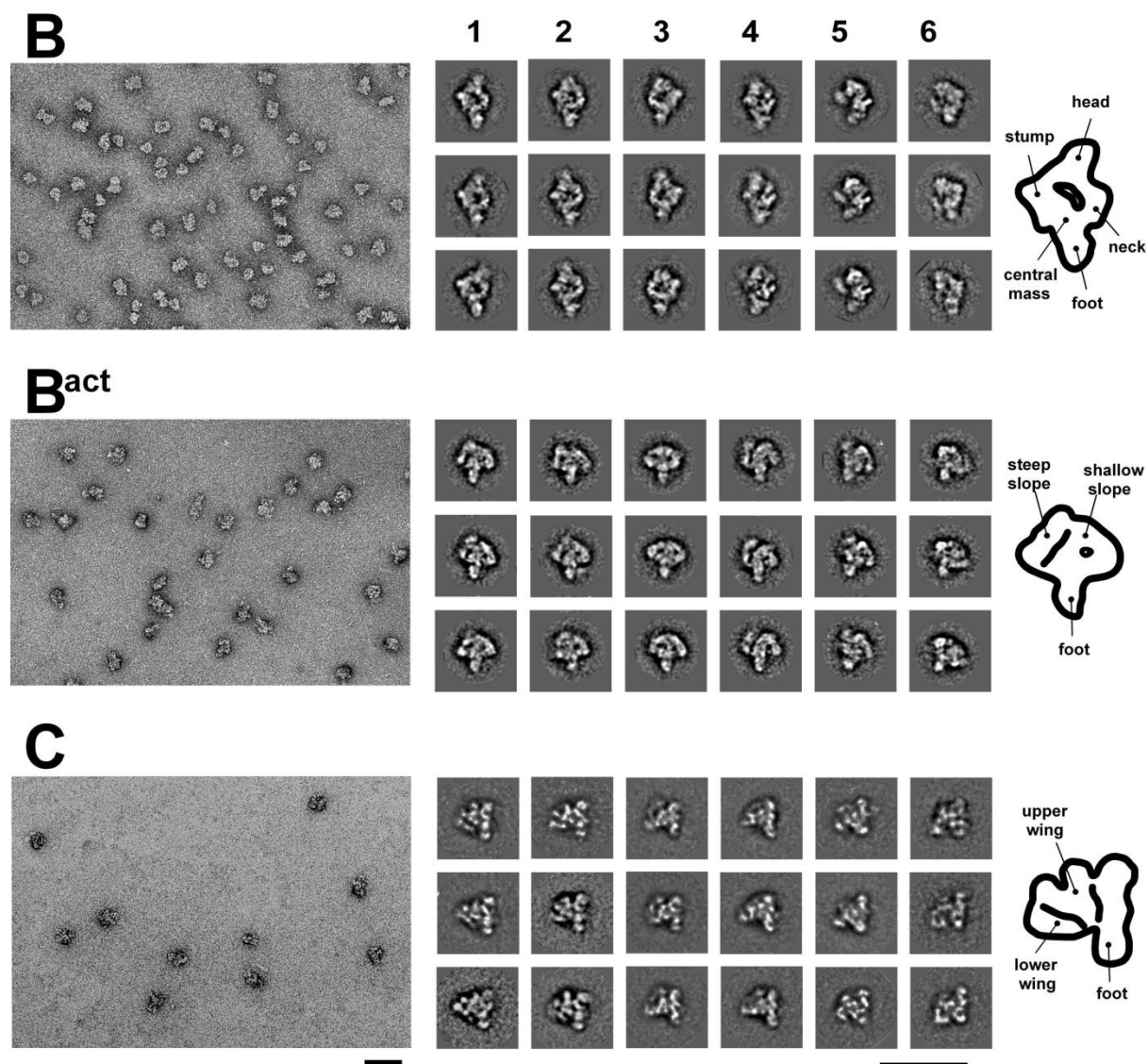


Figure 3.9: Negative stain Electron Microscopy of yeast spliceosomes. Overview of negatively stained samples is shown in the left panels. Representative class averages are shown in the galleries in the middle (numbered 1 to 6), starting with the most frequently observed class, for which a schematic drawing is shown on the right. All three particles display a short protuberance that in the class averages is shown pointing downward (foot). Some structural features are labeled. Names introduced by Boehringer (Boehringer, Makarov et al. 2004) for the human B complex are used also for the yeast B complex. A small fraction of images typical of the most frequent classes of complex B^{act} was also detected in the C complex preparation. Scale bars, 50 nm (Fabrizio, Dannenberg et al. 2009)

Complex C. The C complex was assembled on M3-ActACAC and exhibits also in most image classes an approximately straight element (Fig. 3.9, lowest block). Here, the axis is always on the right-hand side of the particle in the “foot-down” orientation (Fig. 3.9, columns 1–4). Less frequent forms include those shown in columns 5 and 6

(Fig.3.9). In summary, the image classes of complex C appear less compact than those of B^{act}. Thus, the analysis of the EM images of the three purified complexes reveals structures of about the same size but with quite different morphology. The most pronounced structural differences are seen between B and B^{act}. Complex B^{act} and C also exhibit differences, but some views possess similar main features.

3.6 Isolation and characterization of early spliceosomal complexes isolated from the Yeast *S. cerevisiae*

As described above, we have purified *in vitro* assembled spliceosomal complexes B, B^{act} and C from yeast and revealed that yeast spliceosomes contain fewer proteins than metazoans and that each functional stage is very homogeneous and well suited for three dimensional structure analyses. Next, we wanted to obtain more insights into the very early steps of spliceosomal assembly. Little is known about the compositional organization of early spliceosomal complexes harboring the U1 and U2 snRNPs, which together with several non-snRNP proteins are involved in juxtaposing the functional sites of the pre-mRNA. Here, we have stalled yeast spliceosomes at the commitment complex (CC) stage prior to pre-spliceosome (A complex) formation. Therefore we used the temperature-sensitive (ts) yeast strain carrying the mutant of the Prp5 helicase, termed *prp5-1*, where the helicase Prp5 can be heat-inactivated (Ruby, Chang et al. 1993) (see Introduction/Helicases). Previous studies have shown that Prp5 is thought to play an important role for the stable association of the U2 snRNP to form the pre-spliceosome. The stable integration of U2 is the first ATP-dependent step in the splicing cycle and requires the helicase Prp5 (O'Day, Dalbadie-McFarland et al. 1996)

Recognition and pairing of the correct 5', 3' splice sites (SS) and branch point sequence (BPS) of a pre-mRNA are critical events that occur early during spliceosome assembly in metazoans as well as in yeast. Our aim was to investigate in more detail the early events and to obtain more knowledge about the transition from commitment complex to complex A. In addition, it would be interesting to determine how the Prp5-mediated hydrolysis of ATP, promotes the stable association of the U2 snRNP in the pre-spliceosome. Therefore we used our well-established *in vitro* assembly and three steps purification system.

3.6.1 Inactivation or removal of Prp5 stalls the spliceosome assembly at the stage of the CC complex

To stall the spliceosomal assembly at a very early stage of the assembly pathway and prior to the pre-spliceosomal A complex we used extracts made from the yeast temperature-sensitive (ts) mutant strains of Prp5 (*prp5-1*).

After testing the *prp5-1* ts-mutant strains (kindly provided by the lab of John Abelson) for temperature sensitivity, yeast whole cell extract was made according to the protocol (Dannenberg, Fabrizio et al. 2012); see Methods). For the assembly of early complexes we used our wt M3-Act pre-mRNA substrate, ^{32}P -labeled, and whole cell extract made from the ts-strain *prp5-1* and a concentration of ATP of 2.0 mM. After heat-inactivation of the extract at 35°C, we incubated the reaction with the pre-mRNA substrate at 23°C for 50' and incubated the sample under standard splicing conditions. Subsequently, we up scaled the experiments and purified the complexes obtained. The purification strategy was the same as for the B, B^{act} and C complexes.

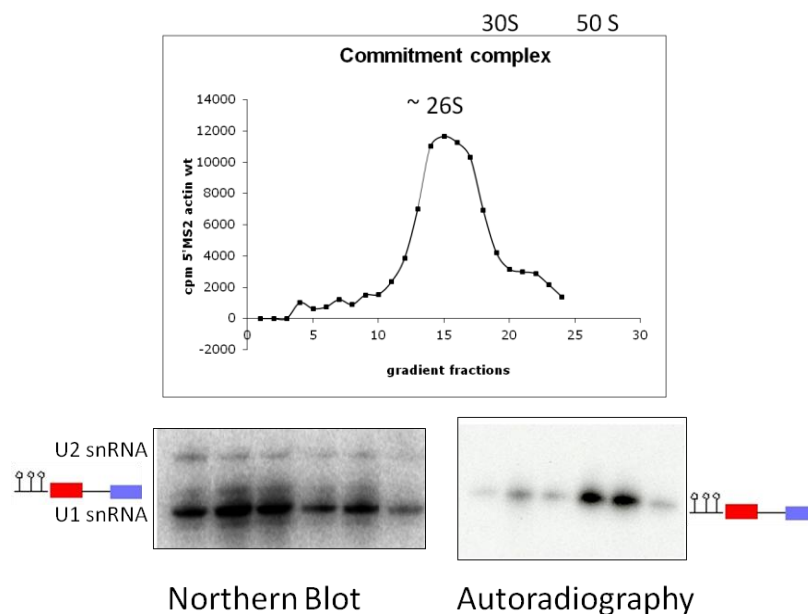


Figure 3.10: Northern Blot and autoradiography of the RNA-PAGE of the commitment complex. Profile of affinity-purified Commitment complex separated on a glycerol gradient centrifuged for 3 hours at 60.000 r.p.m. in a Sorvall TH660 rotor. The radioactivity contained in each gradient fraction was determined by Cherenkov counting. Sedimentation coefficients were determined by analyzing the UV absorbance of fractions of a reference gradient containing prokaryotic ribosomal subunits. Lower (B): RNA from gradient fractions (#14-18), were separated by denaturing PAGE and visualized by autoradiography and Northern Blot analysis. RNA identities are indicated on the right.

The gradient profile of the distribution of the radioactive labeled pre-mRNA in the complex, compared to co-sedimentation of 30 S and 50 S ribosomal subunits, revealed a sedimentation coefficient of ~26S for our stalled complex. RNA PAGE and Northern blot analysis of the purified complex showed that it contained exclusively pre-mRNA and U1 snRNPs, thus this complex had the characteristics of a CC (Fig. 3.10).

Following these preliminary studies, the protein composition of the isolated complexes has been determined by mass spectrometry. The mass spectrometry data revealed a full set of U1 snRNP proteins, all Sm proteins and the early protein factors Msl5 and Mud2, which indicated that our complex was a commitment complex 2 (CC2) (Fig. 3.11). Thus, our complexes stalled at the stage of the early commitment complex, were stable for mass spectrometry analysis. These complexes might be well suited for further studies, i.e. reconstitution of the pre-spliceosomal A complex or for further investigations concerning the role of the ATP-driven stable association of the U2 snRNP with the spliceosome.

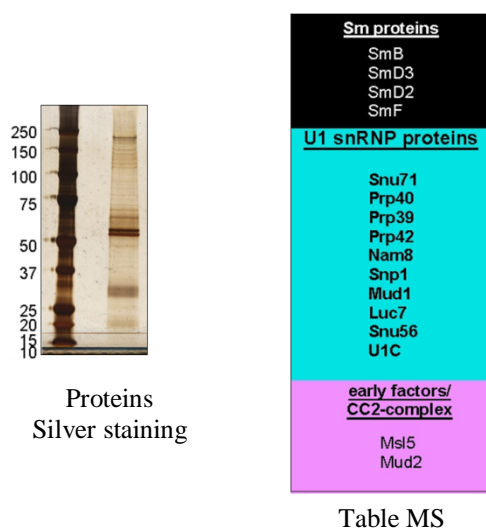


Figure 3.11: Proteins of the Commitment complex. On the left: Proteins of affinity-purified commitment complexes were analyzed by PAGE and silver staining. On the right: Table of Proteins found in our preparations of commitment complexes isolated from yeast as revealed by MS.

If one compares the protein content analyzed by silver or coomassie stained gels of the early CC complex with the one of B and B^{act} complexes (see Figures 3.3 and 3.5

above), one can observe a dramatic difference in the number of proteins which are associated with each individual complex.

Yeast Protein name ^a	Systematic Gene name	MW (kD)	Number of peptides sequenced in Prp5-1 inactive and ATP depleted complex preparations ^b		Description	Human protein name
			Prp5-1 inact. #1	Prp5-1 ATP depl. #1		
U1snRNP proteins						
Snu71	YGR013W	71.4	8			S164
Prp40	YKL012W	69.0	6			PRP40B
Prp39	YML046W	74.7	5			PRPF39
Prp42	YDR235W	155.0	5			PRPF39
Nam8	YHR086W	57.0	1			TIA1/TIAR
Snp1	YIL061C	34.4	2			U1-70K
Mud1	YBR119W	34.8	3			U1-A
Luc7	YDL087C	30.2	3			LUC7B
Snu56	YDR240C	56.4	2			
Yhc1	YLR298C		-			U1-C
Sm proteins						
SmB	YER029C	22.4				B
SmD2	YLR275W	12.8	1			D2
SmD3	YLR147C	11.2				D3
SmF	YPR182W	9.7				F
Commitment complex associated proteins						
Msl5		53.0	21			BBP1
Mud2	YKL074C	60.0	17			U2AF65
Poly (A+) RNA-binding protein, involved in mRNA export from the nucleus to the cytoplasm						
Hrb1/To m34	YNL004W	49.1	2	2	export of mRNAs	PABPC4L
Npl3	YDR432W	45.4	2		export of mRNAs	SFRS4
Cft1		15.3	3	4	involved in poly(A) site recognition and required for both pre-mRNA cleavage and polyadenylation	
Pab1		64.5	3	30	Poly(A) polymerase, one of three factors required for mRNA 3'-end polyadenylation	
Pta1		27.6	1			
Fip1		35.8	3		Polyadenylation factor	
Pat1	YCR077C	88.5	9	25	Polyadenylation factor	PATL1

Table 3.2

Peptides sequenced in the CC preparations obtained from yeast extracts heat-inactivated for Prp5-1 (inactive) and additionally ATP depleted. Proteins were identified by LC-MS/MS after three steps purification and separation by PAGE. Numbers represent the absolute numbers of peptides sequenced for a protein found in each preparation. The table contains information about the *S.cerevisiae* protein, the systematic gene name, and the calculated molecular weight in kDa. The last column contains the name of the human protein to aid comparison with previous studies of human spliceosomal complexes. Proteins are grouped in organizational and/or functional subgroups.

Additionally, to investigate the role of ATP at the early steps of spliceosomal assembly and to see whether there is a difference in the recruitment of spliceosomal factors to the early complex, we repeated the experiments with ATP-depleted whole cell extracts made from functional, not heat-inactivated *prp5-1* strains. As revealed by MS, no changes in peptide numbers sequenced for proteins recruited to early spliceosomes were detected when the extract was ATP-depleted (Table 2).

3.7 Investigation of the protein rearrangements at the catalytic core of the spliceosome as revealed by dual color FCCS

In the first part of our work we isolated spliceosomal complexes from the yeast *S.cerevisiae* and obtained important information of the proteome and the three dimensional structure of spliceosomal B, B^{act} and C complexes. Such a characterization of the protein content of spliceosomal complexes was done for the first time and gave important insights of the protein dynamics at the core of the spliceosome during assembly and step 1 catalysis. To identify the factors recruited at distinct stages of spliceosome assembly, has helped us to understand better the mechanistic aspects of the catalytic activation and the process of pre-mRNA splicing in general. Our MS analysis showed a dramatic change of the protein factors which were recruited and released during catalytic activation and spliceosome assembly.

While the studies summarized above provide initial indications of the dynamics of the spliceosome's protein composition during its catalytic activation, they provide only little information about the degree of weakening or stabilization of the binding affinity of individual proteins or about the order in which proteins are bound to the spliceosome or dissociate from it. For example, there is disagreement in the literature as to the binding behavior of the U2 SF3a/b proteins during the catalytic phase of the yeast spliceosome. Depending on the conditions under which the catalytically active spliceosomes are isolated, these proteins are reported to be “completely absent” to “stoichiometrically present”. In view of our observation of the reduced peptide numbers sequenced for the U2 proteins in our affinity-purified first step spliceosomes, as compared to the B^{act} and B complexes, we wanted to learn more about their binding behavior during catalytic activation and first step of splicing. Indeed, our previous results led to the question whether the U2 SF3a/b proteins are just

destabilized or even released from the spliceosome during the catalysis of the first step of the splicing reaction. To address this and additional questions, we applied the technique of dual color Fluorescence-cross correlation spectroscopy (dcFCCS) to study the dynamics of protein factors during the catalytic activation of the spliceosome mediated by Prp2 helicase. DcFCCS had to fulfill some important properties, for example it should allow us to measure the dynamics of the spliceosome in solution, i.e. in thermodynamic equilibrium and it should deliver quantitative data about the protein factors of interest.

The dcFCCS technique is an optimal method to study the dynamics of spliceosomal protein recruitment and dissociation, because i) it is a versatile and very sensitive method and requires sample concentrations in the low nM range, ii) it allows real time measurements in solution and in thermodynamic equilibrium and iii) provides quantitative data and is suitable for the elucidation of dissociation constants. The biochemical set up for using dcFCCS (reviewed in (Haustein and Schwillle 2007)) was already well established in our laboratory by Dr. Peter Odenwalder and Dr. Thomas Ohrt and the technical setup for dcFCCS was done in collaboration with Prof. Jorg Enderlein and Mira Prior, from the III. Institute of Physics, University of Gottingen.

First we applied a strategy to stall the spliceosome assembly at the B^{act} complex using the *prp2-1* strain. As demonstrated by the work of Kim and Lin (Kim and Lin 1996) the Prp2 helicase functions before the first step of splicing and can be heat inactivated in the temperature sensitive strain *prp2-1*. As a result, the spliceosome assembly can be stalled at the stage of an activated, but not yet catalytically active complex. In the work of Warkocki et al., 2009 an *in vitro* reconstitution system was established in our laboratory using this temperature-sensitive mutant of the RNA helicase Prp2 and the M3-Act wt substrate, to investigate the role of Prp2 in catalytic activation (Warkocki, Odenwalder et al. 2009). It could be demonstrated that B^{act} spliceosomes stalled prior to the first step by inactivating Prp2 could be purified. The protein composition of these complexes, termed B^{actΔPrp2}, was characteristic for spliceosomes which have not yet undergone first step and are thus pre-catalytic. Importantly, it was shown that the complexes were able to catalyze efficient step 1 when supplemented with recombinant Prp2, Spp2 and first step factor Cwc25 and step 2 when supplemented with Prp16, Slu7/Prp18 and Prp22 in the presence of ATP (Warkocki, Odenwalder et al. 2009).

Second, we chose proteins of interest, which were suitable for the investigation of the compositional dynamics of the spliceosome during conversion from the B^{act} to the B* complex (adapted from Warkocki et al, 2009), i.e. the proteins Cwc24, Cwc27, Yju2, Bud 13, a factor of the RES complex and the U2 snRNP-associated SF3a factor Prp11 and SF3b factor Cus1. The majority of these factors are recruited to the spliceosome during its activation (see Table 1).

3.8 Generation of doubly labeled spliceosomes for dcFCCS measurements

Our experimental strategy is outlined in Figure 3.12. The (stable) core spliceosome was tagged with the red fluorescent dye Atto647N at the 5' end of actin pre-mRNA. For this purpose, a wild-type actin pre-mRNA that included three binding sites for MS2 phage coat protein upstream of the first exon (M3Act) was prepared by transcription *in vitro* with T7 RNA polymerase in the presence of a 10-fold molar excess of guanosine-5'-O-monophosphorothioate (5'-GMPS) over unmodified GTP. The gel-purified pre-mRNA was then allowed to react with a 100-fold excess of Atto-647N maleimide, whereby the 5'-terminal phosphorothioate group of the M3Act reacted with the C=C-double bond of the maleimide group of the dye, forming, almost quantitatively, the stable thioether product Atto647N -M3Act (see Methods; (Ohrt, Prior et al. 2012)). We confirmed that Atto647N-M3Act was as active in a splicing assay *in vitro* as unmodified M3Act pre-mRNA (data not shown, experiment done by Dr. Peter Odenwalder from our laboratory).

The individual proteins were genetically fluorescently labeled by constructing yeast strains (in collaboration with Dr. Thomas Ohrt and Dr. Patrizia Fabrizio; see Methods; (Ohrt, Prior et al. 2012)) that expressed the protein of interest with a C-terminal EGFP (enhanced green fluorescent protein) fusion domain on the basis of the temperature-sensitive *Prp2-1* strain, containing the mutated ATPase Prp2 which is needed to stall the spliceosome assembly at the stage of B^{act} (i.e., B^{act} Δ Prp2) (Fig. 3.12). The following spliceosomal proteins were expressed stably as EGFP fusion proteins: Cus1, Prp11, and Bud13 (members of the SF3b, SF3a, and RES protein complexes, respectively), and Cwc24, Cwc27 and Yju2. All constructed strains grew like the unmodified strain *prp2-1*. Next we checked whether the tagged proteins and the labeled RNA substrate were able to assemble spliceosomal complexes in our *in vitro*

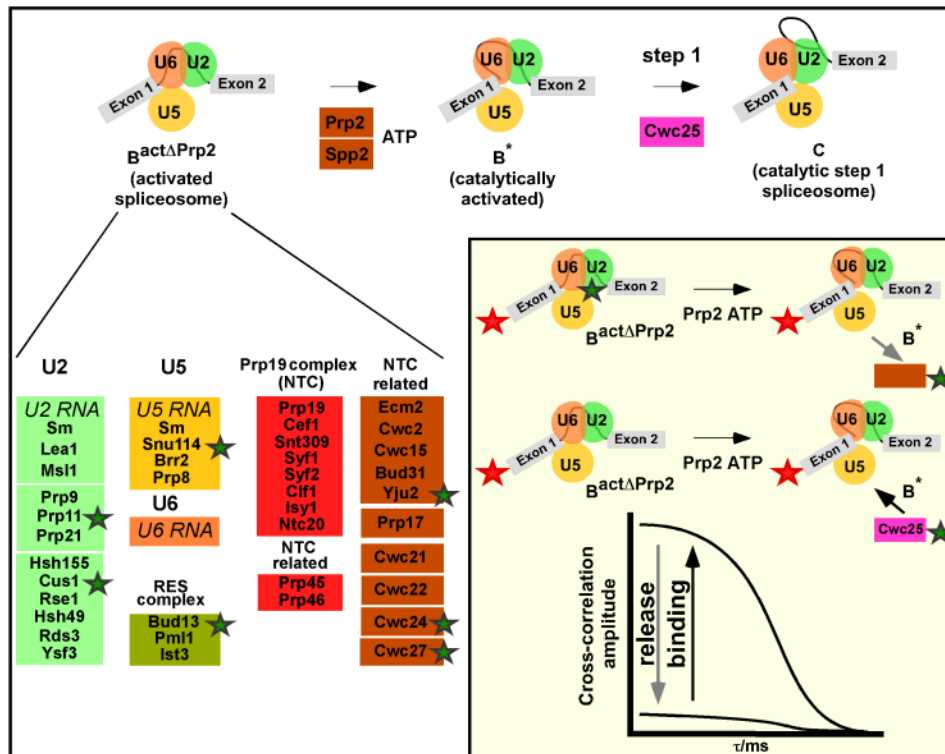


Figure 3.12: Experimental design and example of data. The Prp2-deficient spliceosomal complex $B^{\text{act}\Delta\text{Prp2}}$ (stalled through the inactivation of Prp2) is catalytically activated by the addition of Prp2 together with Spp2 and ATP. This leads to complex B^* , which on binding the step1 factor Cwc25, catalyses the the first step of splicing and forms the C complex. U2/5/6 snRNPs are shown as circles. The composition of the activated spliceosome is shown underneath; green stars indicate the spliceosomal proteins that were tagged with EGFP. (Inset) Release or recruitment of an EGFP-labeled protein (green star) from/to the spliceosome (carrying Atto647N, red star). The cross-correlation amplitude at short correlation time t is proportional to the amount of doubly labeled spliceosomes (adapted from (Ohrt, Prior et al. 2012)).

reconstitution system. Therefore we used the labeled RNA substrate Atto647N-M3-Act wt together with the different yeast whole cell extracts made from the constructed EGFP strains in comparison with unlabeled substrate or *prp2-1* extracts. After assembly and separation of the $B^{\text{act}\Delta\text{Prp2}}$ complexes by glycerol gradient centrifugation, the pooled peak fractions from the gradient were loaded on an affinity-selection column containing amylose beads. The bound complexes were washed one time with G-150 buffer (containing 150 mM KCl) and two times with G-75 (containing 75 mM KCl) and were subsequently eluted with 20 mM Maltose. For real-time dcFCCS measurements, reactions were carried out in a final volume of 60 μl

with a final complex concentration of 1.1 nM. The eluted fractions were supplemented with ten times excess of recombinant proteins and instead of the 10x rescue mix (used for reconstitution on beads), the reaction conditions were only adjusted to final concentrations of 2.5 mM MgCl₂ and 2 mM ATP (or other analogues) in buffer G-75 in a final volume of 60 μ l. The reactions were incubated at 23°C for 45 min and subjected subsequently to dcFCCS measurement. Indeed, all EGFP-tagged extracts and substrates were able to form B^{act Δ Prp2} spliceosomes and all tested preparations led to equal amounts of spliceosomal particles stalled prior to first step of splicing. Even all purified complexes were able to perform first step when supplemented with recombinant proteins required for the activation and for the first step of splicing.

3.8.1 Stability of the binding of EGFP fusion proteins to the B^{act Δ Prp2} complex under dcFCCS conditions

First we performed some preliminary experiments to set up our dcFCCS conditions. For dcFCCS measurement our complexes had to fulfill two important requirements (i) they had to be stable at least for ~ 3 h and (ii) we had to avoid the aggregation of our complexes during dcFCCS measurement. Toward this goal, we used the well-known protein Snu114. Snu114 is a GTPase that remains stably bound to the spliceosome during the whole splicing cycle (Bartels, Urlaub et al. 2003). We found that the B^{act Δ Prp2} complexes which contained the Snu114-EGFP fusion protein showed constant high cross-correlation between the green label (protein) and the red label (RNA), Fig. 3.13, column 1, indicating that the B^{act Δ Prp2} complexes do not dissociate under the conditions used for dcFCCS. When we induced the catalytic activation of our Snu114-EGFP-B^{act Δ Prp2} complexes by incubating them with recombinant Prp2/Spp2 proteins plus 2.0 mM ATP for 45 min at 23°C, we observed an almost quantitative conversion (>90%) of the 45 S B^{act Δ Prp2} complex to the slower migrating 40 S B* complex (see Cwc24-EGFP experiments; Fig.3.17, shown for Cwc24-EGFP complexes and also demonstrated for unlabeled spliceosomes in (Warkocki, Odenwalder et al. 2009)).

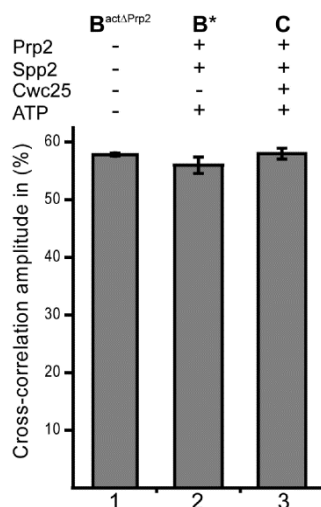


Figure 3.13: Binding behavior of Snu114-EGFP fusion protein to the spliceosome analyzed by dcFCCS. Affinity-purified $B^{\text{act}\Delta\text{Prp2}}$ complexes assembled on Atto647N-M3Act, carrying Snu114-EGFP (column 1), were complemented with Prp2, Spp2, and ATP (column 2) and Cwc25 (column 3). After incubation (45 min at 23°C; see Methods), dcFCCS measurements were then performed at complex concentrations of 1.0 nM. Cross-correlation amplitudes derived from two independent preparations are shown for each complex. Error bars indicate the standard deviation from two independent measurements.

As also shown in Fig. 3.13, column 2 the activation of the spliceosome and the conversion from the $B^{\text{act}\Delta\text{Prp2}}$ complex to the B^* complex had no effect on the binding behavior of Snu114-EGFP to the spliceosome. Even addition of Cwc25, which results in the first step spliceosome showed no alteration of the association of Snu114-EGFP with pre-mRNA (Fig. 3.13, column 3) and we observed still a high level of cross correlation between the green label and the red Atto 647N labeled pre-mRNA. The results indicate that Snu114-EGFP remains stably bound in the B^* and C complex under non-stringent conditions, i.e. low salt (75 mM KCl).

To determine the boundary of the stability Snu114-EGFP with the spliceosomal complexes we performed additional salt treatment experiments by increasing the KCl concentration in our experiments for both, $B^{\text{act}\Delta\text{Prp2}}$ and for B^* complexes. Fig. 3.14 shows that up to a concentration of 300 mM KCl we observed high cross correlation and Snu114-EGFP still remained bound to the complexes. By increasing the salt concentration up to 500 mM KCl, dcFCCS measurement was no longer possible

because of precipitation and aggregation of the complexes on the cover slide used for dcFCCS measurement (data not shown, demonstrated by the work of Dr. Peter Odenwalder from our laboratory).

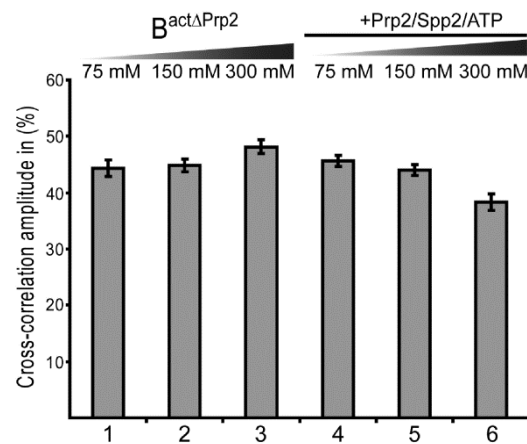


Figure 3.14: Salt-resistance of Snu114-EGFP binding to the spliceosome during catalytic activation. Affinity-purified $B^{\text{act}\Delta\text{Prp2}}$ complexes assembled on Atto647N-M3Act, carrying Snu114-EGFP (columns 1–3), were complemented with Prp2, Spp2, and ATP (columns 4–6). After the standard incubation, increasing concentrations of KCl were added to the samples, which were then subjected to dcFCCS measurements.

Our experiments demonstrated that Snu114-EGFP remained stably associated to the spliceosome even after catalytic activation and high salt conditions as also postulated for native Snu114 (Bartels, Urlaub et al. 2003). In summary, we demonstrated that our complexes were stable enough for dcFCCS measurements after Prp2-mediated activation of purified complexes.

3.8.2 Cwc24 and Cwc27 leave the spliceosome during Prp2-mediated catalytic activation under near-physiological conditions

After the pilot experiments done with our Snu114-EGFP- $B^{\text{act}\Delta\text{Prp2}}$ complexes, we investigated the changes in the binding behavior of Cwc24 upon Prp2-mediated activation. Therefore we first isolated the Cwc24-EGFP- $B^{\text{act}\Delta\text{Prp2}}$ complexes by two steps purification via glycerol gradient centrifugation (10%-30%, 75 mM KCl, in Sorvall SureSpin630 rotor) and affinity chromatography on amylose beads. After elution from the amylose beads (in 75 mM/20 mM Maltose), we induced the catalytic

activation by incubating our complexes with recombinant Prp2 and Spp2 proteins and 2.0 mM ATP under non-stringent condition (75 mM KCl). After the incubation for 45 min at 23°C, the activated spliceosomes were directly transferred on the cover slide for dcFCCS analysis. In the Cwc24-EGFP-B^{actΔPrp2} complex we observed a cross correlation between the green Cwc24 and the red pre-mRNA of ~ 60%. After the Prp2-mediated activation of the spliceosome, the cross correlation between the green and the red label was reduced to less than 5 % in the B* complex as shown in Fig. 3.15 column 2.

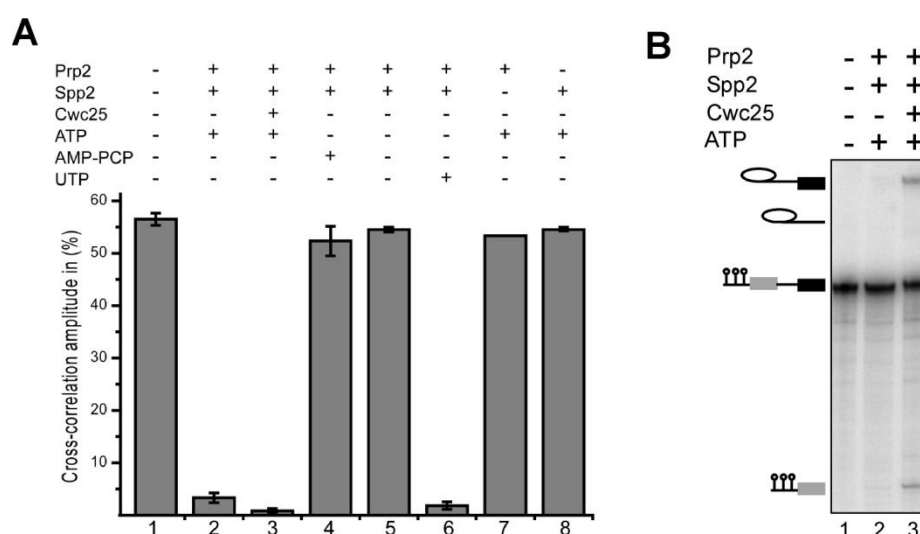


Figure 3.15: Displacement of Cwc24 from the spliceosome during Prp2-mediated catalytic activation, implying its non-involvement in the catalytic step 1 of splicing.

(A) Affinity-purified B^{actΔPrp2} complexes assembled on Atto647N-M3Act carrying Cwc24-EGFP (column 1) were complemented as indicated above each bar or (B) Affinity-purified B^{actΔPrp2} complexes assembled on ³²P-labelled M3Act, carrying Cwc24-EGFP (lane 1) were complemented with Prp2, Spp2 and ATP (lane 2), plus the addition of Cwc25 (lane 3). The positions of the pre-mRNAs, the splicing intermediates and products are indicated on the right.

This observation indicates almost quantitative dissociation of Cwc24-EGFP from the complex during activation. The addition of Cwc25 to form C complex revealed a complete loss of the binding affinity of Cwc24 with the complex as demonstrated in Fig. 3.15, column 3. The cross correlation amplitude went down near to background noise (< 3%) which implies that Cwc24, although essential for pre-mRNA splicing, is not a factor essential for the first step of splicing which occurs in the C complex. In

the presence of non-hydrolysable AMP-PCP or without ATP (columns 4–5), or without Prp2 or Spp2 (columns 7–8), the cross-correlation of ~60% remained unchanged. These results show that the dissociation of Cwc24-EGFP from the spliceosome accompanies the Prp2-mediated transformation of the $B^{\text{act}\Delta\text{Prp2}}$ complex into B^* . The almost complete loss of Cwc24-EGFP from the activated spliceosome is all the more notable, as this protein is very stably bound to the Cwc24-EGFP- $B^{\text{act}\Delta\text{Prp2}}$ complex, as indicated by its presence at 300 mM salt (Figure 3.16, column 3). The dissociation of Cwc24-EGFP during the $B^{\text{act}\Delta\text{Prp2}}$ to B^* complex transition also occurred efficiently in the presence of UTP (Fig. 3.15, column 6), consistent with the fact that Prp2 has a broad rNTP specificity (Kim, Smith et al. 1992). As yeast Brr2 is strictly ATP-specific, it is very unlikely that Brr2 ATPase activity is involved in the displacement of Cwc24 from the spliceosome, suggesting that this dissociation is solely due to the action of Prp2.

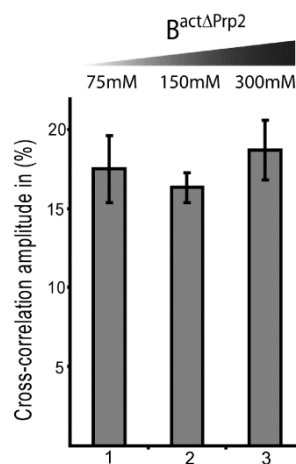


Figure 3.16: Salt resistance of Cwc24-EGFP binding to the spliceosome during Prp2-mediated activation.

Affinity-purified $B^{\text{act}\Delta\text{Prp2}}$ complexes assembled on Atto674N-M3Act wt pre-mRNA carrying the Cwc24-EGFP protein were eluted from the amylose matrix and were treated with increasing salt concentration (75-300 mM KCl) and then incubated on ice for 30 min before dcFCCS measurement.

Cwc27, although not essential for the growth of yeast under normal physiological conditions (Winzeler, Shoemaker et al. 1999; Giaever, Chu et al. 2002), behaved in a manner similar to Cwc24 (Ohrt, Prior et al. 2012). As with Cwc24, the drop in cross-

correlation was seen after incubation with Prp2, Spp2 and ATP, but not when any of these components was absent from the reaction mixture; in addition, ATP could be replaced by UTP but not by AMP-PCP. We conclude that both Cwc24 and Cwc27 lose their affinity for – or are displaced from – the spliceosome upon catalytic activation of the $B^{\text{act}\Delta\text{Prp2}}$ complex.

3.8.3 Cwc24 is essential for the first step of splicing *in vitro* but it is not required for catalysis of the splicing reaction *per se*

The above results indicate that Cwc24 dissociates almost quantitatively from the spliceosome during or after its catalytic activation, thus suggesting that it is not required for the actual first step of splicing. To determine whether the essential protein Cwc24 is required for the actual catalytic step, affinity-purified $B^{\text{act}\Delta\text{Prp2}}$ complexes assembled on ^{32}P -labelled M3Act pre-mRNA (Fig. 3.15 B, lane 1) were complemented with Prp2, Spp2 and ATP to allow the dissociation of Cwc24 (lane 2). Cwc25 was then added (lane 3). The spliceosomes from which Cwc24 had dissociated (Fig. 3.15 A, column 3), were capable of carrying out catalytic step 1 of splicing (Fig. 3.15 B, lane 3), supporting the idea that Cwc24 is required before the action of Prp2 and not for catalytic step 1 *per se*.

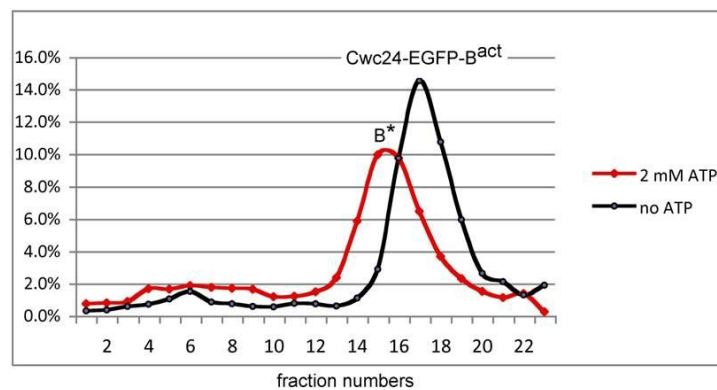


Figure 3.17: Catalytic activation of the Cwc24-EGFP- $B^{\text{act}\Delta\text{Prp2}}$ complex by Prp2.

Profile of affinity-purified Cwc24-EGFP- $B^{\text{act}\Delta\text{Prp2}}$ spliceosomes separated on a glycerol gradient containing 75 mM KCl after incubation with Prp2/Spp2 without the addition of ATP (45S; black line) or with the addition of 2 mM ATP (40S, B* complex; red line). The radioactivity contained in each gradient fraction was measured by Cerenkov counting. Sedimentation coefficients were determined by analyzing the UV absorbance of fractions of a reference gradient containing prokaryotic ribosomal subunits. The y axis shows the percentage of radioactively labeled RNA found in each fraction relative to the amount found in all fractions.

3.8.4 The U2-associated SF3a and SF3b proteins Prp11 and Cus1 remain bound to the B* complex under physiological conditions, but their affinity is weakened at high salt

We observed a reduction of the U2 snRNP associated proteins as revealed by Mass spectrometry analysis (First part of this work; (Fabrizio, Dannenberg et al. 2009)). For this reason we chose the U2 snRNP-associated SF3a protein Prp11 and the SF3b associated protein Cus1 to examine the binding behavior of these individual proteins by dcFCCS as representatives for the U2 snRNP proteins. We therefore constructed Prp11-EGFP and Cus1-EGFP strains and used the whole cell extract made from these strains for our experiments. The experimental procedure was the same as for Cwc24-EGFP and Snu114-EGFP. We purified our B^{actΔPrp2} complexes assembled on Atto674N-M3Act wt pre-mRNA carrying the Prp11-EGFP or Cus1-EGFP protein. After reconstitution with recombinant proteins Spp2, Prp2 and 2.0 mM ATP they were analyzed by dcFCCS. For investigation of the salt stability of these complexes, the samples were treated with different salt concentrations by adding KCl to a final concentration of 150 mM or 300 mM to the samples and incubated for 30 min on ice before measurement. The results, shown in Fig. 3.18., revealed that both proteins, Prp11-EGFP and Cus1-EGFP remained stably bound to the B^{actΔPrp2} complex even at high salt concentrations with a cross correlation of ~45% (Fig. 3.18 A and B, column 1-3). As well after the addition of Prp2, Spp2 and 2.0 mM ATP at a salt concentration of 75 mM KCl, the Prp11-EGFP and Cus1-EGFP stayed associated with the B* complex (Fig. 3.18 A and B, columns 4). Only after increasing the salt concentration from 75 mM KCl up to 300 mM KCl we could observe a dramatic decrease of cross correlation and a weakening of the binding of Prp11-EGFP and Cus1-EGFP from the B* complex (Fig.3.18 A and B, columns 5-6). At 150 mM KCl (column 5) a reduction of 20% of cross correlation could be observed, whereas at 300 mM KCl (column 6) the majority of the proteins, more than 70%, had dissociated from the B* complex. In contrast to the observations of the binding behavior of Snu114-EGFP, which remained stably bound even under high salt conditions, we demonstrated that the U2-SF3a/b proteins were tightly bound to the pre-catalytic spliceosome, but their binding is weakened after Prp2 action and the catalytically activation of the spliceosome, becoming salt-sensitive. However, their affinity to the B* complex is

higher than that of Cwc24-EGFP or Cwc27-EGFP. Even after addition of recombinant Cwc25, i.e. upon C complex formation, Cus1 and Prp11 remained bound to the spliceosome at a salt concentration of 75 mM KCl (data not shown).

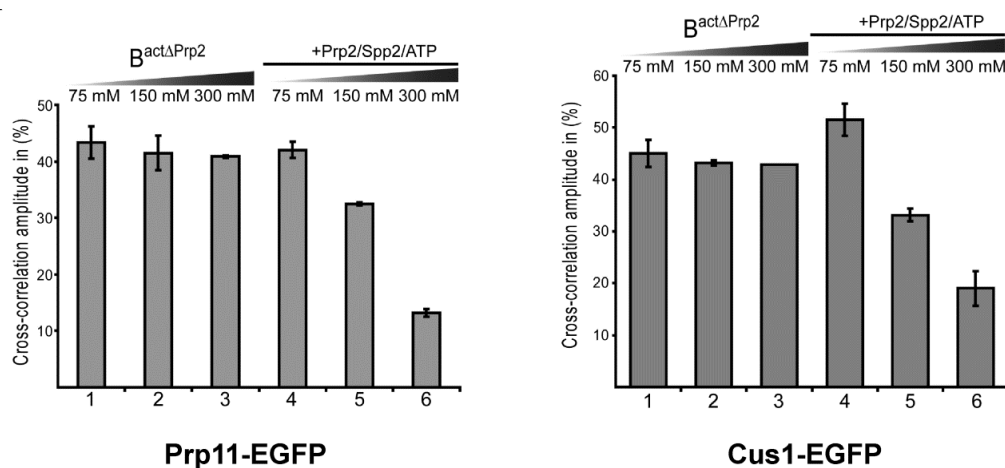


Figure 3.18: Binding of U2 SF3a/b proteins Prp11-EGFP and Cus1-EGFP to the spliceosome is made salt-sensitive by the Prp2-mediated catalytic activation. Affinity-purified Bact Δ Prp2 complexes were assembled on Atto674N-M3Act wt, carrying Prp11-EGFP (A) or Cus1-EGFP (B). The complexes were incubated with increasing salt concentrations before (columns 1-3) and after addition of Prp2, Spp2 and ATP (columns 4-6).

3.8.5 The binding of the RES complex protein Bud13 is weakened during catalytic activation

The pre-mRNA Retention and Splicing (RES) complex plays an important role in nuclear retention of un-spliced pre-mRNAs. The yeast RES complex consists at least of three proteins: Ist/Snu17, Pml1 and Bud13. Our previous results confirmed the data from the literature that the RES complex associates with the spliceosome before step 1 of splicing, as we showed for the yeast spliceosomal B complex (Dziembowski, Ventura et al. 2004);(Fabrizio, Dannenberg et al. 2009). For investigating the binding behavior of the RES complex to the spliceosome, we chose the protein Bud13 as a representative for the RES complex and we applied the same experimental strategy using dcFCCS described above. The cross correlation intensity of the Bud13-EGFP-B^{act} Δ Prp2 under non-stringent conditions (75 mM KCl) was at ~ 28% between the green

labeled protein Bud13-EGFP and the red labeled pre-mRNA (Fig. 3.19, column 1), but was reduced by almost 50% (down to ~15%) when treated with high salt concentrations (300 mM KCl; Fig. 3.19, column 3) in the Bud13-EGFP-B^{actΔPrp2} complex.

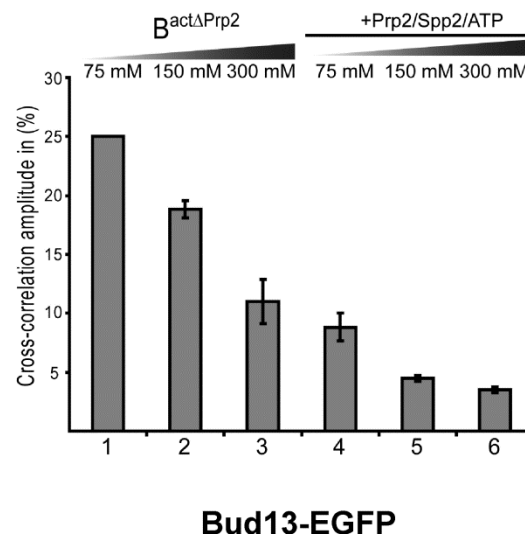


Figure 3.19: Displacement of Bud13-EGFP from the spliceosome during Prp2-mediated catalytic activation. Affinity-purified B^{actΔPrp2} complexes assembled on Atto647N-M3Act, carrying Bud13-EGFP (columns 1–3), were complemented with Prp2, Spp2, and ATP (columns 4–6). After incubation, increasing concentrations of KCl were added and dcFCCS was performed as above.

In comparison to the binding strength of Cwc24-EGFP and Snu114-EGFP, we observed a weaker association of Bud13-EGFP with the spliceosomal B^{actΔPrp2} complex. Even more significant was the dramatically reduced affinity of Bud13-EGFP for the B^{*} complex after Prp2-mediated activation of the Bud13-EGFP-B^{actΔPrp2} complex under high salt conditions (300 mM KCl, Fig. 3.19, column 6). At these stringent conditions Bud13-EGFP was almost displaced from the spliceosome after catalytic activation (Fig. 3.19, column 5 and 6). This observation is congruent with the idea that the members of the RES complex remain bound to the spliceosome until the Prp2-mediated catalytic activation of the spliceosome takes place, to avoid the premature release of unspliced pre-mRNA from the nucleus. It was demonstrated by Dziembowski et al. that inactivation of these proteins causes leakage of unspliced pre-mRNA from the nucleus (Dziembowski, Ventura et al. 2004).

3.8.6 Binding of Yju2 to the spliceosome is strengthened upon catalytic activation

Yju2 is a novel splicing factor known to be associated with components of the NTC and to play a role in pre-mRNA splicing, both in vivo and in vitro. Yju2 is recruited to the spliceosome prior the action of Prp2 and the first step of splicing at the stage of the B^{act} complex. Its role is in promoting step 1 of splicing after Prp2-mediated structural rearrangement of the spliceosome (Liu, Chen et al. 2007).

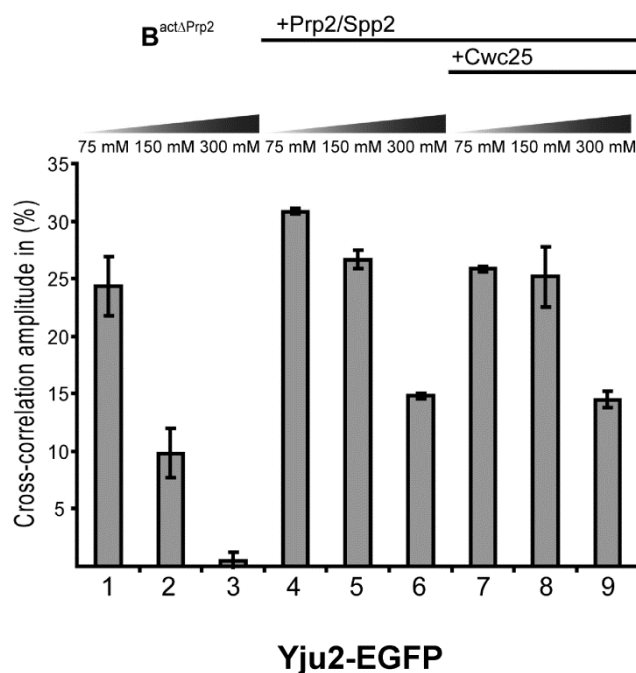


Figure 3.20: Strengthening of binding of Yju2-EGFP to the spliceosome upon catalytic activation. Affinity-purified B^{actΔPrp2} complexes assembled on Atto647N-M3Act, carrying Yju2-EGFP (columns 1–3), were complemented with Prp2, Spp2, and ATP (columns 4–6), or with Prp2, Spp2, ATP, and Cwc25 (columns 7–9). After standard incubation, increasing concentrations of KCl were added.

The investigation of the binding affinity of Yju2-EGFP to purified spliceosomal complexes revealed that Yju2-EGFP has a lower affinity for the B^{actΔPrp2} complex than for B* complex as demonstrated by dcFCCS data. Under non-stringent condition, Yju2-EGFP seemed to be associated with the B^{actΔPrp2} complex, but already at a concentration of 150 mM KCl more than 50% of the Yju2-EGFP was dissociated

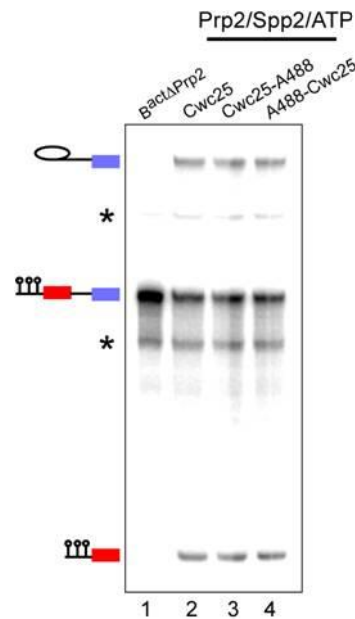
from the complex and at 300 mM KCl the dissociation was complete (Fig. 3.20, column 1-3). Interestingly, after the Prp2-mediated activation of the spliceosome, the binding affinity of Yju2-EGFP protein was higher for the B* complex than for the corresponding B^{actΔPrp2} (Fig. 3.20, column 4). The higher binding affinity was more prominent at 150 mM and 300 mM KCl (Fig. 3.20, column 5 and 6). We concluded that the Prp2-dependent rearrangement of the spliceosome changes the binding affinity of Yju2 for the spliceosome from low to high. The addition of Cwc25, leading to the first step spliceosome had no additional effect on the binding strength of Yju2-EGFP to the C complex. Moreover, the affinity of Yju2 was minimally affected by the first step of splicing (Fig. 3.20, column 7-9).

3.8.7 Prp2-mediated catalytic activation of the spliceosome creates also a high affinity binding site for Cwc25 in the spliceosome

We showed in our experiments described above, that the Prp2-mediated rearrangement of the spliceosome is accompanied by changes of the binding affinity of many proteins. Some were only destabilized during activation like the U2 snRNP associated SF3a/b proteins, other were displaced completely, i.e. Cwc24, Cwc27 or Bud13 or their binding was even enhanced like the factor Yju2. The essential factor for promoting the first step of splicing is Cwc25 as shown in Warkocki et al., 2009. To investigate the role and the binding affinity of Cwc25 during pre-mRNA splicing we conjugated the green fluorescent dye Alexa488N-maleimide to Cwc25 via cyteines which were linked to the protein at the C or N terminus of the protein. After labeling the overexpressed and purified protein (in collaboration with Dr. Jana Schmitzova and Dr. Thomas Ohrt) a second step of purification was performed to remove unbound Alexa488N-maleimide. Fluorescently labeled protein was obtained with a label efficiency of ~ 70% (see Methods).

Next steps were to test whether fluorescently labeled Cwc25 was functional or whether Alexa488N-maleimide interferes with spliceosome assembly. Therefore, we purified B^{actΔPrp2} complexes assembled on Atto647N-M3Act pre-mRNA as already described, and complemented them with Prp2, Spp2, ATP, and either unlabeled recombinant Cwc25 or its N or C terminus labeled versions. As shown in Figure 3.21,

all Cwc25 preparations we have tested led to the identical step 1 efficiencies (done by Dr. Peter Odenwalder from our laboratory).



Figures 3.21: Functional assay using Cwc25-Alexa488N-maleimide. Complexes

assembled on Atto647N-M3Act undergo the first step of splicing when complemented with Prp2, Spp2, ATP and Cwc25 labelled with the fluorescent dye Alexa488. B^{act}ΔPrp2 complexes assembled on Atto647N-M3Act (lane 1) were purified, eluted from the amylose matrix and complemented with Prp2, Spp2, ATP and Cwc25 (lane 2), or fluorescently labelled Cwc25 (lanes 3 and 4). Two preparations of Cwc25, C-terminally (lane 3) and N-terminally labelled (lane 4) were used. RNA was analysed on an 8% polyacrylamide–urea gel and visualised by autoradiography. The positions of the pre-mRNAs and the splicing intermediates are indicated on the left. Asterisks: uncharacterised pre-mRNA bands (Assay done by Dr. Peter Odenwalder, Figure kindly provided by Dr. Peter Odenwalder).

Next, we studied the recruitment of Cwc25 to the spliceosome in more detail.

Therefore, using extracts from the *prp2-1* strain, B^{act}ΔPrp2 complexes were assembled on Atto647N-M3Act. After gradient separation and affinity-purification, the bound complexes were transferred into a new 1,5 ml Eppendorf tube and complemented with Prp2, Spp2, Cwc25-Alexa488 (C-terminally labeled) and ATP or only with Cwc25-Alexa488. Reaction mixtures were incubated for 45 min at 23°C and transferred back into the chromatography columns for washing. After washing the reconstituted

complexes twice with G-75 buffer to remove unbound Cwc25-Alexa488, the complexes were analyzed by dcFCCS (Fig. 3.22).

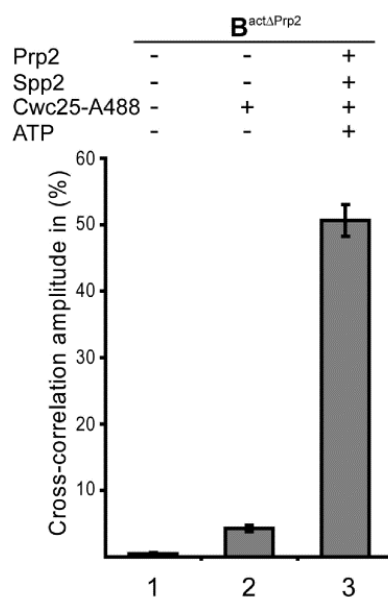


Figure 3.22: Catalytic activation by Prp2 creates a high-affinity binding site for Cwc25 in the spliceosome. $B^{\text{act}\Delta\text{Prp2}}$ complexes assembled on Atto647N-M3Act (column 1) were complemented on the amylose matrix with C-terminally labeled Cwc25-Alexa488 (column 2) or Cwc25-Alexa488 together with Prp2, Spp2 plus ATP (column 3). After incubation, the complexes were washed and eluted with maltose, and dcFCCS measurements were performed (this experiment was repeated for this work according to the protocol of Dr. Peter Odenwalder).

$B^{\text{act}\Delta\text{Prp2}}$ complexes complemented with Cwc25-Alexa488 displayed only a background cross-correlation of <5% (column 2). On the other hand, when the $B^{\text{act}\Delta\text{Prp2}}$ complex was supplemented with Prp2, Spp2, ATP, and Cwc25-Alexa488, it showed a cross correlation amplitude of ~ 50% (Fig. 3.22, column 3). Accordingly, Cwc25 binds efficiently to the spliceosome only after ATP-hydrolysis by Prp2 and rearrangement of the structure of the spliceosome, i.e. only after the release or destabilization of several proteins. This suggests that the remodeling of the spliceosome by Prp2 helicase generates a binding site for Cwc25 in the spliceosome. To study how the affinity of Cwc25 changes during catalytic activation of the spliceosome, we determined quantitatively the binding constants for Cwc25 at the $B^{\text{act}\Delta\text{Prp2}}$ and B^* stages, i.e., immediately before and after catalytic activation by Prp2

done in parallel experiments by Dr. Peter Odenwalder (Computational analysis of the data was done by Mira Prior, III. Institute of Physics, University of Gottingen; data not shown) (Ohrt, Prior et al. 2012). The results of these additional experiments were in line with our results, thus, we conclude that the Prp2-dependent rearrangement of the spliceosome generates a high-affinity binding site for Cwc25. In conclusion dcFCCS is a high resolution and quantitative technique for the investigation of highly dynamic complexes like the spliceosome and we have obtained important insights about protein dynamics at the catalytic core of the spliceosome during pre-mRNA splicing in yeast.

4. Discussion

In this work we established a method to isolate and to purify spliceosomal complexes from the yeast *S. cerevisiae* stalled at defined stages of spliceosome assembly for the first time (Dannenberg, Fabrizio et al. 2012); (Fabrizio, Dannenberg et al. 2009) We characterized the proteome of the B, B^{act} and C complexes and could give first insights into the protein dynamics and the two-dimensional (2D) structural changes during transition from B to B^{act} and from B^{act} to C complexes during pre-mRNA splicing as revealed by Mass spectrometry (MS) and Electron microscopy (EM) analyses. During the conversion from B to B^{act} to C, the compositional changes are accompanied by structural remodeling of the spliceosome which results in changes of the S values of the individual complexes, 40S for B complex, 45S for B^{act} and 40S for C complexes. EM studies revealed that these compositional changes correlate with structural changes during both transitions, B to B^{act} and B^{act} to C. Our results give insights into the highly dynamic RNP machine that undergoes many changes in composition and conformation.

4.1 The structural dynamics of the spliceosome are modulated by multiple DExD/H-box RNA helicases, the driving forces of the spliceosome

Among these helicases are Prp5 and Prp2, which are essential ATPase required prior to the first step of pre-mRNA splicing. The DEAD-box ATPase Prp5 enables stable U2 snRNP association with the branch point sequence (BPS). We showed here that the use of temperature-sensitive mutants of Prp5 (*prp5-1*) led to accumulation of early, pre-spliceosomal complexes, identified by MS as commitment complex 2 (CC2). Another important helicase, the DEAH-box ATPase Prp2, is known to promote a structural rearrangement that transforms the B^{act} into the catalytically activated B* complex. Our MS results already revealed that a number of proteins are affected by the Prp2-mediated catalytic activation. Consequently, a second approach of this work was to deepen our previous results by studying the modulation of the binding strength of individual proteins to the yeast spliceosome during catalytic

activation by Prp2 in a quantitative manner. Therefore, we applied the technique of dual color Fluorescence Cross Correlation Spectroscopy (dcFCCS) which was established during this work in collaboration with Dr. Thomas Ohrt, Dr. Peter Odenwalder, Mira Prior and Prof. Jorg Enderlein. The combination of our established three-step purification strategy (Fabrizio, Dannenberg et al. 2009); (Dannenberg, Fabrizio et al. 2012) together with *in vitro* reconstitution of functional spliceosomes (Warkocki, Odenwalder et al. 2009) and with the dcFCCS technique made it possible to shed some light on the nature of the release/loss of splicing factors during the crucial remodeling step of catalytic activation. This is the first example where purified, catalytically active spliceosomes were investigated directly in solution and in equilibrium. By dcFCCS we showed that the U2 SF3a/SF3b proteins Prp11 and Cus1 are destabilized and Cwc24, Bud13 and Cwc27 are released from the spliceosome after Prp2-mediated catalytic activation. Furthermore, we demonstrated that high affinity binding sites are created for the step 1 factors Yju2 and Cwc25 during catalytic activation, consistent with their requirement for step 1 catalysis. This work demonstrates that Prp2 has a major role in the structural remodeling and in the multiple rearrangements at the core of the spliceosome.

4.2 The protein composition of yeast spliceosomes is less complex than that of metazoan spliceosomes

If one compares the proteome of the yeast B, B^{act} and C complexes with spliceosomal complexes isolated from other species, i.e. *Drosophila* or human spliceosomes, it is obvious that the yeast spliceosome has significantly less proteins than metazoan spliceosomes. The human and the *Drosophila* B complex isolated under similar non-stringent conditions contain ~ 110 proteins (Deckert, Hartmuth et al. (2006); (Herold, Will et al. 2009), whereas the yeast B complex comprises ~ 60 proteins. The most drastic difference was shown for the purified Bact complexes from human with more than ~ 140 proteins compared to the yeast Bact complex with only ~ 40 proteins (Bessonov, Anokhina et al. (2010)). A similar minimal protein composition like for the yeast B^{act} complex was revealed for the yeast C complex, which is composed of only ~ 50 proteins in yeast versus ~ 110 proteins in human (Bessonov, Anokhina et al.

(2008). As a result we can conclude that the number of proteins of each yeast complex is less than half compared to human spliceosomal complexes (Fig 4.1.). We identified in total, ~ 90 proteins in the three isolated yeast complexes.

The proteins identified here include the majority of proteins which were found to be associated with previously isolated yeast complexes such as the purified penta-snRNP and the Cef1-associated complex (Ohi and Gould (2002); Stevens, Ryan et al. (2002)). Established splicing factors that were known to contribute to pre-mRNA splicing as revealed by genetics or other techniques, which were not found in our three complexes, include those that were only loosely associated and lost during purification, such as Prp28 and Sad1 or those that act even earlier in pre-mRNA splicing, e.g. Npl3 or Mud2 and Msl5 which were however found associated with the early pre-spliceosomal Commitment Complex that we have also isolated, purified and characterized in this work (Table 3.2 and Figure 4.1).

4.3 Isolation and characterization of early spliceosomal complexes from yeast

Here, we have also purified yeast spliceosomes stalled at the commitment complex (CC) stage prior to prespliceosome (A complex) formation using a temperature sensitive yeast strain, which carries the mutant Prp5 protein (named *prp5-1*). The DEAD-box Prp5 is an essential, RNA dependent ATPase present in the CC that functions in subsequent A complex formation containing both the U1 and U2 snRNPs. Our stalled 26S complex contained exclusively pre-mRNA and U1 snRNPs. The protein composition of this complex has been determined by MS and contained in addition to all known U1 proteins, three additional splicing factors: Mud2, Msl5 and Npl3, thus has all the characteristics of a CC2. In yeast two kinds of commitment complexes have been identified, termed CC1 and CC2. The CC1 is characterized by a faster mobility and is dependent on the presence of the 5'SS and the U1 snRNP, which binds to the 5'SS in an ATP-independent manner. CC2 has a lower mobility and needs the 5'SS and a functional BPS for proper formation.

The presence of Mud2, Msl5 and Npl3 in our MS analyses suggests that our isolated early complex is CC2. Npl3 is a SR-like protein in *S. cerevisiae* that was recently shown to be required for efficient co-transcriptional recruitment of the splicing

machinery. It is involved in the recruitment of splicing factors to chromatin-associated transcripts. Npl3 was shown to promote efficient splicing of a large subset of genes via co-transcriptional recruitment of U1 and U2 snRNPs (Kress, Krogan et al. 2008); (Moehle, Ryan et al. 2012). SR and hnRNP proteins in metazoans are best understood for their role in alternative and constitutive splicing, although they have also been implicated in additional steps in gene expression, including mRNA export, translation, and even transcription itself (Singh and Valcarcel 2005); (Long and Caceres 2009); (Dreyfuss, Kim et al. 2002). The yeast *S. cerevisiae*, contains at least three genes with a canonical SR protein domain structure: one or more RNA recognition motifs and a domain enriched in arginine-serine-di-peptides (Long and Caceres 2009); (Manley and Krainer 2010). It was shown that deletion of Npl3 causes splicing defects. The affected genes were exclusively those encoding ribosomal proteins which represent the major class of intron containing genes in budding yeast, in other respects alternative splicing is extremely rare in yeast (Kress, Krogan et al. 2008; Long and Caceres 2009); (Moehle, Ryan et al. 2012). Recent experiments demonstrated that Npl3 remains associated with mRNA after splicing is completed (Moehle, Ryan et al. 2012). The fact that we found Npl3 only associated with our CC2 might be due to our purification strategy. Likely, Npl3 might be tightly associated with early spliceosomal complexes consistent with its suggested role of co-transcriptional recruitment of the splicing machinery.

Mud2 is a splicing factor known to be involved in early pre-mRNA splicing events and it has been shown to interact with the highly conserved BPS in yeast and with the U1 snRNP (Krämer et al., 1996). Msl5/BBP (homologue to SF1) is a branch point binding protein and recognizes the intron BPS UACUAAC in the pre-mRNA transcripts during spliceosome assembly. Msl5 is recruited to the spliceosome at a very early stage of assembly. Mud2 has been identified as the yeast homolog of U2AF65, the large subunit of U2AF that interacts with the polypyrimidine tract 3' to the mammalian BPS (Kistler and Guthrie 2001). In previous studies it was shown that Mud2 interacts with Msl5/BBP splicing factor and Sub2.

Sub2 was completely absent from our purified complexes (i.e. CC, B, Bact and C). Sub2 is a DEAD-box helicase, which acts very early in pre-mRNA splicing. Sub2 belongs to the DExD/H-box ATPase family, like Prp5 and Prp2, and is one of the helicases which play a role in both pre-mRNA splicing and mRNA export. Like the

helicase Sub2, Prp5, was absent from our purified complexes. Prp5 and hydrolysis of ATP are required for stable binding of the U2 snRNP with the pre-mRNA in the presence of Cus2 which is thought to be the first ATP-dependent step in the splicing cycle (Liao, Colot et al. 1992); (Ruby, Chang et al. 1993);(Perriman, Barta et al. 2003). The reason for the absence of Prp5 in our CC preparations is that we used a thermo sensitive mutant of Prp5 (*prp5-1*), which is heat-inactivated and lost, thus blocking spliceosome assembly at the stage of CC2. However, Prp5 was never detected with high peptide numbers in our spliceosomes due to the fact that Prp5 acts at the stage of the pre-spliceosomal A complex prior to the formation of the B complex. We also could not detect the U2 snRNP associated protein Cus2 in our CC2. Cus2 belongs to the members of the RNA recognition motif (RRM) family of RNA binding proteins and it was suggested to mediate a functional interaction between the U2 snRNA and/or the U2 associated SF3a complex protein Prp11 and Prp5 (Yan, Perriman et al. 1998). The work by Perriman and Ares suggested a model for the interplay between Cus2, Prp5 and the U2 snRNP in which Prp5 might be needed for the ATP-dependent removal of Cus2 from the U2 snRNP leading to subsequent stable integration of the U2 snRNP into the spliceosome (Perriman, Barta et al. 2003). The absence of Cus2 in our complexes could be explained by the absence of U2 snRNPs in our CC2 preparations. It might be that Cus2 is recruited together with U2 to the spliceosome to stabilize the binding of the U2 snRNA/snRNP until its stable integration into the spliceosome. To promote this, the Prp5-mediated removal of Cus2 is needed (Perriman, Barta et al. 2003). Our isolated CC2 could be used in the future for *in vitro* reconstitution of A complexes upon addition of purified U2 snRNPs and recombinant Prp5. In addition it would be interesting to investigate how the Prp5-mediated hydrolysis of ATP promotes the stable association of the U2 snRNP in the pre-spliceosome

4.4 Evolutionary conservation of yeast spliceosomes

The large number of proteins found associated with human spliceosomal complexes are due to the higher amount of regulated splicing in the metazoan system whereas, as mentioned above, alternative splicing is nearly completely absent in yeast. However, most of the identified splicing factors found in our purified complexes have a human

homolog and thus, are evolutionarily conserved in humans. Remarkably, more than 85% of the yeast splicing factors listed in Table 3.1 have a clear evolutionarily conserved counterpart (Fig. 4.1). The comparison of the proteome of metazoan and yeast spliceosomes revealed an evolutionarily conserved core design of the splicing machinery. In Fig 4.1 are shown the protein factors which associates with human spliceosomes without an obvious conserved counterpart in yeast. There are ~ 80 proteins without a yeast homolog, known to play a role in regulating alternative splicing, i.e. among others SR and hnRNP proteins (Wahl, Will et al. (2009)). A set of about ten SR and hnRNP proteins and several U2-related proteins are present in early human spliceosomes but essentially absent from yeast (Fig. 4.1). We expected that one or more yeast SR-like or hnRNP proteins would be found in early yeast spliceosomal complexes (e.g. A complex). Indeed we found the yeast SR-like protein Npl3 associated with our early pre-spliceosomal CC2 (Table 3.1). Indeed, Npl3 was also recently shown to promote the recruitment of the U1 snRNP to the pre-mRNA (Kress, Krogan et al. 2008). The human splicing machinery contains many regulatory proteins needed for alternative splicing. The majority of these regulatory protein factors are only required in certain situations and are loosely associated with the human spliceosome. Obvious counterparts for many of these proteins are not present in yeast. For example, the members of the PPIase family (peptidyl-prolyl cis/trans isomerase) are represented with seven proteins in the human spliceosomes, but only one PPIase, NY-CO-10, shows 28% identity (45% similarity) with the yeast Cwc27, which harbors a PPIase domain. This lead us to conclude that the yeast splicing machinery is less complex than that of metazoan due to the limited amount of regulated splicing.

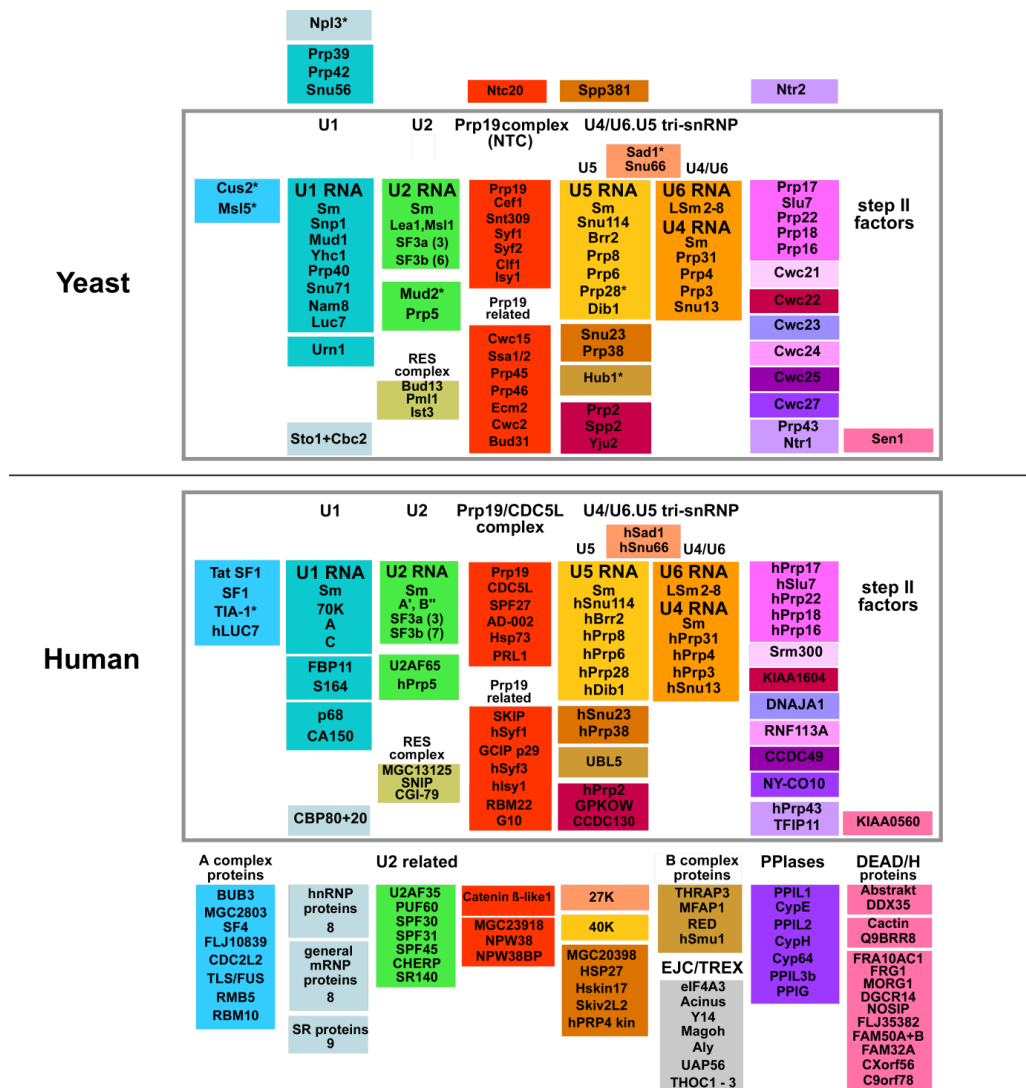


Figure 4.1: The yeast splicing machinery is less complex than that of humans

Upper rectangle: Yeast proteins (yeast nomenclature) evolutionarily conserved between yeast and man, associated with purified yeast B, Bact, and C complexes, are placed inside of the rectangle. Proteins above the rectangle do not have a human counterpart. Lower rectangle: Human proteins (human nomenclature) evolutionarily conserved between yeast and man, associated with purified human A, B, and C complexes, are placed inside of the rectangle. Proteins below the rectangle were found associated with purified human spliceosomal complexes, but the majority of them do not have a yeast counterpart (Behzadnia, Golas et al. 2007); (Bessonov, Anokhina et al. 2008). Numbers indicate the total number of individual proteins in a particular group. (Asterisks) Proteins that do have homologs in yeast or human but were not found or found loosely associated with purified spliceosomal complexes; yeast Msl5, Npl3, Mud2, and Hub1 were found with low peptide numbers in the 20S–25S peak shown in the results section for the B complex and Msl5, Npl3 and Mud2 were found in the commitment complex. Cus2, Prp28, and Sad1 were not detected by MS and are included for completeness, as well as human TIA-1, which is the homolog of yeast Nam8. Proteins are grouped according to snRNP association, function, presence in a stable heteromeric complex, or association with a particular spliceosomal complex, as indicated (Fabrizio, Dannenberg et al. 2009).

4.5 Spliceosomal dynamics during catalytic activation

Comparative proteomics of human and *Drosophila* spliceosomal complexes showed a dramatic exchange of proteins during the transition from B to C complexes. More than 60 proteins are exchanged during catalytic activation of the metazoan splicing machinery (Bessonov, Anokhina et al. (2008); (Herold, Will et al. 2009). Our studies show that the yeast spliceosome is also in a highly dynamic state during its assembly and step 1 catalysis. The most dramatic compositional change in the yeast spliceosome occurred during the transition from the pre-catalytic B complex to the activated B^{act} complex. During the step of activation, the entire U1 snRNP is released, whereas the tri-snRNP undergoes massive remodeling. This entails dramatic structural rearrangements that at the RNA level involve unwinding of the U4/U6 duplex and the formation of U2/U6 base-pairing, a reorganization that is exceptional among RNP machines (Wahl, Will et al. (2009). Concomitant with the unwinding of the U4/U6 duplex, all U4 and U6 snRNP associated proteins are released from the spliceosome as well, together with factors that link the U5 snRNP to the U4/U6 di-snRNP (Fig. 4.2)(Hacker, Sander et al. 2008). As a consequence, our B^{act} complexes lack all U4/U6 snRNP specific proteins and several U5 snRNP proteins, except Brr2, Prp8 and Snu114 which are present throughout the whole splicing cycle (Fig.4.2). In total ~ 35 proteins are lost during the transition from the B to the B^{act} complex. Subsequently after the disruption of the U4/U6 duplex and the loss of pre-catalytic binding partners, new partners have to be provided to stabilize the U6 snRNA interaction with pre-mRNA and the U2 snRNA. The factors which are recruited during the formation of the U2/U6/pre-mRNA base-pairing interaction were unclear at the start of this work, as well as the precise time at which such proteins are recruited. Here, we could demonstrate that 12 known splicing factors were recruited at the time of spliceosomal activation and that the eight proteins of the NTC-complex become more stably bound (Fig. 4.2, B^{act}, and compare with B complex). As a result of this reproducible observation we regard these factors as characteristic for the yeast spliceosomal B^{act} complex and named them NTC-related proteins.

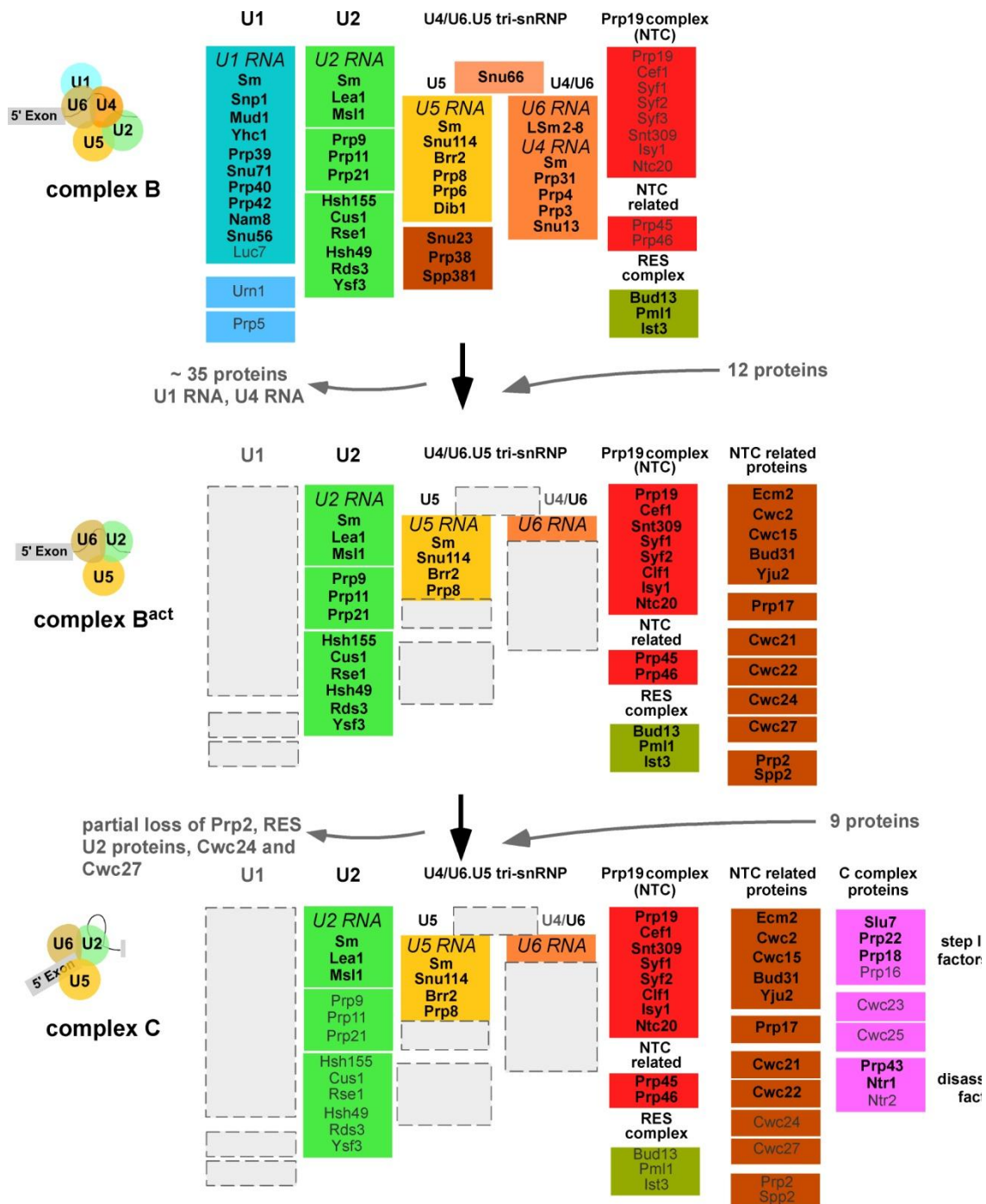


Figure 4.2: Compositional dynamics during catalytic activation

The protein composition of the yeast B, B^{act}, and C complexes was determined by MS. Proteins (yeast nomenclature) are grouped as described in the legend of Figure 4.1. The relative abundance of proteins is indicated by light (substoichiometric amounts) or dark (stoichiometric amounts) lettering and is based on the relative number of peptides sequenced (Table 3.1) (Fabrizio, Dannenberg et al. 2009)

The proteins recruited to the Bact complex can be divided into two classes: (i) those most probably required to establish and/or stabilize the U2/U6 base-pairing interaction (e.g. Cwc24, Ecm2 and Cwc2 a protein that contains a RNA recognition motif [RRM] (Hogg, McGrail et al.) and (ii) those more directly required to promote step 1, such as Prp2, Spp2, and Yju2. U6 snRNA not only engages in novel base pairing interactions with U2 and the pre-mRNA but also new protein-RNA interactions are established (Wahl, Will et al. 2009). It was postulated that members of the NTC complex and NTC-related proteins play an important role in restructuring the U6 and U2 snRNAs, and it was previously shown by Chan et al. (2003) that proteins of the NTC play a critical role in tethering and stabilizing the U6 and U5 snRNAs at the time of activation (Chan, Kao et al. 2003) NTC-dependent stabilization of U6 is mediated through remodeling of U6 snRNP, which includes the stabilization of U6/5'SS base pairing interaction, and destabilization of Lsm proteins from U6 (Chan, Kao et al. 2003). Additional rearrangements are required to shape and juxtapose evolutionarily conserved sequences of U6 snRNA (e.g. the internal stem-loop structure (ISL) with the pre-mRNA 5'SS for catalysis of the first step. One of the proteins that influence the catalytic conformation of the RNA network in the spliceosome is Cwc2 which interacts physically with Prp19 (Hogg, McGrail et al.). Recent data from our laboratory indicate that Cwc2 interacts with the catalytically important ISL of U6 snRNA and the pre-mRNA substrate in B^{act}, B* and C complexes (Rasche, Dybkov et al. 2012). Thus, it might play a crucial role in positioning the catalytic site into an active structure. The U2 snRNP is also substantially remodelled during splicing, with an apparent destabilization of SF3a and SF3b proteins prior to formation of the C complex, which suggested that they are not required after step 1 (Bessonov, Anokhina et al. 2008); (Fabrizio, Dannenberg et al. 2009). Thus, a large number of structural and compositional rearrangements accompany the assembly and catalytic process of the spliceosome. As mentioned above, the activation of the spliceosome and splicing catalysis requires formation of an active catalytic centre. In this context, the Prp2 DEAH-box ATPase is known to act subsequently of the U4/U6 unwinding by the helicase Brr2 but just prior to step 1 of splicing catalysis. It was suggested that Prp2 is released from the spliceosome upon ATP hydrolysis. We could show that Prp2 is recruited very stably to the spliceosome at the stage of the Bact complex, and it remains stably bound to this pre-catalytic

complex, as determined by the high peptide numbers analyzed by MS. This suggested that Prp2 cannot hydrolyze ATP in this specific spliceosomal "snapshot", otherwise it would dissociate from it. This observation led us to conclude that the B^{act} complex is not yet catalytically activated. This is further confirmed by the high S value of our B^{act} complex (45S) and is consistent with previous studies that showed that, prior to ATP hydrolysis, the spliceosome has a higher S value than it has after ATP hydrolysis by Prp2 (Kim and Lin (1996)). Despite the fact that we used a concentration of 2.0 mM ATP during the assembly of our B^{act} complexes, Prp2 is "trapped" in B^{act}. This is because our B^{act} complexes were assembled on the truncated M3-Act Δ 6 pre-mRNA substrate and were able to undergo pre-catalytic activation in the presence of high ATP but not to proceed to catalytic activation and step 1 catalysis. As step 1 catalysis occurs in our complex C when we used the M3-Act Δ 31 pre-mRNA, which is only 25 nucleotides longer downstream of the BPS, this led us to speculate that a longer RNA stretch downstream of the BPS may be required - either directly or as a protein-binding site - to stimulate ATP hydrolysis and/or support the structural rearrangements that occurs during Prp2-mediated ATP hydrolysis and release. This assumption was in line with previous studies which postulated the importance of the length of the intron downstream of the BPS for step 1 catalysis (Rymond, Torrey et al. (1987), Cheng (1994), Fabrizio, Dannenberg et al. (2009)). In addition, cross-linking experiments demonstrated contacts of the essential Prp2 DEAH-box ATPase with this intron region (Teigelkamp, McGarvey et al. (1994)). Thus, B^{act} represents a spliceosome prior to the final catalytic step mediated by Prp2. Therefore we suggest that one or more factors present in our purified spliceosomal C complex may be required for promoting step 1 (i.e. Cwc25) (Fabrizio, Dannenberg 2009).

The proteomic analysis of C complexes showed that at least nine proteins are recruited at the time of C complex formation and step 1 catalysis, these factors are named the C complex proteins (Figure 4.2). One of them is Cwc25, an essential spliceosomal factor that was recently shown to promote the first step of splicing and suggested to bind at or near the branch site of the pre-mRNA after Prp2 action (Warkocki, Odenwalder et al. (2009), (Tseng, Liu et al. 2011)). We found Cwc25 only with low peptide numbers in the C complex (Table 3.1), indicating that Cwc25 had already acted (i.e. by promoting step 1 catalysis) and additional factors required for its

dissociation (i.e. Prp16, Slu7 and Prp18, see below) have already entered (Ohrt, Odenwalder et al., manuscript submitted).

If one compares our purified pre-catalytic, but activated B^{act} complex with the first step spliceosome C complex, it is obvious that this transition also entails a dramatic remodeling. Our first step spliceosome showed a lower S value (40S) than did the B^{act} complex. This remodeling was also accompanied by a destabilization of Prp2 and its co-factor Spp2 as determined by the decrease of peptide numbers analyzed by MS (Table 3.1). Additionally we observed a decreased number of peptides for proteins belonging to the U2 associated SF3a and SF3b complexes. The SF3a/b proteins are required at early stages in the splicing cycle, but it is not yet clear whether they are required after step 1. We will discuss further the importance of the destabilization of the U2 SF3a/b proteins during the transition from complex B^{act} to C below, together with our dcFCCS data.

The proteomic analysis of C complexes showed also a recruitment of spliceosomal factors which are known to act at later stages of the splicing reaction and include also the so-called “second step factors” that comprise Prp16, Slu7, Prp18 and Prp22 (Umen and Guthrie (1995). Prp17 is also a second step factor but it is already present at the time of B^{act} complex formation, which is consistent with recent observation that Prp17 plays a role in step 1 of the splicing reaction (Sapra, Khandelia et al. 2008). Thus, Prp17 can be considered as a *bona fide* step 1 factor. Surprisingly, we also detected all members of the trimeric disassembly NTR complex (Ntr1, Ntr2 and Prp43) in our C complex preparations. The NTR plays a role at a later stage of the splicing cycle, during the disassembly of the spliceosome after completion of splicing. One explanation for the unexpected association of the NTR with the spliceosome is that the splicing machinery might initiate turnover of the stalled spliceosomes due to the mutation or the lack of the 3'SS in our pre-mRNA substrate (Pandit, Lynn et al. 2006).

In summary, the proteins present in complex C likely comprise the complete list of proteins required to maintain a functional RNP machine in which step 1 is catalyzed (Fig. 4.2) As the complete set of known step 2 factors is present in complex C, this indicates that also step 2 could occur under certain conditions and on a wild-type pre-

mRNA substrate. The limited number of proteins recruited during the B^{act} to C transition revealed by this work has already offered the possibility of investigating step 1 and 2 catalysis *in vitro* using purified components of known composition (Warkocki, Odenwalder et al. 2009) and also gave us the opportunity of learning more about protein dynamics during catalytic activation and step 1 catalysis as revealed by dcFCCS in the second part of this work (Ohrt, Prior et al. 2012).

4.6 Compositional dynamics correlate with structural changes

Our EM analyses showed that the B, B^{act} and C complexes exhibit distinct typical shapes (Figure 4). Complex B images have triangular/rhombic shapes which are very similar to corresponding images obtained for human and *Drosophila* B complexes (Deckert, Hartmuth et al. 2006), (Herold, Will et al. 2009). In addition, structural features which were first described for the human complex (Boehringer, Makarov et al. 2004), like head, neck, stump and foot, are also discernible in the yeast B complex. This suggests that higher order interactions and the general spatial organization of spliceosomal subunits are also conserved among metazoans and yeast. The most evident difference between B complexes from yeast and man lies in the size of the head region, which is substantially smaller in yeast. The structural heterogeneity observed for complex B's head domain in other organisms (Boehringer, Makarov et al. 2004);(Deckert, Hartmuth et al. 2006), is also seen in the yeast complex, but here the degree of heterogeneity is less pronounced. B and B^{act} are structurally very different, in agreement with substantial differences in protein/RNA composition and the profound compositional remodeling during the B to B^{act} transition. Remodeling also leads to a change in sedimentation behavior – from 40 to 45S – during this activation step.

Our EM studies indicated that there are profound structural differences also between the 2D class averages of B^{act} and C. This is also reflected in the S value which drops from 45S to 40S for the less compact appearing C complex. The reason for the observed structural differences were found only in later studies (Warkocki, Odenwalder et al. 2009) and result from remodeling event occurring concomitant with the transformation of the B^{act} complex into the B* complex which is a pre-requisite

for 5'SS cleavage in complex C. Thus, consistent with mechanistic differences between B^{act} and C, their 2D structures suggest differences in their spatial organization. EM immunolabeling of spliceosomal components and 3D reconstructions may allow a more precise determination of the structural differences between B^{act} and C spliceosomes.

4.7 Suitability of dual color Fluorescence Cross Correlation Spectroscopy (dcFCCS) for investigating spliceosomal protein dynamics

With the experiments done in this work we demonstrated that dcFCCs is, in combination with the established *in vitro* reconstitution system of functional spliceosomes, a powerful approach to investigate dynamics of purified spliceosomes. For dcFCCS measurements, yeast spliceosomes were stalled before step 1 by using the temperature-sensitive mutant *prp2-1* yielding a $B^{\text{act}\Delta\text{Prp2}}$ spliceosome. It was shown by the work of Warkocki et al (2009) that highly purified $B^{\text{act}\Delta\text{Prp2}}$ can be catalytically activated to form B^* when supplemented with recombinant Prp2 and Spp2 splicing factors (Warkocki, Odenwalder et al. 2009). Purified $B^{\text{act}\Delta\text{Prp2}}$ complexes assembled on actin pre-mRNA labeled at its 5' end with the red fluorescent dye Atto647N were used. Proteins were labeled *in vivo* by fusing the protein of interest with a fluorescent protein EGFP (enhanced green fluorescent protein) by genetic modification. As in any study involving the introduction of bulky labels, there was a risk of label-induced impaired behavior. In the system described here, neither the label on the pre-mRNA nor those on the various proteins impaired the activity of the spliceosomes examined. The resulting doubly fluorescent-labeled and purified spliceosomal complexes were analyzed before and after catalytic activation by Prp2 and were found to be stable under our dcFCCS conditions as demonstrated for Snu114-EGFP. Snu114 is known to bind to the spliceosome throughout the splicing cycle (Fabrizio, Laggerbauer et al. 1997) (Fabrizio, Dannenberg et al. 2009) and was therefore used as a “positive control” in our experiments. The dcFCCS results of our complexes were sufficiently reproducible and allowed the investigation of the binding and release of the proteins of interest.

4.8 Prp2-mediated transformation of the B^{act} into the B* complex substantially alters the binding affinity of several proteins at the catalytic core of the spliceosome

Although the essential role of Prp2 in the catalytic activation of the spliceosome was established earlier, its mechanism of action has remained enigmatic (Kim and Lin (1996)). The structural change the spliceosome undergoes upon Prp2-mediated, ATP-dependent activation must be profound, given the substantial change in S value seen between the precursor B^{act} Δ Prp2 complex (45S) and the catalytically activated spliceosome B* (40S) (Kim and Lin (1996); Warkocki, Odenwalder et al. (2009)). We expanded our MS data by dcFCCS showing that the binding affinity of at least seven proteins, i.e., the U2 SF3a/b proteins Prp11 and Cus1, the RES complex protein Bud13, Cwc24, Cwc27, Yju2, and Cwc25, is quantitatively and qualitatively altered by Prp2-mediated catalytic activation of the spliceosome. Due to their characteristics in their binding behavior, these proteins can be divided into three groups. The first group comprises Cwc24, Cwc27, and Bud13, which are tightly bound to the B^{act} Δ Prp2 spliceosome and which dissociate almost completely (Cwc24 and Cwc27) or partly (Bud13), even under near-physiological conditions upon Prp2-mediated activation and conversion to the B* complex. The second group includes the SF3a/b proteins Prp11 and Cus1, whose binding to the spliceosome is weakened by the catalytic activation thus becoming salt-sensitive, such that they dissociate from the B* complex at higher salt concentrations, while staying associated with the B* spliceosome at non-stringent conditions (Fig. 3.18). The third group contains proteins whose binding to the spliceosome is enhanced during the B^{act} to B* transition and includes Yju2 (which is recruited at the stage of the B^{act} complex and which is more weakly bound prior to catalytic activation) and Cwc25 (which before the transition was not bound at all and is thus recruited to B*). Both proteins are known to be required for the first catalytic step that is catalyzed by complex B*.

4.9 Cwc24 functions in the generation of an active spliceosome but is not required for splicing catalysis *per se*

There is little known about the function of Cwc24 and Cwc27 in splicing. Cwc27 contains a peptidylprolyl isomerase and also has an evolutionarily conserved counterpart in the human spliceosome, NYCO-10 (Ohi, Link et al. (2002); Fabrizio, Dannenberg et al. (2009), but nevertheless, Cwc27 is not essential for the growth of *S. cerevisiae* under standard conditions (Winzeler, Shoemaker et al. (1999), Giaever, Chu et al. (2002). In contrast, Cwc24 is known to be essential for yeast growth, and it is needed for the splicing of the U3 snoRNA precursor *in vivo* (Goldfeder and Oliveira (2008). Our results that Cwc24 and Cwc27 dissociate almost quantitatively from the spliceosome during or after the Prp2-mediated catalytic activation of the spliceosome (Fig. 3.15) was the first indication that they are not required for catalysis of the splicing reaction *per se*. This fact led us to investigate the role of Cwc24 in splicing in more detail. The depletion and reconstitution experiments, done in our laboratory, confirmed that the presence of Cwc24 is necessary for splicing to proceed through the first catalytic step *in vitro* (Ohrt, Prior et al. 2012). Surprisingly, they also showed that Cwc24 is not required during the actual catalysis; catalytically activated B* complexes that had lost all of their Cwc24 were still able to perform the first catalytic step of splicing efficiently when complemented with the step 1 factor Cwc25 (Fig. 3.14B). Thus, the function of Cwc24 must be to assist in the assembly or the maturation of the activated spliceosome B^{act}. Consequently, we regard Cwc24 as an assembly factor for the B^{act} complex that is probably involved in generating the correct structure or conformation of the B^{act} complex. Therefore it will be interesting to find out which proteins of the B^{act} complex are direct interaction partners of Cwc24 and whether it also binds to spliceosomal RNAs or the pre-mRNA.

Earlier in this work, we showed that the proteins of the RES complex are recruited to the spliceosome at the time of the B complex and that it is stoichiometrically present in B^{act} (Table 3.1 and Figure 4.2). Our dcFCCS results demonstrate that the RES protein Bud13 loses its affinity for the B* complex. Previous studies showed that the RES complex is not essential for yeast viability, but is required for efficient splicing *in vitro* and *in vivo*. The work by Dziembowski et al. (2004) demonstrated that the inactivation of these proteins causes leakage of unspliced pre-mRNA from the

nucleus (Dziembowski, Ventura et al. (2004). Our present results are consistent with the idea that the RES proteins remain associated with the spliceosome until Prp2-mediated catalytic activation of the spliceosome and first step of catalysis to prevent the premature nuclear release of unspliced pre-mRNA.

4.10 Sf3a/b proteins remain bound to the B* spliceosome under near-physiological conditions, but their binding is reduced at high salt

Our dcFCCS data revealed clearly that Prp2-mediated ATP hydrolysis affects the binding affinity of the SF3a/b complexes (Fig. 3.18). We demonstrated that representative proteins of the Sf3a/b complex, Prp11 and Cus1, remained bound to the spliceosome under physiological salt conditions (i.e. 75 mM KCl). However, a destabilization of their interaction with the B* complex could be analyzed by the loss of their binding affinity at higher salt conditions. In human B/B^{act} complex, several SF3a/b proteins bind to the pre-mRNA on both sides of the BS (Gozani, Potashkin et al. (1998), and a similar function may likely be ascribed to their counterparts in yeast. Indeed, Hsp155, the yeast homolog of human SF3b155, cross-links to pre-mRNA close to the BPS (McPheeters and Muhlenkamp (2003). Thus, the destabilization of proteins, losing their binding affinity upon Prp2-mediated ATP hydrolysis, could expose the BPS adenosine for nucleophile attack at the 5'SS phosphodiester bond, due to rearrangement of the spliceosome near the BPS.

There are somewhat conflicting reports regarding the fate of the U2-associated SF3a/b proteins during catalytic activation. Our MS data showed that the U2 SF3a/b proteins were represented in similar quantities in B and B^{act}, nevertheless, in the C complex their presence was reduced to 20%–30%. In the B* and C complexes, prepared from B^{actΔPrp2} by complementation *in vitro*, the same U2 proteins were found by MS to be similarly abundant in the B^{actΔPrp2}, B*, and C complexes (Warkocki, Odenwalder et al. (2009). In a recent paper (Lardelli et al. 2010), it was reported that endogenous yeast C complexes arrested *in vivo* by the effect of a cold-sensitive Prp16 mutant and subsequently purified from whole yeast extracts contained virtually no U2 proteins. In the present work, we found that, under dcFCCS conditions (i.e., spliceosomes reconstituted *in vitro* under near-physiological conditions and at ~1 nM

concentration), the U2 proteins Prp11 and Cus1 are not released either from complex B* or from complex C. We believe that the results shown here correspond most closely to physiological reality because dcFCCS allows spliceosomes to be investigated directly in solution and in equilibrium without requiring biochemical/physical perturbation of the sample. The differences described above could be due simply to the U2 proteins having an intermediate binding affinity after catalytic activation of the spliceosome so that their continued presence in B* and/or C complexes is sensitive to small changes in the spliceosome's physical environment. Since in all cases, either truncated pre-mRNAs or mutated RNA helicases were used to arrest the spliceosome at the desired stage, it is also possible that, in extract, discard mechanisms are responsible for the removal of the U2 proteins from dead-end spliceosomal complexes. Very recently it was shown in our laboratory that the U2 SF3a/b proteins remain bound to the spliceosome during the entire spliceosomal cycle and the U2 snRNP is released during disassembly of the spliceosome as an intact particle (Fourmann, Schmitzova et al. 2013).

4.11 Prp2 action creates high-affinity binding sites for the step 1 factors Yju2 and Cwc25 in the catalytically activated spliceosome

Yju2 is one of the factors which needs the ATP-dependent Prp2-mediated activation of the spliceosome for stable integration. Of all the proteins studied here by dcFCCS, Yju2 has the lowest affinity for the B^{actΔPrp2} spliceosome and can be completely removed from it at 300 mM salt. After Prp2-mediated catalytic activation, the spliceosome's binding affinity for Yju2 is strongly enhanced, and its association becomes largely salt-resistant. These results evidenced that Prp2 has to function before Yju2 to create a high-affinity binding site for stable integration. Thus, it is possible to conclude that the stable integration of Yju2 is Prp2-dependent. Additionally we demonstrated that the first step factor Cwc25 is recruited after Prp2 has acted. No peptides were found for Cwc25 in our Bact complex preparations as revealed by MS analysis. However, *via* dcFCCS we clearly showed that after catalytic activation a strong binding site is created in the B* spliceosome for the step 1 factor Cwc25.

4.12 Substantial Prp2-mediated remodeling during catalytic activation of the spliceosome

The ability to isolate and to purify spliceosomal complexes stalled at distinct stages of the splicing cycle and to characterize their proteome was a milestone towards the understanding of the ongoing processes at the core of the splicing machinery during its activation. We showed a dramatic change in the protein composition during the transition from the B^{act} to C complex, including the destabilization of the U2 proteins and RES complex as revealed by MS. Thus, to expand our MS data, we measured the effect of the catalytic activation on the binding strength of at least seven proteins in this first application of dcFCCS to functional spliceosomes. Of these, Bud13, Prp11 and Cus1, all belong to multiprotein complexes containing additional proteins. Bud13 is a member of the RES complex, which comprises two additional proteins, Prp11 and Cus1 belong to the U2 snRNP associated multiprotein complexes SF3a/b which consist of two (SF3a) or six additional proteins (SF3b) (see Figure 4.2). The dcFCCS results from this work are in line with our MS data. Thus, we imply that the interaction of at least 17 proteins with the spliceosome is affected by the Prp2-mediated catalytic activation of the spliceosome (Fig. 4.3).

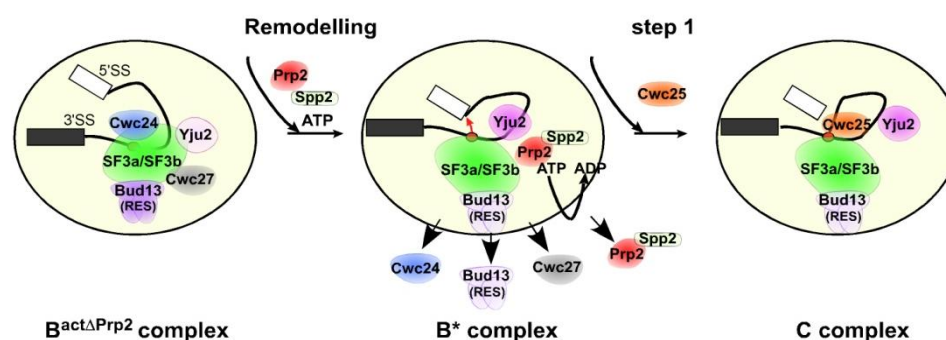


Figure 4.3: Schematic representations of the substantial remodeling the B^{act} spliceosome undergoes during the Prp2/ATP-mediated catalytic activation.

Cwc24, Cwc27, the RES protein Bud13, Prp2 and Spp2 are released while the U2 SF3a/b proteins are destabilized by Prp2/ATP such that the BS adenosine becomes available for a nucleophile attack at the 5' SS phosphodiester bond. At the same time high affinity binding sites are created for Yju2 and Cwc25, which are required to promote the first step of splicing (adapted from (Ohrt, Prior et al. 2012)).

Based on our data we addressed the question whether Prp2 is the only ATPase/helicase responsible for these dramatic rearrangements at the catalytic core of the spliceosome. The MS analysis of $B^{\text{act}\Delta\text{Prp2}}$ complexes from the work of Warkocki et al. (2009) showed a complete absence of the other helicases Prp5, Sub2 and Prp28, which are required for earlier steps of spliceosome assembly. The only spliceosomal helicase that is stoichiometrically present in the B^{act} complex is Brr2, which is known to trigger together with the GTPase Snu114 the precatalytic activation of the spliceosome by disrupting U4/U6 interaction (Bartels, Klatt et al. 2002); (Small, Leggett et al. 2006).

It was recently shown that the obligate ATPase Brr2, together with Prp43, functions in the dissociation of the post-splicing complexes that contain the intron lariat (Arenas and Abelson 1997); (Small, Leggett et al. 2006), suggesting that Brr2 could also be involved in catalytic activation, together with Prp2. However, we demonstrated earlier that the Prp2-dependent shift in S value from $\sim 45\text{S}$ to $\sim 40\text{S}$ during catalytic activation takes place in the presence of all rNTPs (not only ATP) (Warkocki, Odenwalder et al. 2009). In this work we showed that, upon Prp2-mediated catalytic activation, the dissociation of individual proteins, such as Cwc24-EGFP, occurs in the presence of UTP with efficiency equal to that in the presence of ATP (Fig. 3.15). Based on our results we can exclude the possibility that Brr2 contributes to spliceosome remodeling during catalytic activation due to the fact that yeast Brr2 hydrolyzes only ATP and no other rNTP, while Prp2 is rNTP unspecific (Kim, Smith et al. 1992). This would imply that Prp2 alone is responsible for the many changes in molecular interactions that take place during the transformation of B^{act} into the B^* spliceosome.

The assumption that Prp2 is alone responsible for the ongoing processes at the time of catalytic activation at the spliceosome's core suggests a cascade of remodeling steps during the B^{act} to B^* complex transition. One possible consideration for such a substantial remodeling model would be that Prp2 has only a single substrate and that only one protein is displaced from the network of intermolecular interactions in the B^{act} complex and that this process triggers all subsequent rearrangements. A possible Prp2 target could be Cwc24, as it is very stably bound in the B^{act} complex but loses its binding affinity during the transition to the B^* complex (Fig. 3.15). In this context,

the recent demonstration of a direct interaction between Cwc24 and Cef1 is of interest (Goldfeder and Oliveira 2008). Cef1 is a core protein of the NTC complex, which acts as a major assembly platform, integrating and coordinating many molecular interactions in B^{act} and B* complexes (Tsai, Chow et al. 1999); (Hogg, McGrail et al.). An alternative primary target of Prp2 could be one of the U2 SF3a/b proteins, which are known to interact with the pre-mRNA near the BPS. We cannot entirely exclude, however, that Prp2 may act on a number of targets, altering in succession the binding affinities of various proteins. This question could potentially be answered by performing a time-resolved analysis of the dissociation of various proteins and by determining the number of ATP molecules that are hydrolyzed during the transformation of a B^{act} Δ Prp2 to a C complex.

It is also unclear which RNA structure(s) in the spliceosome is/are the primary target(s) of Prp2/ATPase activity or whether Prp2 affects protein-protein interactions directly. Prp2 has been cross-linked to the region between the BPS and the 3'SS (Teigelkamp, McGarvey et al. 1994), raising the possibility that Prp2 modulates interactions between the BPS region and the U2 proteins. Alternatively, contact with this stretch of RNA might merely be required to stimulate Prp2/ATPase activity. It is also possible that Prp2/ATPase activity modulates the U2 RNA conformation during catalytic activation (Hilliker, Mefford et al. 2007); (Perriman and Ares 2007), which, in turn, could lead to the rearrangement of protein-RNA and protein-protein interaction at the catalytic core. Clearly, more information is needed about the direct contact sites of Prp2 on the B^{act} spliceosome and about the timing of the Prp2-mediated structural changes of the spliceosome to understand this important and profound structural reorganization step. In conclusion, the studies described in this work show that our isolated and purified complexes are well suited for structural and biochemical investigations and that dcFCCS can contribute significantly to these sophisticated investigations using reconstituted, highly purified spliceosomes.

5. Future perspectives

Our recently established affinity-based methods allowed us to isolate and characterize yeast spliceosomal complexes at defined functional stages (Dannenberg et al, 2012). In addition, it gave us the opportunity to carry out an investigation of the poorly understood conformational rearrangements in the spliceosome's catalytic core that occur prior to and during/after step 1 catalysis, using several approaches described in detail in this work. For example, by applying fluorescence-spectroscopic methods such as dcFCCS (in collaboration with Prof. J. Enderlein, Univ. of Göttingen) coupled with an *in vitro* reconstitution system (Warkocki, Odenwalder et al. 2009), we investigated the dynamics of the spliceosome's protein composition during catalytic activation by the RNA helicase/ATPase Prp2. We show that the binding affinity of a surprisingly high number of proteins is significantly changed during catalytic activation, suggesting remarkable Prp2-mediated structural rearrangements in the spliceosome's catalytic core (Ohrt, Prior et al. 2012). We have already expanded our studies and followed structural changes and the kinetics of protein recruitment/release during step 2 catalysis by dcFCCS. Our data show that the step 2 factors Slu7 and Prp18 are needed to displace the step 1 factor Cwc25 from the spliceosome and that this displacement occurs immediately before step 2 catalysis and, in addition another RNA helicase/ATPase, Prp16, is involved (Ohrt et al., submitted). Thus, these studies have already paved the way for a deeper understanding of the action of Prp16, a crucial RNA helicase essential for step 2 catalysis. Additional studies including essential RNA helicases/ATPases required after step 2 catalysis, as for example Prp22 and Prp43, will also be undertaken in the future, to follow structural changes and the kinetics of protein recruitment/release during their action by dcFCCS and FRET (with Prof. J. Enderlein).

Additional main goals will also be to investigate molecular details of the transformation of the yeast Commitment complex to A complex and the pre-catalytic B to B^{act} complex, both of which involve dramatic structural rearrangements. For example, the latter rearrangement includes the displacement of all U4/U6 proteins and the stable integration of about 20 new proteins [i.e. the Prp19 (NTC) complex and the NTC-related proteins] into the newly formed B^{act} complex (Fabrizio et al., 2009). This will be performed by complementing purified B complexes with recombinantly

expressed NTC and NTC-related proteins (in collaboration with Dr. Vlad Pena). With this system we will dissect the requirements for the Brr2-mediated dissociation of the U4/U6 base pairing which initiates activation and the role of proteins in restructuring the U6 and U2 snRNAs and in assembling the catalytic core RNP domain. Additionally, our isolated CC2 could be used for *in vitro* reconstitution of A complexes upon addition of purified U2 snRNPs and recombinant Prp5.

In collaboration with Prof. H. Stark's group, we have obtained a 3D Cryo-EM structure of the yeast B^{act} complex at 20-25 Å resolution. To learn more about the structural organisation of individual snRNPs, we will localise important proteins and RNA regions within the B^{act} complex by immunoelectron microscopy. Using genetically tagged proteins, it would now be possible to map the position of selected proteins (e.g., Cwc2, Prp2 and Prp19) in purified yeast B^{act} complexes, providing initial insight into the location of the spliceosome's catalytic centre. A second major focus will be to determine the spliceosome's 3D structure at higher resolution, which we will pursue mainly by a combination of single-particle electron cryomicroscopy (with Prof. H. Stark). Our EM studies will be conducted mainly on reconstituted and purified yeast spliceosomes – with the hope of isolating sufficient quantities of all of the interesting intermediates formed during spliceosome activation and catalysis – with the goal of obtaining cryo-EM structures with 10-15 Å resolution or even higher. In collaboration with Prof. H. Stark, our laboratory is currently testing a variety of methods, including the optimization of buffer and pH conditions and mild crosslinking procedures, to optimize stabilization and thus reduce conformational heterogeneity of spliceosomes. At the same time, we will extend our EM studies to locate specific proteins and RNA regions to other spliceosomal complexes (i.e. B and C). The topographical data obtained in this way, in combination with biochemical and cross linking data on the spatial organisation of RNAs and proteins, will be of great value for the interpretation of the 3D cryo-EM structures. With the availability of 3D cryo-EM maps of yeast spliceosomes at higher resolution in the near future, crystal structures of individual spliceosomal proteins can be fit into the 3D EM maps, and should thus greatly facilitate our understanding of the organisation of the spliceosome.

6. References

- Abovich, N., P. Legrain, et al. (1990). "The yeast PRP6 gene encodes a U4/U6 small nuclear ribonucleoprotein particle (snRNP) protein, and the PRP9 gene encodes a protein required for U2 snRNP binding." *Mol. Cell Biol.* **10**(12): 6417-6425.
- Abu Dayyeh, B. K., T. K. Quan, et al. (2002). "Probing interactions between the U2 small nuclear ribonucleoprotein and the DEAD-box protein, Prp5." *J Biol Chem* **277**(23): 20221-20233.
- Arenas, J. E. and J. N. Abelson (1997). "Prp43: An RNA helicase-like factor involved in spliceosome disassembly." *Proc. Natl. Acad. Sci. USA* **94**(22): 11798-11802.
- Bach, M. and R. Lührmann (1991). "Protein-RNA interactions in 20S U5 snRNPs." *Biochim. Biophys. Acta* **1088**(1): 139-143.
- Bach, M., G. Winkelmann, et al. (1989). "20S small nuclear ribonucleoprotein U5 shows a surprisingly complex protein composition." *Proc. Natl. Acad. Sci. USA* **86**(16): 6038-6042.
- Bartels, C., C. Klatt, et al. (2002). "The ribosomal translocase homologue Snu114p is involved in unwinding U4/U6 RNA during activation of the spliceosome." *EMBO Reports* **3**(9): 875-880.
- Bartels, C., H. Urlaub, et al. (2003). "Mutagenesis Suggests Several Roles of Snu114p in Pre-mRNA Splicing." *J Biol Chem* **278**(30): 28324-28334.
- Behzadnia, N., M. M. Golas, et al. (2007). "Composition and three-dimensional EM structure of double affinity-purified, human prespliceosomal A complexes." *Embo J* **26**(6): 1737-1748.
- Bessonov, S., M. Anokhina, et al. (2010). "Characterization of purified human Bact spliceosomal complexes reveals compositional and morphological changes during spliceosome activation and first step catalysis." *RNA* **16**(12): 2384-2403.
- Bessonov, S., M. Anokhina, et al. (2008). "Isolation of an active step I spliceosome and composition of its RNP core." *Nature* **452**(7189): 846-850.
- Blum (1987). "Improved silver staining of plant proteins, RNA and DNA in polyacrylamide gels." *Electrophoresis*.
- Boehringer, D., E. M. Makarov, et al. (2004). "Three-dimensional structure of a pre-catalytic human spliceosomal complex B." *Nat Struct Mol Biol* **11**(5): 463-468.
- Boon, K. L., T. Auchynnikava, et al. (2006). "Yeast ntr1/spp382 mediates prp43 function in postspliceosomes." *Mol Cell Biol* **26**(16): 6016-6023.
- Brow, D. A. (2002). "Allosteric cascade of spliceosome activation." *Annu. Rev. Genet.* **36**: 333-360.
- Brow, D. A. and C. Guthrie (1988). "Spliceosomal RNA U6 is remarkably conserved from yeast to mammals." *Nature* **334**(6179): 213-218.
- Caspary, F. and B. Séraphin (1998). "The yeast U2A'/U2B complex is required for pre-spliceosome formation." *EMBO J.* **17**(21): 6348-6358.
- Chan, S. P., D. I. Kao, et al. (2003). "The Prp19p-associated complex in spliceosome activation." *Science* **302**(5643): 279-282.
- Chanfreau, G., S. A. Elela, et al. (1997). "Alternative 3'-end processing of U5 snRNA by RNase III." *Genes Dev* **11**(20): 2741-2751.

- Cheng, S. C. (1994). "Formation of the yeast splicing complex A1 and association of the splicing factor PRP19 with the pre-mRNA are independent of the 3' region of the intron." Nucleic Acids Res. **22**(9): 1548-1554.
- Company, M., J. Arenas, et al. (1991). "Requirement of the RNA helicase-like protein PRP22 for release of messenger RNA from spliceosomes [see comments]." Nature (London) **349**(6309): 487-493.
- Cordin, O., D. Hahn, et al. (2012). "Structure, function and regulation of spliceosomal RNA helicases." Curr Opin Cell Biol **24**(3): 431-438.
- Dalbadie-McFarland, G. and J. Abelson (1990). "PRP5: a helicase-like protein required for mRNA splicing in yeast." Proc. Natl. Acad. Sci. USA **87**(11): 4236-4240.
- Dannenber, J., P. Fabrizio, et al. (2012). Affinity purification of spliceosomal and small nuclear ribonucleoprotein complexes. Handbook of RNA biochemistry; Weinheim: Wiley-VCH. 2.Ed., (in Press).
- Das, R., Z. Zhou, et al. (2000). "Functional association of U2 snRNP with the ATP-independent spliceosomal complex E." Mol. Cell **5**(5): 779-787.
- Deckert, J., K. Hartmuth, et al. (2006). "Protein composition and electron microscopy structure of affinity-purified human spliceosomal B complexes isolated under physiological conditions." Mol Cell Biol **26**(14): 5528-5543.
- Dreyfuss, G., V. N. Kim, et al. (2002). "Messenger-RNA-binding proteins and the messages they carry." Nat Rev Mol Cell Biol **3**(3): 195-205.
- Dziembowski, A., A. P. Ventura, et al. (2004). "Proteomic analysis identifies a new complex required for nuclear pre-mRNA retention and splicing." EMBO J **23**(24): 4847-4856.
- Fabrizio, P. and J. Abelson (1990). "Two domains of yeast U6 small nuclear RNA required for both steps of nuclear precursor messenger RNA splicing." Science **250**(4979): 404-409.
- Fabrizio, P., J. Dannenberg, et al. (2009). "The evolutionarily conserved core design of the catalytic activation step of the yeast spliceosome." Mol Cell **36**(4): 593-608.
- Fabrizio, P., B. Lagerbauer, et al. (1997). "An evolutionarily conserved U5 snRNP-specific protein is a GTP-binding factor closely related to the ribosomal translocase EF-2." EMBO J. **16**(13): 4092-4106.
- Fabrizio, P., D. S. McPheeters, et al. (1989). "In vitro assembly of yeast U6 snRNP: a functional assay." Genes Dev **3**(12B): 2137-2150.
- Fenn, J. B., M. Mann, et al. (1989). "Electrospray ionization for mass spectrometry of large biomolecules." Science **246**(4926): 64-71.
- Földes-Papp, Z. (2005). "How the molecule number is correctly quantified in two-color fluorescence cross-correlation spectroscopy: corrections for cross-talk and quenching in experiments." Curr Pharm Biotechnol **6**(6): 437-444.
- Földes-Papp, Z. and R. Rigler (2001). "Quantitative two-color fluorescence cross-correlation spectroscopy in the analysis of polymerase chain reaction." Biol Chem **382**(3): 473-478.
- Fourmann, J. B., J. Schmitzova, et al. (2013). "Dissection of the factor requirements for spliceosome disassembly and the elucidation of its dissociation products using a purified splicing system." Genes Dev **27**(4): 413-428.
- Frank, D. N., H. Roiha, et al. (1994). "Architecture of the U5 small nuclear RNA." Mol Cell Biol **14**(3): 2180-2190.

- Giaever, G., A. M. Chu, et al. (2002). "Functional profiling of the *Saccharomyces cerevisiae* genome." *Nature* **418**(6896): 387-391.
- Golas, M. M., B. Sander, et al. (2003). "Molecular Architecture of the Multiprotein Splicing Factor SF3b." *Science* **300**(5621): 980-984.
- Goldfeder, M. B. and C. C. Oliveira (2008). "Cwc24p, a novel *Saccharomyces cerevisiae* nuclear ring finger protein, affects pre-snoRNA U3 splicing." *J Biol Chem* **283**(5): 2644-2653.
- Gottschalk, A., G. Neubauer, et al. (1999). "Identification by mass spectrometry and functional analysis of novel proteins of the yeast [U4/U6.U5] tri-snRNP." *Embo J* **18**(16): 4535-4548.
- Gottschalk, A., G. Neubauer, et al. (1999). "Identification by mass spectrometry and functional analysis of novel proteins of the yeast [U4/U6.U5] tri-snRNP." *EMBO J* **18**(16): 4535-4548.
- Gottschalk, A., J. Tang, et al. (1998). "A comprehensive biochemical and genetic analysis of the yeast U1 snRNP reveals five novel proteins." *RNA* **4**(4): 374-393.
- Gozani, O., J. Potashkin, et al. (1998). "A potential role for U2AF-SAP 155 interactions in recruiting U2 snRNP to the branch site." *Mol. Cell Biol.* **18**(8): 4752-4760.
- Hacker, I., B. Sander, et al. (2008). "Localization of Prp8, Brr2, Snu114 and U4/U6 proteins in the yeast tri-snRNP by electron microscopy." *Nat Struct Mol Biol* **15**(11): 1206-1212.
- Hartmuth, K., H. Urlaub, et al. (2002). "Protein composition of human prespliceosomes isolated by a tobramycin affinity-selection method." *Proc Natl Acad Sci U S A* **99**(26): 16719-16724.
- Haustein, E. and P. Schwillle (2007). "Fluorescence correlation spectroscopy: novel variations of an established technique." *Annu Rev Biophys Biomol Struct* **36**: 151-169.
- Herold, N., C. L. Will, et al. (2009). "Conservation of the protein composition and electron microscopy structure of *Drosophila melanogaster* and human spliceosomal complexes." *Mol Cell Biol* **29**(1): 281-301.
- Hilliker, A. K., M. A. Mefford, et al. (2007). "U2 toggles iteratively between the stem IIa and stem IIc conformations to promote pre-mRNA splicing." *Genes Dev* **21**(7): 821-834.
- Hogg, R., J. C. McGrail, et al. "The function of the NineTeen Complex (NTC) in regulating spliceosome conformations and fidelity during pre-mRNA splicing." *Biochem Soc Trans* **38**(4): 1110-1115.
- Jurica, M. S., L. J. Licklider, et al. (2002). "Purification and characterization of native spliceosomes suitable for three-dimensional structural analysis." *RNA* **8**(4): 426-439.
- Jurica, M. S. and M. J. Moore (2002). "Capturing splicing complexes to study structure and mechanism." *Methods* **28**(3): 336-345.
- Kastner, B., N. Fischer, et al. (2008). "GraFix: sample preparation for single-particle electron cryomicroscopy." *Nat Methods* **5**(1): 53-55.
- Kettling, U., A. Koltermann, et al. (1998). "Real-time enzyme kinetics monitored by dual-color fluorescence cross-correlation spectroscopy." *Proc Natl Acad Sci U S A* **95**(4): 1416-1420.

- Kim, S. H. and R. J. Lin (1996). "Spliceosome activation by PRP2 ATPase prior to the first transesterification reaction of pre-mRNA splicing." *Mol Cell Biol* **16**(12): 6810-6819.
- Kim, S. H., J. Smith, et al. (1992). "The purified yeast pre-mRNA splicing factor PRP2 is an RNA-dependent NTPase." *EMBO J* **11**(6): 2319-2326.
- Kiss, T. and B. E. Jady (2004). "Functional characterization of 2'-O-methylation and pseudouridylation guide RNAs." *Methods Mol Biol* **265**: 393-408.
- Kistler, A. L. and C. Guthrie (2001). "Deletion of MUD2, the yeast homolog of U2AF65, can bypass the requirement for sub2, an essential spliceosomal ATPase." *Genes Dev* **15**(1): 42-49.
- Konarska, M. M., J. Vilardeell, et al. (2006). "Repositioning of the reaction intermediate within the catalytic center of the spliceosome." *Mol Cell* **21**(4): 543-553.
- Kosowski, T. R., H. R. Keys, et al. (2009). "DEXD/H-box Prp5 protein is in the spliceosome during most of the splicing cycle." *RNA* **15**(7): 1345-1362.
- Kress, T. L., N. J. Krogan, et al. (2008). "A single SR-like protein, Npl3, promotes pre-mRNA splicing in budding yeast." *Mol Cell* **32**(5): 727-734.
- Kretzner, L., A. Krol, et al. (1990). "Saccharomyces cerevisiae U1 small nuclear RNA secondary structure contains both universal and yeast-specific domains." *Proc Natl Acad Sci U S A* **87**(2): 851-855.
- Laemmli, U. K. (1970). "Cleavage of structural proteins during the assembly of the head of bacteriophage T4." *Nature* **227**(5259): 680-685.
- Lardelli, R. M., J. X. Thompson, et al. "Release of SF3 from the intron branchpoint activates the first step of pre-mRNA splicing." *RNA* **16**(3): 516-528.
- Lesser, C. F. and C. Guthrie (1993). "Mutations in U6 snRNA that alter splice site specificity: implications for the active site." *Science* **262**(5142): 1982-1988.
- Liao, X. C., H. V. Colot, et al. (1992). "Requirements for U2 snRNP addition to yeast pre-mRNA." *Nucleic Acids Res.* **20**(16): 4237-4245.
- Liu, Y. C., H. C. Chen, et al. (2007). "A novel splicing factor, Yju2, is associated with NTC and acts after Prp2 in promoting the first catalytic reaction of pre-mRNA splicing." *Mol Cell Biol* **27**(15): 5403-5413.
- Long, J. C. and J. F. Cáceres (2009). "The SR protein family of splicing factors: master regulators of gene expression." *Biochem J* **417**(1): 15-27.
- Lopez, P. J. and B. Seraphin (1999). "Genomic-scale quantitative analysis of yeast pre-mRNA splicing: implications for splice-site recognition." *Rna* **5**(9): 1135-1137.
- Makarov, E. M., O. V. Makarova, et al. (2002). "Small Nuclear Ribonucleoprotein Remodeling During Catalytic Activation of the Spliceosome." *Science* **298**(5601): 2205-2208.
- Makarova, O. V., E. M. Makarov, et al. (2002). "Protein 61K, encoded by a gene (PRPF31) linked to autosomal dominant retinitis pigmentosa, is required for U4/U6*U5 tri-snRNP formation and pre-mRNA splicing." *EMBO J* **21**(5): 1148-1157.
- Makarova, O. V., E. M. Makarov, et al. (2004). "A subset of human 35S U5 proteins, including Prp19, function prior to catalytic step 1 of splicing." *EMBO J* **23**(12): 2381-2391.
- Manley, J. L. and A. R. Krainer (2010). "A rational nomenclature for serine/arginine-rich protein splicing factors (SR proteins)." *Genes Dev* **24**(11): 1073-1074.

- Mann, M., R. C. Hendrickson, et al. (2001). "Analysis of proteins and proteomes by mass spectrometry." Annu Rev Biochem **70**: 437-473.
- McPheeters, D. S. and P. Muhlenkamp (2003). "Spatial organization of protein-RNA interactions in the branch site-3' splice site region during pre-mRNA splicing in yeast." Mol Cell Biol **23**(12): 4174-4186.
- Merril, C. R., D. Goldman, et al. (1981). "Ultrasensitive stain for proteins in polyacrylamide gels shows regional variation in cerebrospinal fluid proteins." Science **211**(4489): 1437-1438.
- Moehle, E. A., C. J. Ryan, et al. (2012). "The yeast SR-like protein Npl3 links chromatin modification to mRNA processing." PLoS Genet **8**(11): e1003101.
- Moore, M. J., C. C. Query, et al. (1993). Splicing of precursors to mRNA by the spliceosome. RNA World. A. Gesteland. Cold Spring Harbor, New York, Cold Spring Harbor Laboratory Press: 303-357.
- Moore, M. J. and P. A. Sharp (1993). "Evidence for two active sites in the spliceosome provided by stereochemistry of pre-mRNA splicing." Nature (London) **365**(6444): 364-368.
- Mouaikel, J., C. Verheggen, et al. (2002). "Hypermethylation of the cap structure of both yeast snRNAs and snoRNAs requires a conserved methyltransferase that is localized to the nucleolus." Mol Cell **9**(4): 891-901.
- Mütze, J., T. Ohrt, et al. (2011). "Fluorescence correlation spectroscopy in vivo." Laser & Photonics Reviews **5**(1): 52-67.
- Neubauer, G., A. Gottschalk, et al. (1997). "Identification of the proteins of the yeast U1 small nuclear ribonucleoprotein complex by mass spectrometry." Proc. Natl. Acad. Sci. USA **94**(2): 385-390.
- Newman, A. J. (1997). "The role of U5 snRNP in pre-mRNA splicing." EMBO J **16**(19): 5797-5800.
- Nilsen, T. W. (1998). RNA-RNA interactions in nuclear pre-mRNA splicing. RNA Structure and Function. R. W. S. a. M. Grundber-Manago. Cold Spring Harbor, New York., Cold Spring Harbor Laboratory Press: 279-307.
- O'Day, C. L., G. Dalbadie-McFarland, et al. (1996). "The *Saccharomyces cerevisiae* Prp5 protein has RNA-dependent ATPase activity with specificity for U2 small nuclear RNA." J. Biol. Chem. **271**(52): 33261-33267.
- Ohi, M. D. and K. L. Gould (2002). "Characterization of interactions among the Cef1p-Prp19p-associated splicing complex." RNA **8**(6): 798-815.
- Ohi, M. D., A. J. Link, et al. (2002). "Proteomics analysis reveals stable multiprotein complexes in both fission and budding yeasts containing Myb-related Cdc5p/Cef1p, novel pre-mRNA splicing factors, and snRNAs." Mol Cell Biol **22**(7): 2011-2024.
- Ohrt, T., M. Prior, et al. (2012). "Prp2-mediated protein rearrangements at the catalytic core of the spliceosome as revealed by dcFCCS." RNA **18**(6): 1244-1256.
- Ohrt, T., W. Staroske, et al. "Fluorescence cross-correlation spectroscopy reveals mechanistic insights into the effect of 2'-O-methyl modified siRNAs in living cells." Biophys J **100**(12): 2981-2990.
- Pandit, S., B. Lynn, et al. (2006). "Inhibition of a spliceosome turnover pathway suppresses splicing defects." Proc Natl Acad Sci U S A **103**(37): 13700-13705.

- Perriman, R., I. Barta, et al. (2003). "ATP requirement for Prp5p function is determined by Cus2p and the structure of U2 small nuclear RNA." Proc Natl Acad Sci U S A **100**(24): 13857-13862.
- Perriman, R. J. and M. Ares, Jr. (2007). "Rearrangement of competing U2 RNA helices within the spliceosome promotes multiple steps in splicing." Genes Dev **21**(7): 811-820.
- Query, C. C., M. J. Moore, et al. (1994). "Branch nucleophile selection in pre-mRNA splicing: evidence for the bulged duplex model." Genes Dev **8**(5): 587-597.
- Rasche, N., O. Dybkov, et al. (2012). "Cwc2 and its human homologue RBM22 promote an active conformation of the spliceosome catalytic centre." EMBO J **31**(6): 1591-1604.
- Ricka, J. and T. Binkert (1989). "Direct measurement of a distinct correlation-function by fluorescence cross-correlation." Physical Review A **39**(5): 2646-2652.
- Rosbash, M. and B. Séraphin (1991). "Who's on first? The U1 snRNP-5' splice site interaction and splicing." Trends Biochem. Sci. **16**(5): 187-190.
- Ruby, S. W., T. H. Chang, et al. (1993). "Four yeast spliceosomal proteins (PRP5, PRP9, PRP11, and PRP21) interact to promote U2 snRNP binding to pre-mRNA." Genes Dev **7**(10): 1909-1925.
- Rymond, B. C. and M. Rosbash (1985). "Cleavage of 5' splice site and lariat formation are independent of 3' splice site in yeast mRNA splicing." Nature (London) **317**(6039): 735-737.
- Rymond, B. C., D. D. Torrey, et al. (1987). "A novel role for the 3' region of introns in pre-mRNA splicing of *Saccharomyces cerevisiae*." Genes Dev **1**(3): 238-246.
- Sambrook, J., D. W. Russell, et al. (1989). "Molecular Cloning: A Laboratory Manual." Cold Spring Harbor, NY: Cold Spring Harbor Laboratory Press.
- Sapra, A. K., P. Khandelia, et al. (2008). "The splicing factor Prp17 interacts with the U2, U5 and U6 snRNPs and associates with the spliceosome pre- and post-catalysis." Biochem J **416**(3): 365-374.
- Schwer, B. and C. H. Gross (1998). "Prp22, a DExH-box RNA helicase, plays two distinct roles in yeast pre-mRNA splicing." EMBO J **17**(7): 2086-2094.
- Schwille, P., F. J. Meyer-Almes, et al. (1997). "Dual-color fluorescence cross-correlation spectroscopy for multicomponent diffusional analysis in solution." Biophys J **72**(4): 1878-1886.
- Shevchenko, A., M. Wilm, et al. (1996). "Mass spectrometric sequencing of proteins silver-stained polyacrylamide gels." Anal. Chem. **68**(5): 850-858.
- Shevchenko, A., M. Wilm, et al. (1996). "Mass spectrometric sequencing of proteins silver-stained polyacrylamide gels." Anal Chem **68**(5): 850-858.
- Shuster, E. O. and C. Guthrie (1988). "Two conserved domains of yeast U2 snRNA are separated by 945 nonessential nucleotides." Cell **55**(1): 41-48.
- Singh, R. and R. Reddy (1989). "Gamma-monomethyl phosphate: a cap structure in spliceosomal U6 small nuclear RNA." Proc Natl Acad Sci U S A **86**(21): 8280-8283.
- Singh, R. and J. Valcarcel (2005). "Building specificity with nonspecific RNA-binding proteins." Nat Struct Mol Biol **12**(8): 645-653.
- Small, E. C., S. R. Leggett, et al. (2006). "The EF-G-like GTPase Snu114p regulates spliceosome dynamics mediated by Brr2p, a DExD/H box ATPase." Mol Cell **23**(3): 389-399.

- Sontheimer, E. J. (2001). "The spliceosome shows its metal." Nat Struct Biol **8**(1): 11-13.
- Spingola, M., L. Grate, et al. (1999). "Genome-wide bioinformatic and molecular analysis of introns in *Saccharomyces cerevisiae*." RNA **5**(2): 221-234.
- Staley, J. P. and C. Guthrie (1998). "Mechanical devices of the spliceosome: motors, clocks, springs, and things." Cell **92**(3): 315-326.
- Stevens, S. W., I. Barta, et al. (2001). "Biochemical and genetic analyses of the U5, U6, and U4/U6 x U5 small nuclear ribonucleoproteins from *Saccharomyces cerevisiae*." RNA **7**(11): 1543-1553.
- Stevens, S. W., D. E. Ryan, et al. (2002). "Composition and Functional Characterization of the Yeast Spliceosomal Penta-snRNP." Mol. Cell **9**(1): 31-44.
- Studier, F. W. (2005). "Protein production by auto-induction in high density shaking cultures." Protein Expr Purif **41**(1): 207-234.
- Tanaka, N., A. Aronova, et al. (2007). "Ntr1 activates the Prp43 helicase to trigger release of lariat-intron from the spliceosome." Genes Dev **21**(18): 2312-2325.
- Tarn, W. Y., K. R. Lee, et al. (1993). "Yeast precursor mRNA processing protein PRP19 associates with the spliceosome concomitant with or just after dissociation of U4 small nuclear RNA." PNAS **90**(22): 10821-10825.
- Teigelkamp, S., M. McGarvey, et al. (1994). "The splicing factor PRP2, a putative RNA helicase, interacts directly with pre-mRNA." EMBO J. **13**(4): 888-897.
- Tsai, R. T., R. H. Fu, et al. (2005). "Spliceosome disassembly catalyzed by Prp43 and its associated components Ntr1 and Ntr2." Genes Dev **19**(24): 2991-3003.
- Tsai, R. T., C. K. Tseng, et al. (2007). "Dynamic interactions of Ntr1-Ntr2 with Prp43 and with U5 govern the recruitment of Prp43 to mediate spliceosome disassembly." Mol Cell Biol **27**(23): 8027-8037.
- Tsai, W. Y., Y. T. Chow, et al. (1999). "Cef1p is a component of the Prp19p-associated complex and essential for pre-mRNA splicing." J. Biol. Chem. **274**(14): 9455-9462.
- Tseng, C. K., H. L. Liu, et al. (2011). "DEAH-box ATPase Prp16 has dual roles in remodeling of the spliceosome in catalytic steps." RNA **17**(1): 145-154.
- Umen, J. G. and C. Guthrie (1995). "Prp16p, Slu7p, and Prp8p interact with the 3' splice site in two distinct stages during the second catalytic step of pre-mRNA splicing." RNA **1**(6): 584-597.
- Valadkhan, S. and Y. Jaladat (2010). "The spliceosomal proteome: at the heart of the largest cellular ribonucleoprotein machine." Proteomics **10**(22): 4128-4141.
- Valadkhan, S. and Y. Jaladat (2011). "The spliceosomal proteome: at the heart of the largest cellular ribonucleoprotein machine." Proteomics **10**(22): 4128-4141.
- Vijayraghavan, U., R. Parker, et al. (1986). "Mutations in conserved intron sequences affect multiple steps in the yeast splicing pathway, particularly assembly of the spliceosome." EMBO J. **5**(7): 1683-1695.
- Wahl, M. C., C. L. Will, et al. (2009). "The spliceosome: design principles of a dynamic RNP machine." Cell **136**(4): 701-718.
- Wang, Q. and B. C. Rymond (2003). "Rds3p is required for stable U2 snRNP recruitment to the splicing apparatus." Mol Cell Biol **23**(20): 7339-7349.
- Warkocki, Z., P. Odenwalder, et al. (2009). "Reconstitution of both steps of *Saccharomyces cerevisiae* splicing with purified spliceosomal components." Nat Struct Mol Biol **16**(12): 1237-1243.

- Wiest, D. K., C. L. O'Day, et al. (1996). "In vitro studies of the Prp9.Prp11.Prp21 complex indicate a pathway for U2 small nuclear ribonucleoprotein activation." J. Biol. Chem. **271**(52): 33268-33276.
- Will, C. L. and R. Luhrmann (2011). "Spliceosome structure and function." Cold Spring Harb Perspect Biol **3**(7).
- Will, C. L. and R. Luhrmann (2001). "Spliceosomal UsnRNP biogenesis, structure and function." Curr. Opin. Cell. Biol. **13**(3): 290-301.
- Will, C. L. and R. Luhrmann (2006). "Spliceosome Structure and Function." The RNA World.
- Winzler, E. A., D. D. Shoemaker, et al. (1999). "Functional characterization of the *S. cerevisiae* genome by gene deletion and parallel analysis." Science **285**(5429): 901-906.
- Xu, Y. Z. and C. C. Query (2007). "Competition between the ATPase Prp5 and Branch Region-U2 snRNA Pairing Modulates the Fidelity of Spliceosome Assembly." Mol Cell **28**(5): 838-849.
- Yan, D., R. Perriman, et al. (1998). "CUS2, a yeast homolog of human Tat-SF1, rescues function of misfolded U2 through an unusual RNA recognition motif." Mol. Cell Biol. **18**(9): 5000-5009.
- Yean, S. L. and R. J. Lin (1991). "U4 small nuclear RNA dissociates from a yeast spliceosome and does not participate in the subsequent splicing reaction." Mol. Cell Biol. **11**(11): 5571-5577.
- Yean, S. L., G. Wuenschell, et al. (2000). "Metal-ion coordination by U6 small nuclear RNA contributes to catalysis in the spliceosome." Nature **408**(6814): 881-884.
- Zhang, D. and M. Rosbash (1999). "Identification of eight proteins that cross-link to pre-mRNA in the yeast commitment complex." Genes Dev **13**(5): 581-592.
- Zhou, Z., L. J. Licklider, et al. (2002). "Comprehensive proteomic analysis of the human spliceosome." Nature **419**(6903): 182-185.

7. Appendix

7.1 List of abbreviations

3'SS	3' splice site
5'SS	5' splice site
°C	degree celsius
A	adenosine
ADP	adenosine-5'-diphosphate
AMP-PCP	5-adenylyl methylenediphosphonate
APS	ammonium peroxy sulfate
ATP	adenosine-5'-triphosphate
bp	basepair
BPS	branch point sequence
C	cytosine
CC	Commitment complex
Ci	Curie
CV	column volumes
Da	Dalton
dcFCCS	dual-color Fluorescence cross correlation spectroscopy
DNA	deoxyribonucleic acid
dNTPs	deoxynucleotide-5'-triphosphates
DTT	1,4- dithiothreitol
EDTA	ethylendiamine-N, N, N', N'-tetraacetic acid
EM	Electron microscopy
fmol	femtomole
G	guanosine
G-75/150	gradient buffer containing 75 mM or 150 mM KCl
GDP	guanosine-5'-diphosphate
GTP	gunosine-5'-triphosphate
h	hour(s)
kDa	kilo-Dalton
l	liter

Lsm	Like-Sm
μ	micro
μl	microliter
μm	micrometer
μM	micromolar
M	molar
min	minute
ml	milliliter
mM	milimolar
mRNA	messenger RNA
MS	mass spectrometry
n	nano
nM	nanomolar
nmol	nmol
NP-40	Nonidet P-40
nt	nucleotide
NTPs	nucleotide-5'-triphosphates
OD	optical density
PAA	poly-acrylamide
PAGE	poly-acrylamide gel electrophoresis
PCI	phenol-chloroform-isoamylalcohol
PCR	polymerase chain reaction
PEG	polyethylene glycol
pmol	picomole
pre-mRNA	pre-messenger RNA
Prp	pre-mRNA processing
RNA	ribonucleic acid
RNP	ribonucleoprotein
RT	room temperature
S	Svedberg
<i>S. cerevisiae</i>	<i>Saccharomyces cerevisiae</i>
SDS	sodium dodecylsulfate
Sm	“Smith”, patient in which Sm proteins were first discovered

snRNA	small nuclear ribonucleic acid
snRNP	small nuclear ribonucleoprotein
T	thymidine
TBE	tris-borate-EDTA buffer
TE	Tris-EDTA buffer
TEMED	N, N, N', N'-tetramethylethylenediamine
Ts	temperature-sensitive
U	uridine
U snRNA	uridine rich small nuclear ribonucleic acid
U snRNP	uridine rich small nuclear ribonucleoprotein
UV	ultraviolet
YPD	yeast extract, peptone

7.1 Curriculum vitae

Julia Dannenberg

Geburtsdatum: 27. August 1982

Geburtsort: Braunschweig

Staatsangehörigkeit: deutsch

Schulbildung

1989 bis 1995 Grundschule, Hermannshagen (Hann.Münden)

1995 bis 2002 Grotefend-Gymnasium Hann.Münden

Abitur Juni 2002

Studium

10/2002 bis 03/2008 **Studium an der Georg-August-Universität Göttingen im
Diplomstudiengang Biologie**

Hauptfach: Botanik

1. Nebenfach: Immunologie

2. Nebenfach: Physik

Mündliche Prüfungen im Mai 2007

Diplomarbeit März 2007 bis Februar 2008

Titel der Arbeit : „ Isolierung und Charakterisierung der
Proteinzusammensetzung von Spleißosomen aus der Hefe
S.cerevisiae“

angefertigt am MaxPlanck-Institut für biophysikalische Chemie
Göttingen, in der Abteilung für Zelluläre Biochemie

Betreuer: Prof. Reinhard Lührmann

Korreferent: Prof. Ralf Ficner

Promotion

09/2008 bis 03/2013 Promotion bei Prof. Dr. Reinhard Lührmann, Abteilung
Zelluläre Biochemie, Max-Planck-Institut für biophysikalische
Chemie, Göttingen

Titel der Arbeit: “Biochemical and structural characterization of spliceosomes purified at defined stages of assembly from the yeast *S. cerevisiae*”

7.2 List of publications

Fabrizio P, Dannenberg J, Dube P, Kastner B, Stark H, Urlaub H, Lührmann R. „The evolutionarily conserved core design of the catalytic activation step of the yeast spliceosome.“ (Mol Cell. 2009 Nov 25)

Ohr T, Prior M, Dannenberg J, Odenwalder P, Dybkov O, Rasche N, Schmitzova J, Gregor I, Fabrizio P, Enderlein J, Lührmann R. “Prp2-mediated protein rearrangements at the catalytic core of the spliceosome as revealed by dcFCCS”. (RNA 2012)

Dannenberg, J., Fabrizio, P., Will, C., & Lührmann, R. (2012). „Affinity purification of spliceosomal and small nuclear ribonucleoprotein complexes”. In R.K. Hartmann, A. Bindereif, & A. Schön (Eds.), *Handbook of RNA biochemistry* (2.ed.(in press)). Weinheim: Wiley-VCH.

Ohr T, Odenwälder, P., Dannenberg, J., Prior, M., Warkocki, Z., Schmitzová, J., Karaduman, R., Gregor, I., Enderlein, J., Fabrizio, P. and Lührmann, R. “Molecular dissection of step 2 catalysis of yeast pre-mRNA splicing investigated in a purified system” (*in press* (2013)).

7.3 Conferences

“Meeting of the European Associated Laboratory (LEA) on pre-mRNA splicing”, 2009, Göttingen

Präsentation eines Posters mit dem Titel: “Isolation and characterization of early spliceosomal complexes and mRNP from the yeast *S. cerevisiae*”.

“5th International PhD student symposium Horizons in Molecular Biology”, 2008, Göttingen Präsentation eines Posters mit dem Titel: “The evolutionarily conserved core design of the catalytic activation step of the yeast spliceosome.“

“7th International PhD student symposium Horizons in Molecular Biology”, 2010, Göttingen Präsentation eines Posters mit dem Titel: “Characterization and reconstitution of early spliceosomal complexes isolated from the yeast *S. cerevisiae*”

7.4 Acknowledgments

An dieser Stelle möchte ich mich von Herzen bei all denen bedanken, die mich während meiner Doktorarbeit unterstützt und motiviert haben.

Reinhard Lührmann danke ich in erster Linie für die großartige Möglichkeit der Promotion über ein tolles, spannendes Projekt in seiner Abteilung. Ein ganz besonderer Dank gilt ihm aber für seine Großzügigkeit, sein Vertrauen und seine Unterstützung, die er mir in den letzten Jahren entgegengebracht hat und die mir bei der Verwirklichung meines Traumes des Medizinstudiums sehr geholfen und es erst möglich gemacht haben. Vielen Dank dafür, **Reinhard**☺

Mein ganz besonderer und größter Dank gilt **Patrizia Fabrizio** „for being the ultra-best supervisor ever „ ☺ !!!! Während meiner Arbeit hatte ich die beste Betreuung, die man sich vorstellen und wünschen kann. Ich bedanke mich für die großartige Hilfe und Unterstützung, für die Antworten auf all meine Fragen, die zahlreichen Gespräche und Diskussionen, für das Miteinander-Lachen, für die guten und die schlechten Zeiten und alles was sie mir in dieser Zeit gegeben hat. Vielen Dank für die tolle Zeit, du bist großartig☺!

Bei **Thomas Ohrt** bedanke ich mich für die tolle Zusammenarbeit, für seine unbeschreibliche Hilfe und Unterstützung und dafür, dass ich so viel von ihm lernen durfte. Vielen Dank für diese tolle, unvergessliche Zeit und dafür dass du nicht nur ein super Postdoc sondern auch ein toller Freund warst bzw. bist☺!!

Ein herzliches Dankeschön geht an die weiteren Mitglieder meines Prüfungsausschusses: **Prof. Ralf Ficner, Prof. Jörg Enderlein, Prof. Heike Krebber, Prof. Holger Stark, Prof. Jürgen Wienands**

Ein ganz großer Dank geht natürlich an meine Kollegen und Freunde **Carsten, Carli, Cornelius, Irina, Nicolas, Norbert, Olex, Peter O., Ramazan und Thomas O.** (in alphabetischer Reihenfolge☺)!!! Ohne sie wäre die Zeit nur halb so schön gewesen. Danke für die tolle Zeit, die zahlreichen Gespräche und Diskussionen und den riesen Spass, den wir zusammen hatten und dafür, dass ihr immer ein offenes Ohr für mich hattet☺.

Mira Prior danke ich für ihre ausgezeichnete Arbeit, die tolle und witzige Zeit während unserer gemeinsamen Messzeit (an dieser Stelle auch lieben Dank an Flip ☺) und dafür, dass sie mich in die Geheimnisse der Biophysik eingeweiht hat ☺.

Thomas Conrad danke ich für den „just in time delivery service“ gesunder, glücklicher Hefe-Zellen in Kilogramm -Mengen und für die netten Gespräche in der Küche, wenn´s dann doch mal wieder länger gedauert hat ☺ .

Elke Penka danke ich für die zahlreichen Klonierungen und für ihre große Hilfsbereitschaft, **Wiebke Behrens** für die Vorbereitung frischer, aktiver und hochmotivierter Hefe-Extrakte☺.

Holger Stark und seiner Abteilung sowie **Berthold Kastner** danke ich für die tolle Zusammenarbeit und für die Durchführung der EM-Untersuchungen

Monika Raabe, Johanna Lehne, Uwe Pleßmann danke ich für die Durchführung der MS-Analysen.

Henning Urlaub, dem Süßigkeiten-Räuber, danke ich für die zahlreichen lustigen Momente und seine Unterstützung.

Reinhard Rauhaut danke ich für seine großartige Hilfe in allen Lebenslagen und für die netten Gespräche ☺

Jana Schmitzova und **Vlad Pena** für die Hilfe mit rekombinanten Proteinen und eine tolle Zusammenarbeit.

Gabi, Uschi, Gertrud, Claudia, Juliane, Irene, Kami und all den anderen helfenden Händen der Abteilung danke ich für ihre Unterstützung.

Danke **Klaus**, für die vielen interessanten und witzigen Gespräche und Diskussionen ☺

Ein großes Dankeschön auch an all die anderen Mitglieder der Abteilung für eine tolle Atmosphäre und eine gute Zeit.

Daniel danke ich dafür, dass er immer für mich da war, auch in stressigen Zeiten, und immer ein offenes Ohr für mich hatte.

Und als letztes noch ein riesen Dankeschön an meine **Mädels**☺!

7.5 Erklärung

Hiermit versichere ich, dass die Dissertation mit dem Titel “Biochemical and structural characterization of spliceosomes purified at defined stages of assembly from the yeast *S. cerevisiae*” von mir selbstständig und ohne unerlaubte Hilfe angefertigt worden ist.

Göttingen, den 05.03.2013

Julia Dannenberg